ปฏิกิริยาไฮโดรจิเนชันแบบเลือกเกิดของ 1-เฮปไทน์ ในวัฏภาคของเหลวโดยตัวเร่งปฏิกิริยาทอง-แพลเลเดียมบนไทเทเนียมไดออกไซด์

นายประธาน กิตติศักดิ์มนตรี

วิทยานิพนธ์นี้เป็นส่วนหนึ่งของการศึกษาตามหลักสูตรปริญญาวิศวกรรมศาสตรดุษฎีบัณฑิต
สาขาวิชาวิศวกรรมเคมี ภาควิชาวิศวกรรมเคมี
คณะวิศวกรรมศาสตร์ จุฬาลงกรณ์มหาวิทยาลัย
ปีการศึกษา 2556
ลิขสิทธิ์ของจุฬาลงกรณ์มหาวิทยาลัย

LIQUID-PHASE SELECTIVE HYDROGENATION OF 1-HEPTYNE OVER Au-Pd/TiO_2 CATALYSTS

Mr. Prathan Kittisakmontree

A Dissertation Submitted in Partial Fulfillment of the Requirements
for the Degree of Doctor of Engineering Program in Chemical Engineering
Department of Chemical Engineering
Faculty of Engineering
Chulalongkorn University
Academic Year 2013

Thesis Title	LIQUID-PHASE SELECTIVE HYDROGENATION OF 1-HEPTYNE OVER Au-Pd/TiO_2 CATALYSTS
By	Mr. Prathan Kittisakmontree
Field of Study	Chemical Engineering
Thesis Advisor	Associate Professor Joongjai Panpranot, Ph.D.

Accepted by the Faculty of Engineering, Chulalongkorn University in Partial Fulfillment of the Requirements for the Doctoral Degree

.....Dean of the Faculty of Engineering

(Professor Bundhit Eua-arporn, Ph.D.)

THESIS COMMITTEE

.....Chairman

(Associate Professor Anongnat Somwangthanaroj, Ph.D.)

.....Thesis Advisor

(Associate Professor Joongjai Panpranot, Ph.D.)

.....Examiner

(Associate Professor Bunjerd Jongsomjit, Ph.D.)

.....Examiner

(Akawat Sirisuk, Ph.D.)

.....External Examiner

(Assistant Professor Okorn Mekasuwandumrong, D.Eng.)

ประธาน กิตติศักดิ์มนตรี : ปฏิกิริยาไฮโดรจิเนชันแบบเลือกเกิดของ 1-เฮปไทน์ ในวัฏภาคของเหลวโดยตัวเร่งปฏิกิริยาทอง-แพลเลเดียมบนไทเทเนียมไดออกไซด์. (LIQUID-PHASE SELECTIVE HYDROGENATION OF 1-HEPTYNE OVER Au-Pd/TiO_2 CATALYSTS) อ.ที่ปรึกษาวิทยานิพนธ์หลัก: รศ. ดร.จูงใจ ปั้นประณต , หน้า.

ตัวเร่งปฏิกิริยาทอง-แพลเลเดียมบนไทเทเนียมไดออกไซด์ขนาด 100 นาโนเมตร ซึ่งเตรียมด้วยวิธีเคลือบฝังด้วยแพลเลเดียมปริมาณร้อยละ 0.5 โดยน้ำหนัก ตามด้วยวิธี deposition-precipitation ด้วยทองปริมาณร้อยละ 1 โดยน้ำหนัก (Au/Pd/TiO_2_100) และ ตัวเร่งปฏิกิริยา Pd/Au/TiO_2_100 เตรียมขึ้นด้วยลำดับการเติมทองและแพลเลเดียมที่สลับกัน สำหรับตัวเร่งปฏิกิริยา Au/Pd/TiO_2_100 การกระจายตัวของแพลเลเดียมเปลี่ยนแปลงไปในขณะที่เติมทองทำให้เกิดเป็นโลหะผสมทอง-แพลเลเดียมที่มีขนาดเล็ก และทำให้คุณสมบัติเชิงอิเล็กตรอน ของแพลเลเดียมเปลี่ยนไป แต่สำหรับตัวเร่งปฏิกิริยา Pd/Au/TiO_2_100 มีคุณสมบัติเชิงอิเล็กตรอนไม่ต่างจากตัวเร่งปฏิกิริยา Pd/TiO_2_100 นอกจากนี้ไทเทเนียมไดออกไซด์ที่มีขนาด 9 และ 15 นาโนเมตรซึ่งสังเคราะห์ขึ้นโดยวิธีโซลโวเทอร์มอล ถูกนำมาใช้เป็นตัวรองรับสำหรับตัวเร่งปฏิกิริยา Au/Pd/TiO_2 ซึ่งพบว่าโลหะผสมทอง-แพลเลเดียมที่เกิดขึ้นบนไทเทเนียมไดออกไซด์จะมีขนาดเล็กลง ตามขนาดของไทเทเนียมออกไซด์ ดังนี้ TiO_2_9 (เล็กกว่า 1 นาโนเมตร), TiO_2_15 (2-3 นาโนเมตร) และ TiO_2_100 (4-10 นาโนเมตร) สำหรับค่าการเลือกเกิดปฏิกิริยาไปเป็น 1-เฮปทีนของทุกตัวเร่งปฏิกิริยามีค่ามากกว่าร้อยละ 95 เมื่อปฏิกิริยาไฮโดรจิเนชันของ 1-เฮปไทน์เกิดใกล้จะสมบูรณ์ และเมื่อปฏิกิริยาเกิดสมบูรณ์แล้ว จะเกิดปฏิกิริยาไฮโดรจิเนชันของ 1-เฮปทีนไปเป็นเฮปเทนต่อ ซึ่งค่าการเลือกเกิดปฏิกิริยาไปเป็น 1-เฮปทีนของตัวเร่งปฏิกิริยา Au/Pd/TiO_2_100 ลดลงอย่างรวดเร็วเป็นร้อยละ 0 ที่เวลา 120 นาที ในขณะที่ตัวเร่งปฏิกิริยา Au/Pd/TiO_2_9, Au/Pd/TiO_2_15 และ Pd/TiO_2 ยังคงมีค่าการเลือกเกิดปฏิกิริยามากกว่าร้อยละ 40

ภาควิชา วิศวกรรมเคมี ลายมือชื่อนิสิต .....

สาขาวิชา วิศวกรรมเคมี ลายมือชื่อ อ.ที่ปรึกษาวิทยานิพนธ์หลัก .....

ปีการศึกษา 2556

5171870821 : MAJOR CHEMICAL ENGINEERING
KEYWORDS: SELECTIVE HYDROGENATION / 1-HEPTYNE / AU-PD BIMETALLIC CATALYSTS / TIO2

PRATHAN KITTISAKMONTREE: LIQUID-PHASE SELECTIVE HYDROGENATION OF 1-HEPTYNE OVER Au-Pd/TiO_2 CATALYSTS. ADVISOR: ASSOC. PROF. JOONGJAI PANPRANOT, Ph.D., pp.

TiO_2_100 supported Pd-Au catalysts were prepared with Pd (0.5 wt%) by impregnation and then Au (1.0 wt%) by deposition-precipitation (Au/Pd/TiO_2_100) and vice versa (Pd/Au/TiO_2_100). For the former sample, the state of dispersion of Pd on TiO_2 changed during the loading of Au, resulting in the formation of small Au-Pd alloy particles and thus changing the electronic properties of Pd species. The electronic properties of Pd on Pd/Au/TiO_2_100 were not so different from those of monometallic Pd/TiO_2_100. Moreover the nanocrystalline TiO_2 materials (9 and 15 nm) were synthesized by the solvothermal method and employed as the supports for preparation of bimetallic Au/Pd/TiO_2 catalysts. The Pd metal and/or Pd-Au alloy formed on the TiO_2_9 (< 1 nm) were smaller than on TiO_2_15 (2-3 nm) and on TiO_2_100 (4-10 nm). All the catalysts were selective to 1-heptene (> 95%) until close to the complete conversion of 1-hetyne. However, the selectivity of 1-heptene drastically decreased to 0% (which was further hydrogenated to heptane) in 120 minute for the Au/Pd/TiO_2_100 while it still remained > 40% for the Au/Pd/TiO_2_9, Au/Pd/TiO_2_15 and the monometallic Pd/TiO_2 catalyst.

Department: Chemical Engineering Student's Signature .....

Field of Study: Chemical Engineering Advisor's Signature .....

Academic Year: 2013

ACKNOWLEDGEMENTS

I would like to express my special appreciation and thanks to my advisor, Associate Professor Dr. Joongjai Panpranot, who have been a tremendous mentor and for encouraging my research. Her advice on research has been priceless. I attribute the level of my degree to her effort. One simply could not wish for a better or friendlier advisor.

I would also like to thank my committee members, Associate Professor Dr. Anongnat Somwangthanaroj, Associate Professor Dr. Bunjerd Jongsomjit, Dr. Akawat Sirisuk, and Assistant Professor Dr. Okorn Mekasuwandumrong, for serving as my committee members even at hardship. I also want to thank you for letting my defense be an enjoyable moment, and for your brilliant comments and suggestions.

In addition, a thank you to Professor Masahiko Arai and Dr. Shin-Ichiro Fujita for providing my assistance to conduct research at the Graduate School of Engineering, Hokkaido University. They have offered much advice and insight throughout my work there.

In the various laboratories and workshops, I have been blessed with a friendly and cheerful group of fellow student members of the Center of Excellence on Catalysis and Catalytic Reaction Engineering, Department of Chemical Engineering, Chulalongkorn University and members of Chemical Engineering Laboratory, Division of Chemical Process Engineering, Graduate School of Engineering, Hokkaido University.

A special thanks to my family. Words cannot express how grateful I am to my parents for supporting me throughout all my studies at University

Finally, I gratefully thanks to the Dusadeepipat scholarship from Chulalongkorn University, the Thailand Research Fund (TRF), and the Commission on Higher Education for the financial support. I also acknowledge supports from the National Research Council of Thailand (NRCT) and Japan Society for the Promotion of Science (JPS) under the joint research program.

CONTENTS

Page

Page

Page

LIST OF TABLES

LIST OF FIGURES

CHAPTER I
INTRODUCTION

1.1 Rationale

The reactions involving alkyne and alkene hydrogenation have become of both industrial and academic importance. A number of products from these reactions are used in the food (flavors), pharmaceutical (sedatives, anesthetics, vitamins), cosmetics (fragrances), plastics (resins and polymers), and lubricants industries [1]. Such reactions are often carried out in three-phase catalytic systems using batch and semibatch reactors. Different alkynic compounds have been employed as model reactants for evaluation of the liquid-phase selective hydrogenation catalysts under mild reaction conditions such as 1-hexyne [2], 3-hexyne [3], 1-heptyne [1, 4-6], 4-octyne [7], phenylacetylene [8, 9], and 1-phenyl-1-pentyne [10]. Palladium is the most common hydrogenation catalyst used in industry and studied in fundamental research because of its ability to selectively hydrogenate multiple unsaturated hydrocarbons.

Bimetallic catalysts have attracted much attention because of their markedly different properties from either of the constituent metals, and their enhanced catalytic stabilities, activities and/or selectivities. The promotional effect of Au in Pd–Au catalysts has been well established in many catalytic processes. The well-known applications include CO oxidation, selective oxidation of alcohols to aldehydes or ketones, alkenes to epoxides, and oxidation of hydrogen to hydrogen peroxide

hydrogenation [1]. Superior activities of Au–Pd catalysts, as compared to the monometallic Pd or Au nanoparticles, have been attributed to the synergistic effects arisen from both ligand effects and ensemble effects of the Au-Pd alloy [11, 12]. Despite the low reactivity of Au in hydrogenation, Au and Pd–Au catalysts have been studied in the selective hydrogenation of various compounds such as aromatic compounds [13, 14], acetylene [15, 16], 1,3-butadiene [17], 1,3-cyclooctadiene [18], cinnamaldehyde [19], and citral [20]. Different roles of Au addition have been reported in the selective hydrogenation over support Pd catalysts. Deposition of Au particles was used for selective poisoning of Pd surface in the selective hydrogenation of acetylene [15]. In the benzaldehyde hydrogenation in the presence of sulfur, gold acted as only an inert diluent that prevented Pd_4S formation without changing the catalyst activity [21]. A number of studies show that electron transfer between Pd and Au species occurred and was responsible for the improvement in both catalytic activity and selectivity in the hydrogenation reactions [13, 19, 20, 22]. However, it appears that the exertion of electronic interaction between Pd and Au species depended on several factors such as the molar ratio of Au and Pd, the preparation method, the particle morphology, and/or the particle size of Au–Pd alloys [23-26].

Despite the variety of supports being used for preparation of supported Au-Pd catalysts such as γ-Al_2O_3[13, 27], SiO_2 [19, 27], TiO_2 [20, 28], SiO_2-Al_2O_3 [14], zeolite [29], CeO_2 [30], α-Fe_2O_3 [31], and carbon [32, 33], only a few studies systematically reported the influence of support nature on the interaction of Au-Pd species and their corresponding catalytic behaviors.

TiO_2 is one of reducible metal oxides that have received considerable attention as catalyst supports. In the liquid-phase selective hydrogenation of alkyne to alkene, Pd/TiO_2 exhibited the strong metal-support interaction (SMSI) effect, resulting in an improvement of the catalytic performances [34]. However, the SMSI effect in Pd/TiO_2 depended on the properties of the TiO_2 such as the crystalline phase composition and the crystallite size [8, 35]. The TiO_2 supports used for preparation of Au–Pd catalysts in many research works were mostly the commercially available Degussa P25. Solvothemal method is an alternative route for direct (one step) synthesis of pure anatase TiO_2. Particle morphology, crystalline phase, and surface chemistry of the solvothemal-derived TiO_2 can be controlled by regulating precursor composition, reaction temperature, pressure, solvent property, and aging time [34]

In the present work, TiO_2 supported Pd-Au catalysts were prepared by the combination of incipient wetness impregnation (IM) and deposition-precipitation (DP) methods. Such methods are among the most commonly used methods for the preparation of supported monometallic Pd and Au catalysts, respectively. The catalysts were prepared with either loading of Au (1 wt%) first by DP method followed by IM of Pd (0.5 wt%) or preparation of Pd/TiO_2 first by IM before loading of Au by DP. Loading sequence was found to strongly affect the characteristics and catalytic behavior of the bimetallic $Pd–Au/TiO_2$ catalysts prepared in the liquid-phase hydrogenation of 1-heptyne. Moreover, the effect of TiO_2 crystallite size on the catalytic behavior of $Au–Pd/TiO_2$ catalysts was investigated in the selective hydrogenation of 1-heptyne under mild reaction conditions. The catalysts were also

characterized using X-ray diffraction (XRD), transmission electron microscopy (TEM), CO chemisorption, X-ray photoelectron spectroscopy (XPS), diffuse reflectance FTIR (DRIFT) spectra of CO, and UV-Vis spectroscopy.

1.2 Research Objectives

1. To investigate the effect of loading sequence of Au and Pd on the catalytic behavior of the bimetallic Pd–Au/TiO_2 catalysts in the liquid-phase hydrogenation of 1-heptyne.
2. To investigate the effect of TiO_2 crystallite size on the catalytic behavior of Pd/TiO_2 and Au/Pd/TiO_2 catalysts in the liquid-phase hydrogenation of 1-heptyne.
3. To investigate the effect of Pd loading on the catalytic behavior of Pd/TiO_2 and Au/Pd/TiO_2 catalysts in the liquid-phase hydrogenation of 1-heptyne.
4. To investigate the deactivation of Pd/TiO_2 catalyst in the liquid-phase hydrogenation of 1-heptyne and 1-heptene.

1.3 Research Scopes

- Deposition of Au by using the deposition-precipitation method with NaOH and the gold content of 1 wt%.
- Deposition of Pd by using the incipient-wetness impregnation method and the palladium content of 0.5 or 2.0 wt%.
- Synthesis of nano-sized TiO_2 supports by using the solvothermal method with different aging time to obtain different particle sizes. For the micron-sized TiO_2 is purchased from Aldrich.
- Catalyst pretreatment for palladium catalyst by calcination at 500°C in air for 2 hour.
- Reduction of the catalyst under H_2 flow at 40°C for 2 hour before the reaction test.
- Reaction study of Pd/TiO_2 and $Au\text{-}Pd/TiO_2$ catalysts in liquid-phase hydrogenation of 1-heptyne and 1-heptene by using stirring batch reactor (100 ml teflon-lined stainless steel autoclave).
- Characterization of Pd/TiO_2 and $Au\text{-}Pd/TiO_2$ catalysts by using several techniques, such as; X-ray diffraction (XRD), transmission electron microscopy (TEM), CO chemisorption, X-ray photoelectron spectroscopy (XPS), diffuse reflectance FTIR (DRIFT) spectra of CO, and UV-Vis spectroscopy.

1.4 Research Methodology

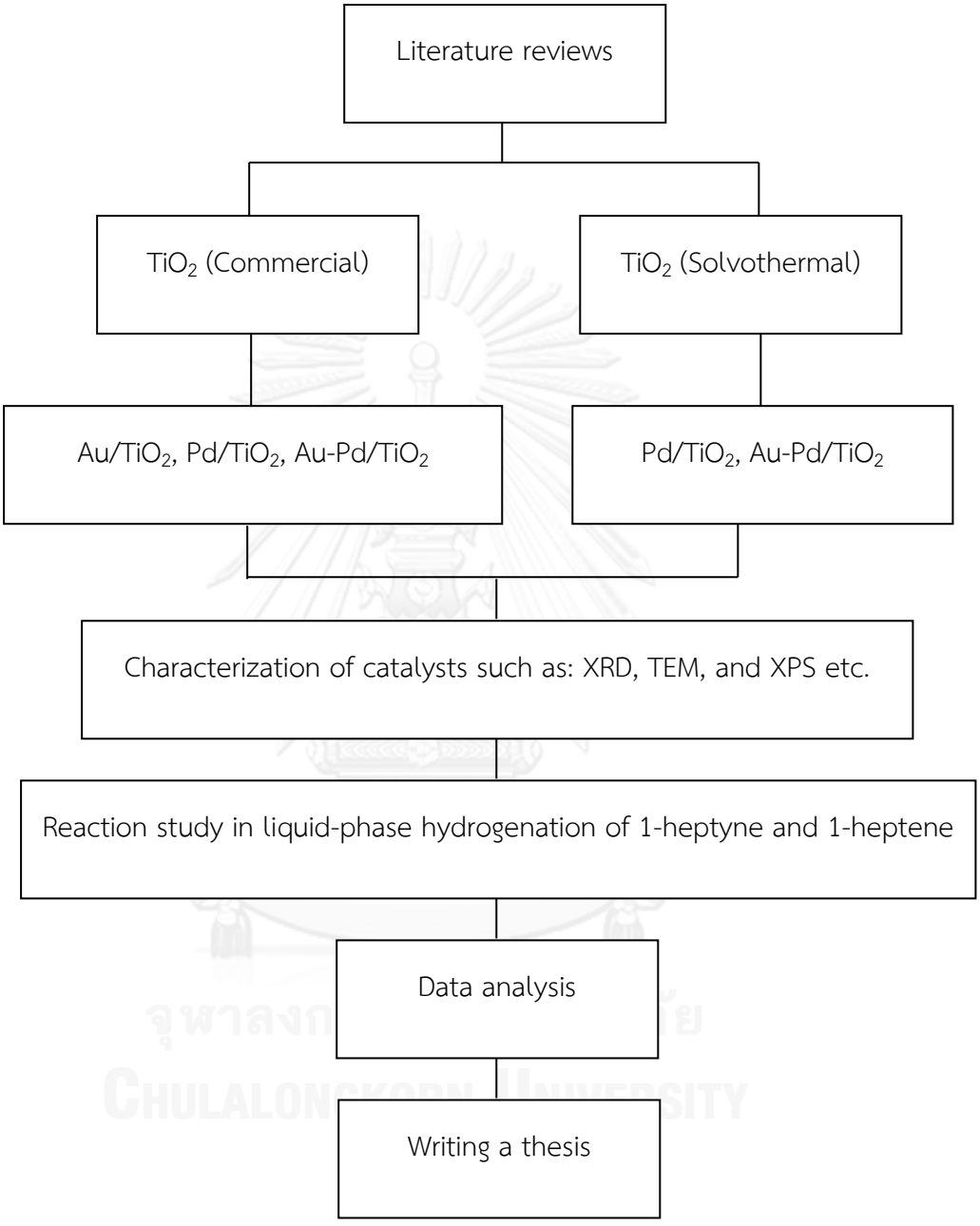

CHAPTER II
BACKGROUND AND LITERATURE REVIEWS

2.1 Hydrogenation of Alkynes

The reactions involving alkyne and alkene hydrogenation have become of both industrial and academic importance. Numerous products obtained from these partial hydrogenation reactions are useful in the synthesis of biologically active compounds, the production of margarine, the lubricant industry and the synthesis of important intermediates for the fine chemicals industry [36]. Hydrogenation processes are often carried out in a small scale in batch reactor. Batch processes are usually most cost effective since the equipment need not to be dedicated to a single reaction. Typically the catalyst is powdered and slurried with reactant; a solvent is usually present to influence product selectivity and to adsorb the reaction heat liberated by the reaction. Since most hydrogenations are highly exothermic, careful temperature control is required to achieve the desired selectivity and to prevent temperature runaway.

Selective hydrogenation of alkynes is an addition of hydrogen to a carbon-carbon triple bond in order to produce only alkenes product. The overall effect of such an addition is the reductive removal of the triple bond functional group. The simplest source of two hydrogen atoms is molecular hydrogen (H_2), but mixing alkynes with hydrogen does not result in any discernable reaction. However, careful hydrogenation of alkynes proceeds exclusively to the alkenes until the former is consumed, at which point the product alkenes is very rapidly hydrogenated to the

alkanes. Although the overall hydrogenation reaction is exothermic, high activation energy prevents it from taking place under normal conditions. This restriction may be circumvented by the use of a catalyst, as shown in the following diagram.

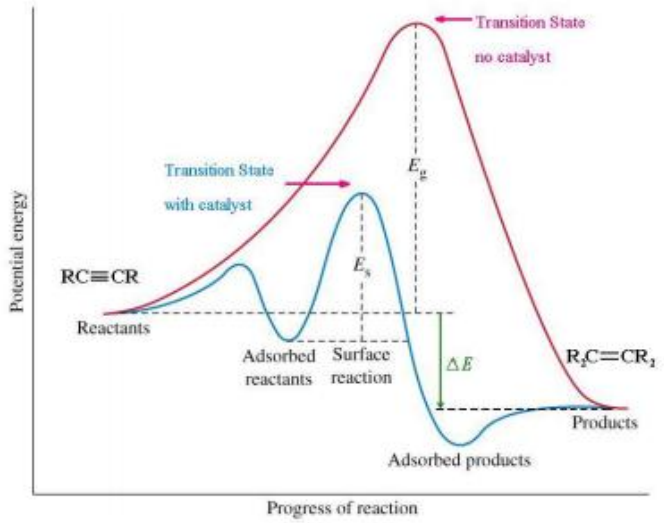

Figure 2.1 Potential energy profiles for non-catalysed and catalysed reactions

Catalysts are substances that change the rate (velocity) of a chemical reaction without being consumed or appearing as part of the product. Catalysts act by lowering the activation energy of the reactions, but they do not change the relative potential energy of the reactions and products. Pd-based catalysts have been known to exhibit high selectivity with respect to semihydrogenation of alkynes to alkenes and have been widely used both in laboratory and industry [37].

Selective hydrogenation of alkynes to alkenes is the reaction which takes place on the surface of the metal catalyst. The mechanism of the reaction can be described in four steps:

Step 1: Hydrogen molecules react with the metal atoms at the catalyst surface. The relatively strong H-H sigma bond is broken and replaced with two weak metal-H bonds.

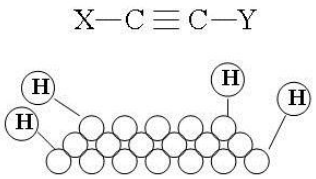

Step 2: The pi bond of the alkyne interacts with the metal catalyst weakening the bond. A hydrogen atom is transferred from the catalyst surface to one of the carbons of the triple bond.

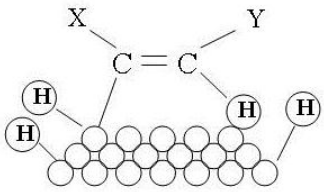

Step 3: The pi bond of the alkyne interacts with the metal catalyst weakening the bond. A second hydrogen atom is transferred from the catalyst surface forming the alkene.

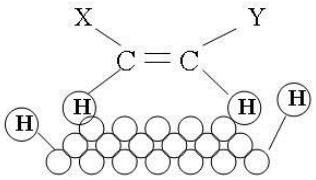

Step 4: The alkene is released from the catalyst's surface allowing the catalyst to accept additional hydrogen and alkene molecules.

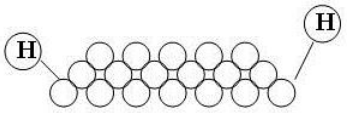

Many papers in the literature deal with the selective hydrogenation of short chain alkynes (C_1-C_4). However, more challenging from an academic and industrial point of view is the semihydrogenation of long chain alkynes such as 1-hexyne [2], 3-hexyne [3], 1-heptyne [1, 4-6], 4-octyne [7]**.** There are a few papers deal with such reaction. For example, O. Mekasuwandumrong et al. [37] implied the good catalytic performances in the liquid-phase selective hydrogenation of 1-heptyne using Pd/TiO_2 nanoparticles synthesized by one-step flame spray pyrolysis (FSP) with Pd loadings 0.5–10 wt%.

C.R. Lederhos et al. [38] studied different low-loaded Pd, Ni and Pd-Ni catalysts were tested for the partial hydrogenation of 1-heptyne. It was found that the Pd 0.5%-Ni1.0% bimetallic catalyst was more active than the Pd monometallic catalyst while both catalysts were very selective for the production of 1-heptene (>95%). These catalysts were however less active than the commercial Lindlar catalyst.

2.2 Gold as the Catalyst

The discovery in the 1980s that finely supported divided nanoparticles of gold could act as catalysts for reactions at low temperatures has to be one of the most fascinating recent observations in chemistry, since most consider gold to be an unreactive metal. Gold for a long time had been considered to be a relatively inert material and particularly unpromising as a catalyst. In particular, due to its stability under most conditions it is really surprising that it can be a highly effective oxidation catalyst. Consequently, a large number of experimental and theoretical studies are being undertaken to try to elucidate the nature of this interesting catalytic activity.

Although most studies of gold catalyst are focused on CO oxidation, the use of gold based catalysts for the hydrogenation reaction has received great attention in the recent years. The first study of the hydrogenation reaction using Au/SiO_2 catalysts was made by Bond [39], which found that the hydrogenation of 1,3-butadiene was occurred and selectively to partial hydrogenation to form butenes. Gold catalyst is not only to hydrogenate 1,3-butadiene, but also found to catalyze hydrogenation of acetylene [26], propyne[40], phenylacetylene [41] and unsaturated aldehydes to unsaturated alcohols [42]. For example, J. Jia and coworker [43] studied the selective hydrogenation of acetylene over Au/Al_2O_3 catalyst. They found that acetylene was hydrogenated to ethylene in the temperature range between 313 and 523 K with 100% selectivity. The activity of the selective hydrogenation of acetylene depends on the size of gold particle of Au/Al_2O_3 catalyst, which a maximum at about 3.0 nm in diameter.

Y. Liu et al. [44] studied liquid phase selective hydrogenation of phthalic anhydride to phthalide over Au/TiO_2 catalyst. The catalysts with different gold loading were prepared by deposition-precipitation method. All the studied Au/TiO_2 catalysts exhibited excellent activity with high selectivity (>92%) to phthalide under mild reaction conditions (180 $^{\circ}C$ and 3.0 MPa H_2). Specially, catalysts with 2-3 wt.% gold loading were highly active and selective for the formation of phthalide. When reused, the catalyst showed a certain deactivation, but still was highly selective to phthalide. The deactivation was attributed to the leaching of gold, collapse of the pore structure and accumulation of organic species on the surface.

There have been some reports about unexpected products on gold catalyst. C. Milone and coworker [45] studied on the hydrogenation of cinnamaldehyde carried out in ethanol under mild conditions (T = 333 K, P_{H2}=1 atm), on the Au/TiO_2 reference catalyst, supplied by the World Gold Council. The reaction was carried out on the as received and on the catalyst reduced at 473 K and 773 K. The behavior of Au/TiO_2 catalyst in the hydrogenation of cinnamaldehyde is of pasticular interest because it is the first time that the formation of the allyl ether is observed during this reaction. The selectivity towards the formation of cinnamyl ethyl ether, measured at 50% of conversion, increases from 19%, on the as received catalysts, up to 33% on the catalysts reduced at 473 K. A further increase of the reduction temperature does not influence the selectivity to cinnamyl ethyl ether.

2.3 Bimetallic Au-Pd Catalysts

Bimetallic catalysts have attracted much attention because of their markedly different properties from either of the constituent metals, and their enhanced catalytic stabilities, activities and/or selectivities. The promotional effect of Au in Pd–Au catalysts has been well established in many catalytic processes. The well-known applications include CO oxidation, selective oxidation of alcohols to aldehydes or ketones, alkenes to epoxides, and oxidation of hydrogen to hydrogen peroxide hydrogenation [1]. Superior activities of Au–Pd catalysts, as compared to the monometallic Pd or Au nanoparticles, have been attributed to the synergistic effects arisen from both ligand effects and ensemble effects of the Au-Pd alloy [11, 12]. Despite the low reactivity of Au in hydrogenation, Au and Pd–Au catalysts have been studied in the selective hydrogenation of various compounds such as aromatic compounds [13, 14], acetylene [15, 16], 1,3-butadiene [17], 1,3-cyclooctadiene [18], cinnamaldehyde [19], and citral [20]. Different roles of Au addition have been reported in the selective hydrogenation over support Pd catalysts. Deposition of Au particles was used for selective poisoning of Pd surface in the selective hydrogenation of acetylene [15]. In the benzaldehyde hydrogenation in the presence of sulfur, gold acted as only an inert diluent that prevented Pd_4S formation without changing the catalyst activity [21]. A number of studies show that electron transfer between Pd and Au species occurred and was responsible for the improvement in both catalytic activity and selectivity in the hydrogenation reactions [13, 19, 20, 22]. However, it appears that the exertion of electronic interaction between Pd and Au species depended on several factors such as the molar ratio of Au and Pd, the

preparation method, the particle morphology, and/or the particle size of Au–Pd alloys [23-26].

L. Prati [46] has used activated carbon or polyvinyl alcohol (PVA) to immobilize Au–Pd sols prepared by in situ reduction (using BH_4^-) of solutions containing Au and Pd salts to prepare Au–Pd bimetallic alloys. Despite slight Pd leaching and particle agglomeration, the Au–Pd alloys showed significantly higher activity towards various alcohol oxidation reactions compared to their monometallic counterparts. Ketchie et al. [47] prepared Au–Pd catalysts using a sol-methodology similar to that of Prati, but reported that both bimetallic and monometallic particles were formed. Analysis by EXAFS indicated that for the bimetallic particles preferential coverage of Pd by Au rather than formation of bimetallic alloy particles occurred, indicating a high degree of sensitivity to specifics of the preparative method.

N. Dimitraatos et al. [48] studied the selective oxidation of glycerol by using mono and bimetallic catalysts based on Au and Pd and supported on graphite. The catalysts were prepared by sol immobilization method. The result showed that the use of a bimetallic system significantly improved the activity with respect to the monometallic system; whereas, the selectivity to glyceric acid showed to be dependent upon the reaction temperature and the preparation method used.

Table 2.1 Physical properties of gold and palladium.

Properties	Pd	Au
Atomic number	46	79
Atomic weight	106.42	196.9665
Electron configuration	[Kr] $4d^{10}$	[Xe] $4f^{14}$ $5d^{10}$ $6s^{1}$
Crystal structure	fcc	fcc
Atomic radius (pm)	137	144
Density ($g \cdot cm^{-3}$)	12.023	19.30
Melting point (K)	1828	1337
Boiling point (K)	3236	3129
Electronegativity	2.20	2.54

2.4 Deposition-precipitation Method (DP)

The method is commonly referred to as deposition-precipitation (DP), because metal hydroxide is supposed to precipitate on the oxide support. It has been widely used for preparing oxide-supported gold catalysts having small gold particle sizes; **Table 2.2** summarises what has been found with TiO_2 support. A typical preparation method is as follows. After adding the support to an aqueous solution of $HAuCl_4$, the pH of the suspension is raised to a fixed value, usually 7 or 8, by adding sodium hydroxide or carbonate, after which it is heated at 343 or 355 K with stirring for 1 h. After thorough washing with water usually at 323 K to remove as much of the sodium and chlorine as possible, the product is dried under vacuum at 373 K, and often calcined in air at higher temperature.

This basic method has numerous variations, such as pH, temperatures of preparation and washing, for instance at room temperature instead of higher temperature, and use of other bases, such as ammonia. Some of the parameters have been systematically investigated in a study using an automated dispenser and various supports. No variation in the results was found whether sodium hydroxide or carbonate or ammonia was used as base. Changes in the ageing period from 2 to 12 h or in temperature (298 and 343 K) did not have any influence either, but there were problems of reproducibility in the preparations that were not found in another study. Whether sodium carbonate was added to the gold solution before or after addition of titania did not produce significant in the results.

Three kinds of processes appear to occur as the pH is raised (Scheme 1): (i) displacement of Cl^- from a complex anion by water, giving a neutral species (steps 1 and 3); (ii) loss of a proton from a neutral hydrated ion (steps 2 and 4); and (iii) hydrolysis by replacement of Cl^- by OH^- (steps 5 and 6) [49]. The equilibrium constants measured by Nechayev and Nikolenko [49] was used as a basis for discussion; they lead to the results shown in Figure 2.2. The neutral $AuCl_3.H_2O$ is major species at about pH 3-4, and at pH 7, which is most often selected in the DP method of catalyst preparation, $AuCl(OH)_3^-$ is probably prevalent. At pH 10 and above, the $Au(OH)_4^-$ anion is the dominant species.

$$[AuCl_4]^- + H_2O \Leftrightarrow AuCl_3(H_2O) + Cl^- \quad (1)$$

$$AuCl_3(H_2O) \Leftrightarrow [AuCl_3(OH)]^- + H^+ \quad (2)$$

$$[AuCl_3(OH)]^- + H_2O \Leftrightarrow AuCl_2(H_2O)(OH) + H^+ + Cl^- \quad (3)$$

$$AuCl_2(H_2O)(OH) \Leftrightarrow [AuCl_2(OH)_2]^- + H^+ \quad (4)$$

$$[AuCl_2(OH)_2]^- + H_2O \Leftrightarrow [AuCl(OH)_3]^- + H^+ + Cl^- \quad (5)$$

$$[AuCl(OH)_3]^- + H_2O \Leftrightarrow [Au(OH)_4]^- + H^+ + Cl^- \quad (6)$$

Scheme 1. Progress of the hydrolysis of the $AuCl_4^-$ ion as the pH is raised.

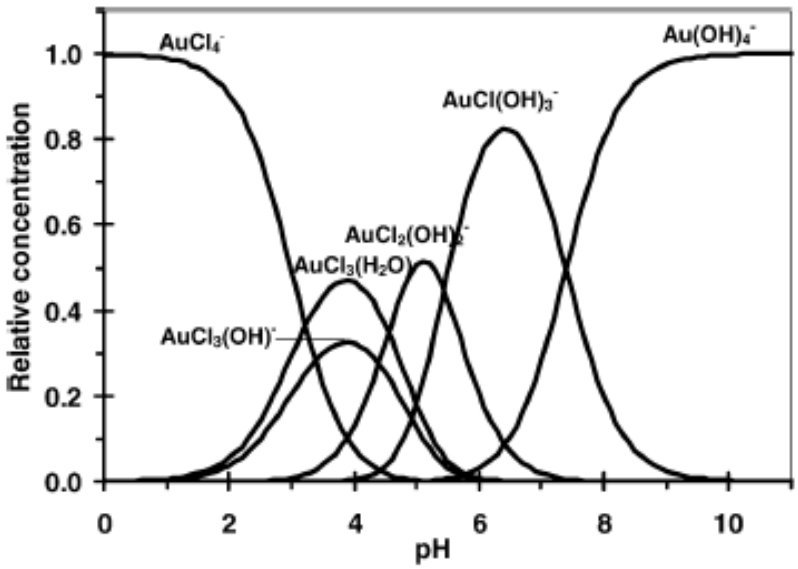

Figure 2.2 Relative equilibrium concentration of gold complexes ($[Cl]^-$ = 2.5×10^{-3} M) as a function of the pH of the solution, calculated with equilibrium constants reported by Nechayev et al.

Table 2.2 Characteristics of Au/TiO_2 catalysts prepared by DP

pH	Au (wt.%)	$T_{calc.}$ (^{o}C)	$T_{red.}$(^{o}C)	d_{Au} (nm)	References
4-12.5	0.08-1	-	-	2-20	[50]
5	2.6-4.8	400	-	2.9-6.1	[51]
5	3.3	400	-	3.2	[52]
6	1.7-3.4	-	-	≥5	[53]
7	2.8-7.5	-	120-500	1.3-8.7	[42]
7	8	25-400	-	1.1-3.5	[54]
7	2	-	-	3.1	[55]
8	1-10	25-500	-	4.5-6.2	[56]
8.1	1.5-5	300	200	2-5, >8	[44]
9	0.06-1.9	-	-	~3	[57]
10	1.8	-	-	3.5	[20]
-	1.5	-	-	3.7 ± 1.5	[40]
-	0.96	-	-	3.4	[58]
-	2.1	400	150	3.3	[59]
-	3	400	-	3.6	[60]

Au/TiO_2 has been prepared by depositing colloidal gold in di-isopropylether onto titania; calcinations at 573 K removed all the organics [61]. Gold particles (~5nm) made in this way were found to sinter much more easily than those made by DP. Gold particles ~2 nm in size made by reducing $HAuCl_4$ with a basic solution of

THPC, (tetrakis (hydroxymethyl) phosphonium chloride) have been deposited on titania and zirconia at pH 2, which is below their PZC: part of the adsorbed ligands were destroyed on exposure to air; calcinations at 673 K removed all the carbon, and gave particles 4-6 nm in size [62, 63].

The effect of preparation method (deposition-precipitation versus sol immobilization method) and reduction method (calcination versus chemical reduction) on Au/TiO_2 catalysts for the liquid phase oxidation of glycerol were studied by N. Dimitratos et al [64]. It was revealed that a different tend existed in terms of activity and distribution of products. The catalytic activity was depended not only on the choice of the reduction method but also on the use of protective agent (PVA, THPC) for the stabilization of the gold colloids. The highest activity was found when a low temperature chemical reduction was employed on the Au/TiO_2 catalyst synthesized by the deposition-precipitation method. Moreover, the use of higher pre-treatment temperature or of a protective agent resulted in a lower activity but could be used to direct selectivity in oxidation reaction.

2.5 Titanium (IV) oxide

Titanium (IV) oxide occurs naturally in three crystalline forms :

1. Rutile, which tend to more stable at high temperatures. The application of almost rutile type is used in industrial products such as paints, cosmetics foodstuffs and sometime found in igneous rocks.

2. Anatase, which tends to be more stable at lower temperatures. This type generally shows a higher photoactivity than the other types of titanium dioxide.

3. Brookite, which is usually found only in minerals and has a structure belonging to orthorhombic crystal system.

A summary of the crystallographic properties of three varieties is given in **Table 2.3**. Both of rutile and anatase type have a structure belonging to tetragonal crystal system but they are not isomorphous (**Figure 2.3**). The two tetragonal crystal types are more common because they are easy to make. Anatase occurs usually in near-regular octahedral, and rutile forms slender prismatic crystal, which are frequently twinned. Rutile is the thermally stable form and is one of two most important ores of titanium.

The three allotropic forms of titanium dioxide have been prepared artificially but only rutile, the thermally stable form, has been obtained in the form of transparent large single crystal. The transformation from anatase to rutile is accompanied by the evolution of ca. 12.6 kJ/mol (3.01 kcal/mol), but the rate of

transformation is greatly affected by temperature and by the presence of other substance which may either catalyze of inhibit the reaction. The lowest temperature at which conversion of anatase to rutile takes place at a measurable rate is ca. 700˚C, but this is not a transition temperature. The change is not reversible; ΔG for the change from anatase to rutile is always negative.

Table 2.3 Crystallographic properties of anatase, brookite, and rutile

Properties	Anatase	Brookite	Rutile
Crystal structure	Tetragonal	Orthorhombic	Tetragonal
Optical	Uniaxial, negative	Biaxial, positive	Uniaxial, negative
Density, g/cm^3	3.9	4.0	4.23
Harness, Mohs scale	$5^1/_2 - 6$	$5^1/_2 - 6$	$7 - 7^1/_2$
Unit cell	$D_4a^{19}.4TiO_2$	$D_2h^{15}.8TiO_2$	$D_4h^{12}.3TiO_2$
Dimension, nm			
a	0.3758	0.9166	0.4584
b		0.5436	
c	0.9514	0.5135	2.953

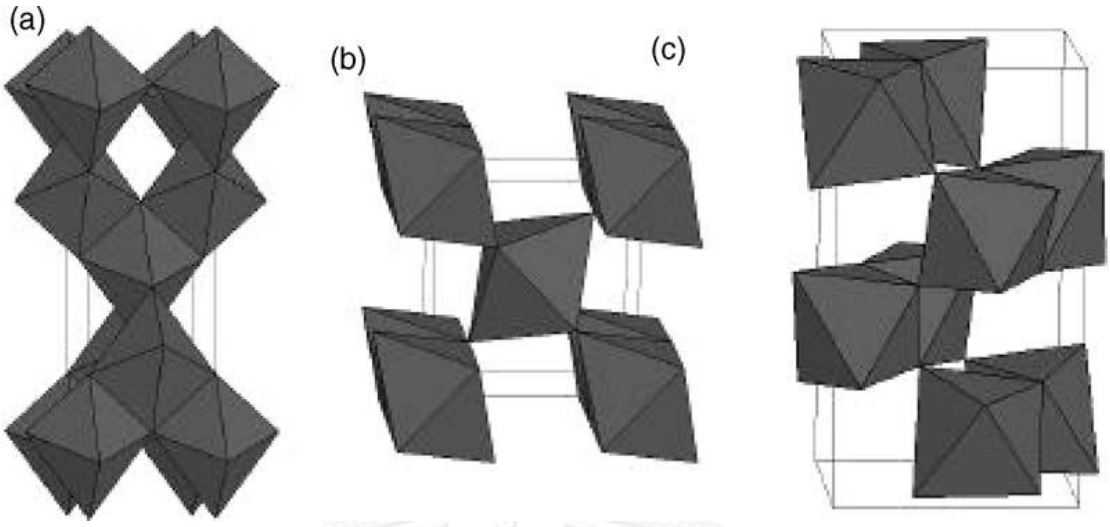

Figure 2.3 Crystal structures of anatase (a), rutile (b), and brookite (c) TiO_2

Brookite has been produced by heating amorphous titanium (IV) oxide, prepared from alkyl titanates of sodium titanate with sodium or potassium hydroxide in an autoclave at 200 to 600 $^{\circ}C$ for several days. The important commercial forms of titanium (IV) oxide are anatase and rutile, and these can readily be distinguished by X-ray diffraction spectrometry.

Since both anatase and rutile are tetragonal, they are both anisotropic, and their physical properties, e.g. refractive index, vary according to the direction relative to the crystal axes. In most applications of these substances, the distinction between crystallographic directions is lost because of the random orientation of large numbers of small particles, and it is mean value of the property that is significant.

Measurement of physical properties, in which the crystallographic directions are taken into account, may be made of both natural and synthetic rutile, natural

anatase crystals, and natural brookite crystals. Measurements of the refractive index of titanium dioxide must be made by using a crystal that is suitably orientated with respect to the crystallographic axis as a prism in a spectrometer. Crystals of suitable size of all three modifications occur naturally and have been studied. However, rutile is the only form that can be obtained in large artificial crystals from melts. The refractive index of rutile is 2.75. The dielectric constant of rutile varies with direction in the crystal and with any variation from the stoichiometric formula, TiO_2; an average value for rutile in powder from is 114. The dielectric constant of anatase powder is 48.

Titanium dioxide is thermally stable (mp 1855˚C) and very resistant to chemical attack. When it is heated strongly under vacuum, there is a slight loss of oxygen corresponding to a change in composition to $TiO_{1.97}$. The product is dark blue but reverts to the original white color when it is heated in air.

2.6 Solvothermal Method

Solvothermal method has been developed for sysnthesis of metal oxide and binary metal oxide with large surface area, high crystallinity and high thermal stability by using solvent as the reaction medium. The solvothermal method is similar to the hydrothermal method except that organic solvents are used instead of water. This method can effectively prevent the products from oxidizing. The solvothermal treatment could be used to control grain size, particle morphology, crystalline phase and surface chemistry by regulating sol composition, reaction temperature, pressure, nature of solvent, additives, and aging time. In particular, the particles prepared by solvothermal method were reported to be larger surface area, smaller particle size, and more stable than those obtained by other methods such as the sol-gel method.

Titanium precursor such as titanium alkoxide, was used as starting material for titania synthesis. It was first suspended in organic solvent in a test tube of autoclave. The crystalline titania was formed at temperature in the range of 200-340 $^{\circ}$C in an autoclave. Autogeneous pressure during the reaction gradually increased as the temperature was raised. It has been reported that physiochemical properties of the synthesized titania depend on the reaction conditions as well as the calcinations temperature. The mechanism of Titanium (IV) tert-butoxide and 1,4-butanediol is shown in **Figure 2.4**.

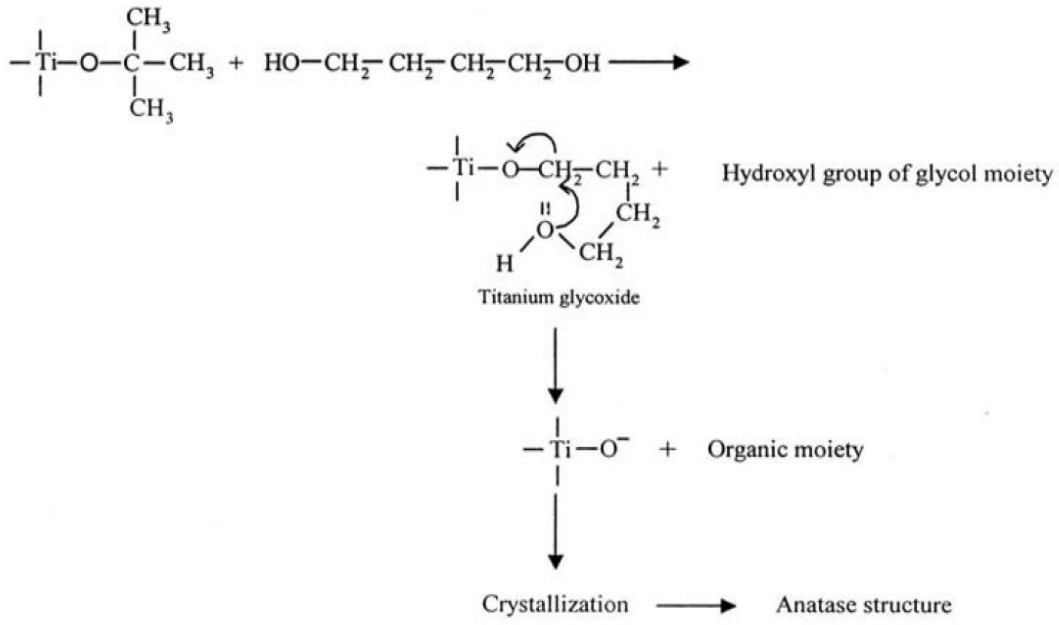

Figure 2.4 Mechanism of solvothermal reaction for the anatase TiO_2 formation

M. Kang et al. [65] synthesized TiO_2 by using the sol-gel and solvothermal method in order to study renders a reliable synthesis procedure of the TiO_2 photocatalyst having the antase structure of nano size. The TiO_2 powder obtained by the solvothermal method at 300°C exhibited a pure anatse structure without any further treatment, while the TiO_2 powder prepared by the sol-gel method was transformed to the anatase structure after thermal treatment at 500°C for 3 h. The TiO_2 powder obtained by the solvothermal method had higher surface area (121 m^2/g) and surface charge (+24.1 mV) than the TiO_2 powder prepared by the sol-gel method (51 m^2/g, +16.4 mV).

C.S. Kim et al. [53] synthesized TiO_2 nanoparticles in toluene solutions with titanium isopropoxide (TIP) as precursor by solvothermal synthetic method. After synthesis at 250 °C for 3 hours with solutions at the weight ratios 10/100, 20/100 and

30/100 nanocrystalline TiO_2 particles are formed and they have a uniform anatase structure with average particle size below 20 nm. Average size of the nanocrystalline particle increases as increasing the amount of TIP precursor in this composition range. For the products obtained from the solution of 5/100 and 40/100, crystalline particles cannot be obtained. The 5/100 of TIP in the mixture might be too small amount to synthesize TiO_2 nanoparticles at 250 ^{o}C and longer time is also needed to obtain adequate size of the particle. In the mixture of 40/100 TIP, the synthetic process of TiO_2 particles may be hindered by agglomeration of the reactants due to surplus of precursor.

W. Payakgul [66] synthesized the titania using thermal decomposition of titatium (V) n-butoxide (TNB) in organic solvents. It is suggested that anatase titania synthesized in 1,4-butanediol is the result from direct crystallization while titania synthesized in toluene is transformed from precipitated amorphous intermediate. Thermal stability of products investigated by calcinations at various temperatures and photocatalytic activity evaluated from ethylene decomposition reaction suggest that amount of defect structures in titania synthesized depends upon the solvent used.

CHAPTER III
EXPERIMENTAL

This chapter describes the experimental procedure used in this research which can be divided into three sections. The details of catalyst preparation are shown in section 3.1. The reaction studies in 1-heptyne and 1-heptene hydrogenation are explained in section 3.2. Finally, the properties of catalyst characterized by various techniques are described in section 3.3.

3.1 Catalyst Preparation

The TiO_2 supports used in this research were an anatase TiO_2. The micron-sized TiO_2 was commercially obtained from Aldrich. The nano-sized TiO_2 was synthesized by the solvothermal method.

3.1.1 Synthesis of TiO_2 Supports via the Solvothermal Method

The chemicals that used to synthesize nano-sized TiO_2 are shown in **Table 3.1**. The TiO_2 support used in this work was synthesized by the solvothemal method as described in Ref. [34] using titanium (IV) tert-butoxide (97%TNB) and 1,4-butanediol (Aldrich) as titanium precursor and solvent. Firstly, 25 g of TNB was suspended in 100 ml of 1,4-butanediol in an inner test tube. The gap between an inner and an outer test tube, 30 ml of 1,4-butanediol is added. After the autoclave was completely purged with nitrogen, it was heated to 300°C at the rate of 2.5°C/min

and held at this temperature for 30 minute (TiO_2_9 nm) and 6 hour (TiO_2_15 nm). After the reaction, the autoclave was cooled down to room temperature. The resulting powder that collected from the test tube was centrifuged in methanol five times and then dried in air at room temperature overnight. The final product obtained was TiO_2 powder. The scheme of apparatus is shown in **Figure 3.1**.

Table 3.1 Chemicals used for synthesis TiO_2

Chemical	Supplier
Titanium (IV) tert-butoxide (97%TNB, $Ti[O(CH_2)_3CH_3]_4$)	Aldrich
1,4-butanediol (1,4-BG, $HO(CH_2)_4OH$)	Aldrich
Methyl alcohol	Aldrich

Table 3.2 The condition used for synthesis TiO_2

Samples	TNB (g)	1,4 Butanediol (ml)	Temperature (^{o}C)	Holding Time (hr)
TiO_2_9	25	100	300	0.5
TiO_2_15	25	100	300	6

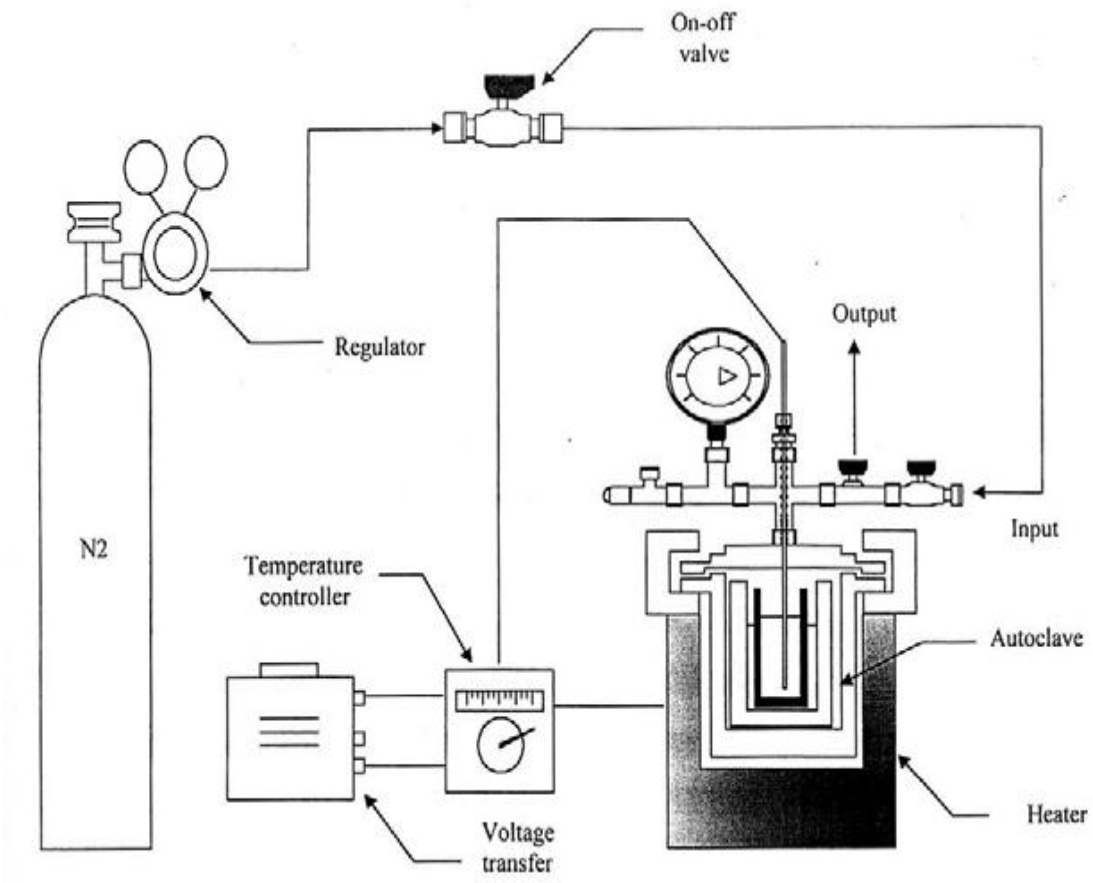

Figure 3.1 The schematic drawing of equipment used for the preparation of TiO_2

3.1.2 Palladium Loading

In this experiment, the palladium was deposited onto the support by incipient wetness impregnation. $PdCl_2$ was used as palladium precursor. The incipient wetness impregnation procedure was follow:

1. $PdCl_2$ was dissolved in hydrochloric acid 0.1 mol/l and heat at 60°C until all the $PdCl_2$ was dissolved.

2. TiO_2 support was impregnated with the $PdCl_2$ solution by incipient wetness technique. The solution of $PdCl_2$ was slowly dropped onto the TiO_2 support.

3. The impregnated support was left at room temperature for 6 hour to assure adequate distribution of metal complex. After that the catalyst was dried in the oven at 110°C for 12 hour.

4. The catalyst was calcined in air at 500°C for 2 hour.

3.1.3 Gold Loading

Gold catalyst was prepared by deposition-precipitation method according to Ref. [42]. Firstly, $HAuCl_4.3H_2O$ which was used as the gold precursor was dissolved in 100 ml of deionized water. The pH was adjusted to 7 by using 0.1 M of NaOH. After 2.0 g of TiO_2 was dispersed in the solution, the pH was readjusted to 7 with NaOH again. The suspension is vigorously stirred for 2 h at 80°C. After 2 h, the suspension is cooled and centrifuged five times with deionized water in order to remove chloride, and then dried at 110°C for 6 h.

Table 3.3 Loading sequence in the catalyst preparation

catalyst	first step	second step
Pd/TiO_2_9	IM Pd	-
2%Pd/TiO_2_9	IM Pd (2 wt%)	
Au/Pd/TiO_2_9	IM Pd	DP Au
Au/2%Pd/TiO_2_9	IM Pd (2 wt%)	DP Au
Pd/TiO_2_15	IM Pd	-
Au/Pd/TiO_2_15	IM Pd	DP Au
Au/TiO_2_100	DP Au	-
Pd/TiO_2_100	IM Pd	-
Pd/Au/TiO_2_100	DP Au	IM Pd
Au/Pd/TiO_2_100	IM Pd	DP Au
DP_IM_Pd/TiO_2_100	IM Pd	DP w/o Au

DP : Deposition-precipitation

IM : Incipient wetness impregnation

The loading of Pd and Au was 0.5wt.% and 1.0wt.%, respectively for all samples.

3.2 Reaction Study

In order to study the characteristic and catalytic properties of these systhesis catalyst, the liquid-phase hydrogenation was required. 1-Heptyne was used as a reactant under an organic solvent as reaction medium.

3.2.1 Chemicals and Reagents

The chemicals and reagents used in the reaction study in the liquid phase hydrogenation are shown in **Table 3.4**

Table 3.4 The chemicals and reagents are used in the reaction

Chemicals and Reagents	Supplier
High purity grade hydrogen (99.99vol.%)	Thai Industrial Gases Limited
1-heptyne	Aldrich
1-heptene	TRADE TCI MARK
1-heptane	Wako
toluene	Fluka

3.2.2 Instruments and Apparatus

The schematic diagram of liquid phase hydrogenation is shown in **Figure 3.2**. The main instruments and apparatus in the reaction study are explained as follow:

- The autoclave reactor

The 100 ml teflon-lined stainless steel autoclave was used as a reactor. Hot plate stirrer with magnetic bar was used to heat up the reactant and to ensure that well mix between the reactant and catalyst.

- Gas Chromatography (GC)

A Gas chromatography equipped with flame ionization detector (FID) with GS-alumina capillary column was used to analyze the feed and product. The operating condition for GC is shown in **Table 3.5**.

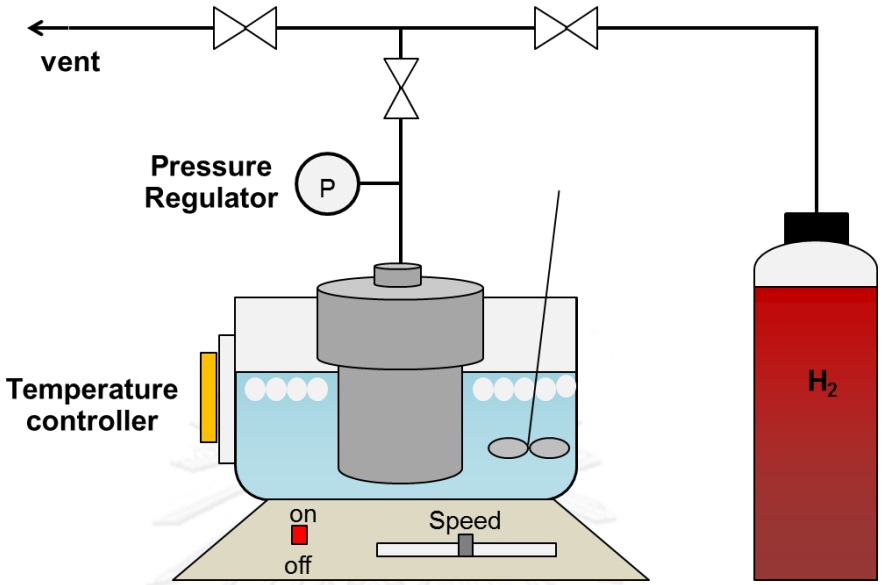

Figure 3.2 The schematic diagram of liquid-phase hydrogenation

Figure 3.3 Teflon-lined stainless steel autoclave reactor of liquid-phase hydrogenation

Table 3.5 The operating condition for GC

Gas Chromatography	Shimadzu GC-14A
Detector	FID
Packed column	GS-alumina (length=30m, I.D.=0.53mm)
Carrier gas	Helium (99.99 vol.%)
Make-up gas	Nitrogen (99.99 vol.%)
Column temperature	200°C
Injector temperature	250°C
Detector temperature	280°C

3.2.3 Liquid-Phase Hydrogenation of 1-Heptyne

Prior to the reaction testing, the catalyst sample was reduced by hydrogen gas at a flow rate of 50cm^3/min at 40°C for 2 h. Then, 0.01 g of the sample was dispersed in 10 cm^3 of toluene containing 2 vol.% 1-heptyne. The effect of mass transfer on the reaction rate was negligible by using a high stirring rate (1000 rpm). The reaction was carried out under flowing hydrogen at 2 bars and 30°C for 10-120 minute. The liquid reactants and products were analyzed by a gas chromatograph equipped with an FID detector.

3.2.4 Liquid-Phase Hydrogenation of 1-Heptene

Prior to the reaction testing, the catalyst sample was reduced by hydrogen gas at a flow rate of 50cm^3/min at 40°C for 2 h. Then, 0.01 g of the sample was dispersed in 10 cm^3 of toluene containing 2 vol.% 1-heptene. The effect of mass transfer on the reaction rate was negligible by using a high stirring rate (1000 rpm). The reaction was carried out under flowing hydrogen at 2 bars and 30°C for 10-120 min. The liquid reactants and products were analyzed by a gas chromatograph equipped with an FID detector.

3.3 Catalyst Characterization

The catalyst was characterized by several techniques such as

3.3.1 X-ray Diffraction (XRD)

The bulk crystal structure and X-ray diffraction (XRD) patterns of all catalysts were determined by the SIEMENS D5000 X-ray diffractometer connected with a computer with Diffract ZT version 3.3 programs for fully control of the XRD analyzer. The experiment was carried out by using CuKα radiation with Ni filter in the 2θ range of 20 to 80 degrees resolution 0.04°. The crystallite size was estimated from line broadening according to the Scherrer's equation.

3.3.2 N_2 Physisorption

The specific surface area of samples were measured through nitrogen gas adsorption at liquid nitrogen temperature (-196°C) using Micromeritics ChemiSorb 2750 Pulse chemisorption System instrument. Before the experiment, the sample was thermally treated at 150°C for 1 h.

3.3.3 Transmission Electron Microscopy (TEM)

The morphology and crystallite size of all catalysts were observed by using JEOL-JEM 200CX transmission electron microscope operated at 100 kV at National

Metal and Materials Technology Center. The average crystallite size was measured by SemAfore program version 5.00.

3.3.4 X-ray Photoelectron Spectroscopy (XPS)

The XPS spectra, the blinding energy and the composition on the surface layer of the catalysts were determined by using an AMICUS photoelectron spectrometer equipped with an Mg K_α X-ray as a primary excitation and KRATOS VISION2 software. XPS elemental spectra were acquired with 0.1 eV energy step at a pass energy of 75 eV. All the binding energies were referenced to the C 1s peak at 285.0 eV of the surface adventitious carbon.

3.3.5 Diffuse Reflectance UV/Vis Spectra

The UV-Vis diffuse reflectance spectra (DSR) were recorded using a Shimadzu UV-3100PC spectrophotometer from 200 to 800 nm.

3.3.6 CO-pulse Chemisorption

The relative percentages of palladium dispersion were determined by CO pulse chemisorption at 40°C using a BEL-METAL-1 system. Approximately 0.1 g of catalyst was reduced under hydrogen flow at 40°C for 2 h, and then helium was purged. The CO was pulsed over the reduced catalyst until the TCD signal from the pulse was constant.

3.3.7 Diffuse Reflectance FTIR (DRIFT) Spectra of CO

The CO adsorbed species on the catalysts were measured using FTIR-620 spectrometer (JASCO) with a MCT detector at a wavenumber resolution of 2 cm^{-1}. He gas was introduced into the sample cell in order to remove the remaining air. The system was switched to hydrogen and heated to 150 °C. The temperature was kept constant for 30 min and then cooled down to the room temperature with He gas. After that, carbon monoxide was flow to the system for 15 min. The IR spectrum of CO adsorbed onto the catalyst was recorded in the 600–4000 cm^{-1} range after the gaseous CO had been purged with flowing He.

CHAPTER IV
RESULTS AND DISCUSSION

4.1 Effect of consequently between Pd and Au on the catalytic behavior of Au-Pd/TiO_2 catalysts in the liquid-phase selective hydrogenation of 1-heptyne

4.1.1Characterization of the catalysts

4.1.1.1 X-Ray Diffraction (XRD)

The XRD patterns of the TiO_2 supports and TiO_2 supported Au–Pd catalysts were carried out at the diffraction angle (2θ) between 20° and 80°, the results are shown in **Figure 4.1**. All the samples showed the characteristic peaks of pure anatase phase titania at 2θ degrees = 25° (major), 37°, 48°, 55°, 56°, 62°, 71°, and 75° without contamination of the other phases such as rutile and brookite [67]. The XRD characteristic peaks corresponding to palladium and gold species were not detected for the Au/TiO_2_100, Pd/TiO_2_100, and Au/Pd/TiO_2_100 because of the low amount of metals present and, probably, the very high intensity of the TiO_2 peaks (due to the large TiO_2 crystallite size 100 nm) compared to the crystallite size of the metals. For the Pd/Au/TiO_2_100, additional peaks at 2θ = 38° and 44° were observed and were indexed to cubic gold metal. The appearance of these Au metallic peaks in the XRD pattern indicated that the Au particles were fairly large in this sample (comparable to the TiO_2).

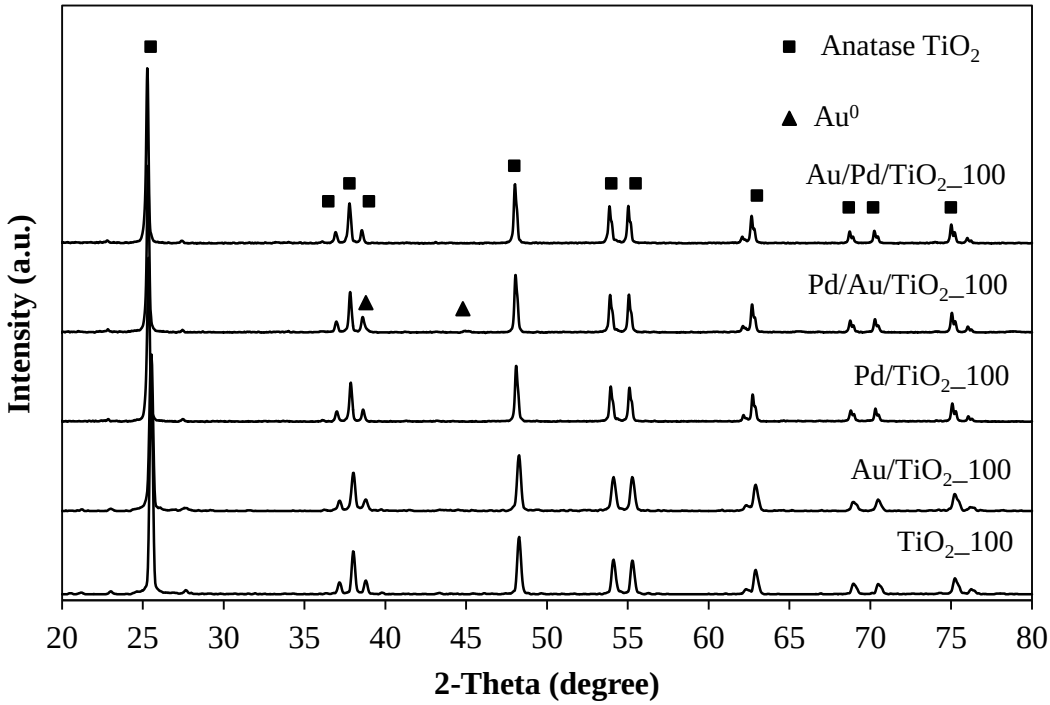

Figure 4.1 XRD patterns of TiO_2_100, Au/TiO_2_100, Pd/TiO_2_100, Pd/Au/TiO_2_100, and Au/Pd/TiO_2_100 catalysts

4.1.1.2 Transmission Electron Microscopy (TEM)

TEM analysis has been carried out in order to physically measure the metal particle sizes and the results are shown in **Figure 4.2-4.6**. The TiO_2 support had a uniform particle size of 0.1–0.2 μm. The metal dispersion of the catalysts can be seen from the TEM images. The average particle sizes of the Au/TiO_2_100 and Pd/TiO_2_100 catalysts were 10.3 and 6.9 nm, respectively. The particle size of Au was larger than expected because it was previously reported that 2–3 nm Au nanoparticles were formed on the P25-TiO_2 by a similar method as used in this work [42]. The formation of larger Au particles may be attributed to the lower surface area of the TiO_2 support used in this study (~10 m^2/g). An adequate support seems to be necessary for preparation of well-dispersed monometallic gold nanoparticles with high activity [68]. In general, gold particles prepared by deposition-precipitation are associated with small particle sizes with a uniform particle size distribution [69] and a closed interaction between the gold particles and the support [39]. The smaller size of Pd particles indicates a better dispersion of palladium on this TiO_2 support.

The TEM images of the bimetallic Pd/Au/TiO_2_100 and Au/Pd/TiO_2_100 are shown in **Figure 4.3 and 4.5**, respectively. For the Pd/Au/TiO_2_100 catalyst, in which Au was loaded on the TiO_2 by deposition-precipitation in the first step followed by impregnation of Pd in the second step, large particles being 30–50 nm in size was observed in addition to some 2–8 nm particles. The larger particles can be attributed to Au^0 particles according to the XRD results. However, further characterization by XPS and UV–Vis spectroscopy (discussed hereafter) suggests the coverage of Au

surface by Pd. The formation of Pd–Au alloy particles with relatively large size (i.e., >30 nm) has often been reported for supported Pd–Au catalysts prepared by co-impregnation of $PdCl_2$ and $HAuCl_4$ [70, 71]. In the present study, Au particles on the Au/TiO_2_100 may be unstable during the impregnation of HCl solution containing $PdCl_2$ and hydrolyzed to form $AuCl_4$ or $Au(OH)Cl_3$ gold species. Under acidic pH, these gold species interacted repulsively with the positively charged TiO_2 surface, resulting in the growth of Au precipitated [72, 73]. The subsequent calcination then resulted in the formation of PdO on both large Au aggregates and the TiO_2 support. For the $Au/Pd/TiO_2$_100 catalyst, in which the Au nanoparticles were deposited on the Pd/TiO_2 by deposition-precipitation in the second step after impregnation and calcinations of Pd, higher metal dispersion was seen from the TEM images (**Figure 4.5**). The sample shows a bimodal particle size distribution of average sizes 1.7 and 7.9 nm.

Figure 4.6 shows TEM image and particle size distribution of the calcined Pd/TiO_2 after being treated under the deposition-precipitatoin conditions in the absence of Au precursor (referred to as DP_IM_Pd/TiO_2_100). Compared to the starting Pd/TiO_2_100, the Pd particle size decreased and the particle size distribution became more uniform on the DP_IM_Pd/TiO_2_100.

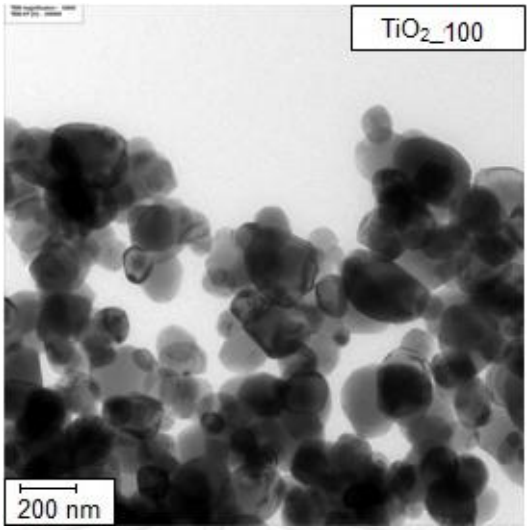

Figure 4.2 TEM image of TiO_2_100 support

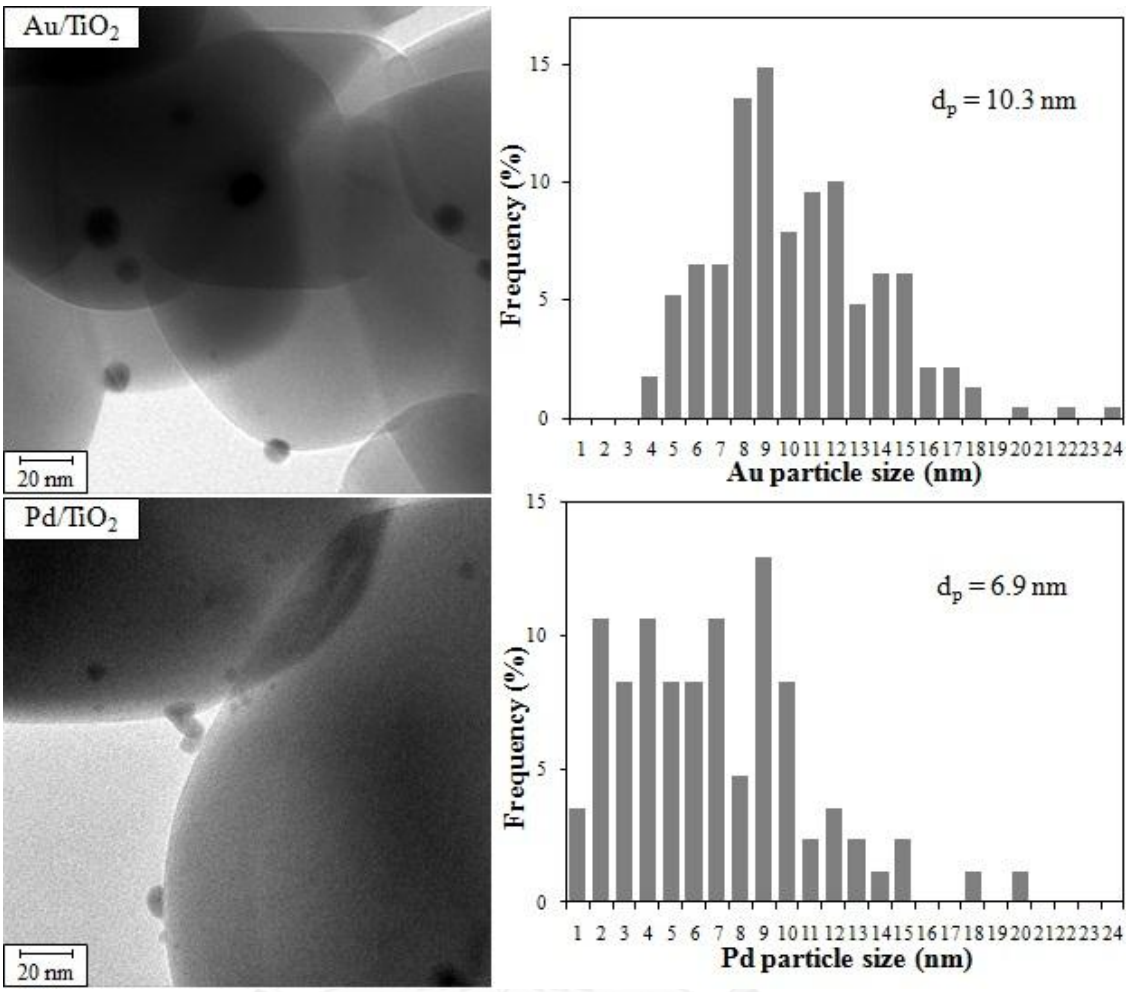

Figure 4.3 TEM images and particle size distribution of TiO_2 supported Au and Pd catalysts

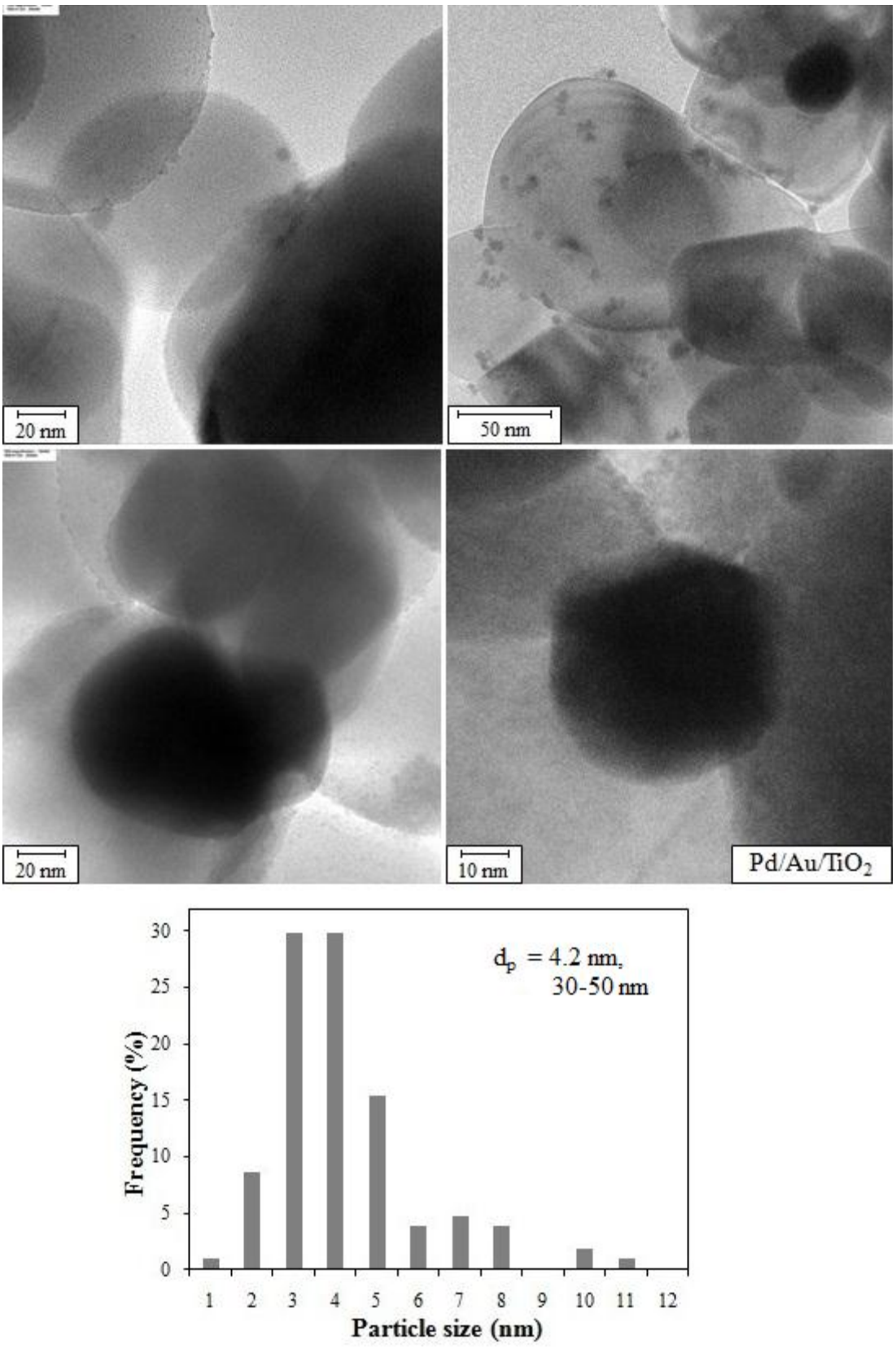

Figure 4.4 TEM images and particle size distribution of Pd/Au/TiO_2_100 catalyst

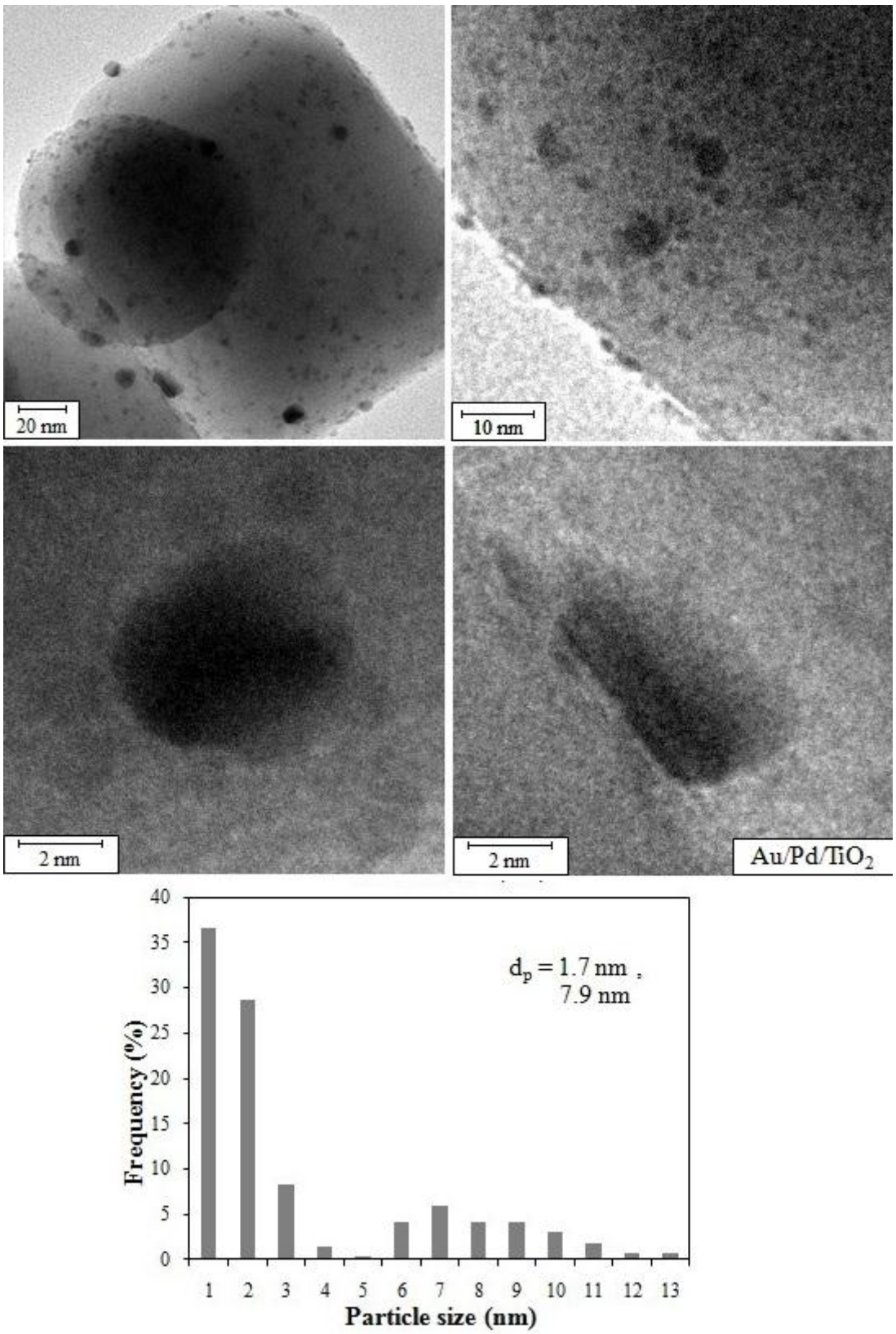

Figure 4.5 TEM images and particle size distribution of Au/Pd/TiO_2_100 catalyst

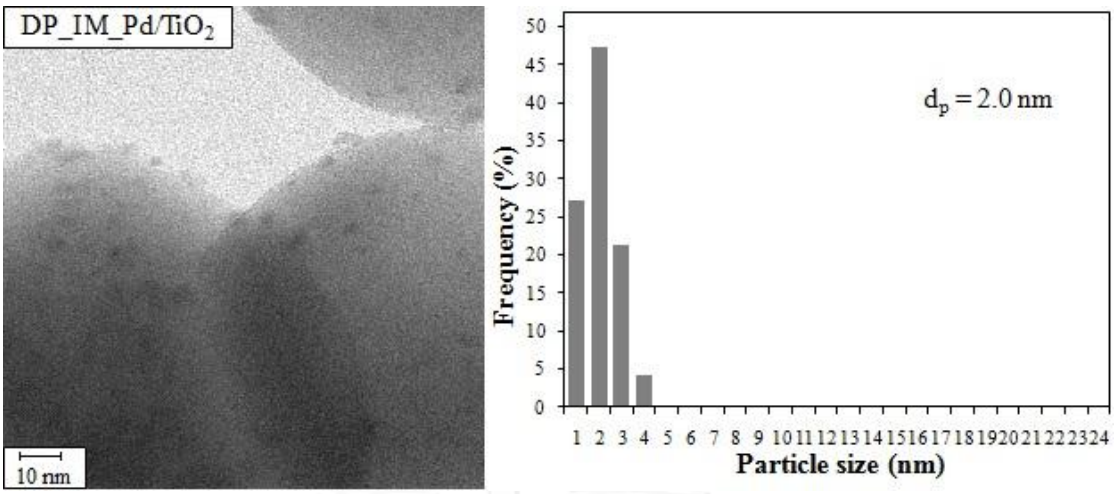

Figure 4.6 TEM images and particle size distribution of DP_IM_Pd/TiO_2_100 catalyst

4.1.1.3 X-ray Photoelectron Spectroscopy (XPS)

Surface compositions of the catalyst were analyzed using a Kratos Amicus X-ray photoelectron spectroscopy. The XPS analysis were carried out with following conditions: Mg Ka X-ray source at current of 20 mA and 12 keV, resolution 0.1 eV/step, and pass energy 75 eV. The operating pressure is approximately $1x10^{-6}$ Pa.

A survey scan was performed in order to determine the elements on the catalyst surface. The elemental scan was carried out in the next step for C 1s, O 1s, Ti 2p, Pd 3d and Au 4f. Binding energies of each element was calibrated internally with carbon C1s at 285.0 eV. Photoemission peak areas are determined by using a linear routine. The deconvolution of complex spectra was done by fitting with Gaussian (70%)-Lorentzian (30%) shapes using VISION2 software equipped with the XPS system.

Prior to the measurements, all the catalysts were reduced ex situ in H_2 flow at 40 ^{o}C for 2 h and kept in a dessicator. The Pd 3d spectra of the catalysts are shown in **Figure 4.7**. For the Pd/TiO_2_100 and Pd/Au/TiO_2_100, the binding energy of Pd $3d_{5/2}$ were detected at 336.5–336.8 eV and were attributed to the presence of palladium in the form of PdO [74]. The binding energy of Pd 3d in the Pd/Au/TiO_2_100 and Pd/TiO_2_100 was essentially similar, suggesting that electronic structure of the surface Pd atoms was not changed in the presence of large Au particles in the case of Pd/Au/TiO_2_100. The presence of PdO on the surface was ascribed to the easy oxidation of Pd upon contact with air at room temperature.

Herzing et al. [70] reported that some surface oxide layer of PdO persisted even after the reduction treatment.

On the other hand, the Pd 3d spectra of the Au/Pd/TiO_2_100 catalyst were fitted by two peaks at higher and lower binding energies of 336.2 eV and 335.2 eV, which were attributed to Pd–Au alloy and metallic Pd^0, respectively[75, 76]. In addition, these Pd particles were highly resistant to oxidation, compared to those of the Pd/TiO_2_100 and Pd/Au/TiO_2_100. Previous studies by Qian and Huang [77] and Yang et al. [19] confirmed that adding Au was helpful to the reduction of Pd^{2+} to metallic Pd, or the protection of Pd^0 from being oxidized into PdO. The atomic percentages of the species at 336.2 eV and 335.2 eV were determined by peak fitting to be 15% and 85%, respectively.

The XPS core level spectra of Au 4f of the various catalysts are shown in **Figure 4.8**. The Au 4f peaks were detected at a range of binding energy (B.E.) of 83.0–83.1 eV for the Au/TiO_2_100 and Au/Pd/TiO_2_100 catalysts, which is typical of metallic gold (B.E. 84.0 ± 0.1) [77]. The Au 4f peaks were not obviously seen for the Pd/Au/TiO_2_100 catalyst. The atomic concentrations of Pd and Au determined by XPS are given in **Table 4.1**. The percentage of Pd on the surface was found to increase in the order: Au/Pd/TiO_2_100 > Pd/Au/TiO_2_100 > Pd/TiO_2_100, whereas that of Au is shown as Au/Pd/TiO_2_100 > Au/TiO_2_100 > Pd/Au/TiO_2_100. The XPS results suggest the coverage of Au surface by Pd for the Pd/Au/TiO_2_100. In contrast, Pd–Au alloy particles with Au rich on the surface may be formed on the Au/Pd/TiO_2_100.

Table 4.1 The binding energies and FWHM of Pd 3d, and Au 4f in sample from XPS results

Sample	Pd $3d_{5/2}$		Au $4f_{7/2}$		Atomic concentration [b]	
	B.E. (eV)	FWHM (eV)	B.E. (eV)	FWHM (eV)	Pd (%)	Au (%)
Au/TiO_2_100	n/a	n/a	83.0	1.176	n/a	0.08
Pd/TiO_2_100	336.5	1.844	n/a	n/a	0.28	n/a
$Pd/Au/TiO_2$_100	336.8	2.794	n.d.	1.352	0.70	n.d.
$Au/Pd/TiO_2$_100	(1) 335.2 (2) 336.2	1.161 1.611	83.1	1.287	(1) 0.91 (2) 0.17	0.67

B.E.; Binding energy, FWHM: Full width at half maximum

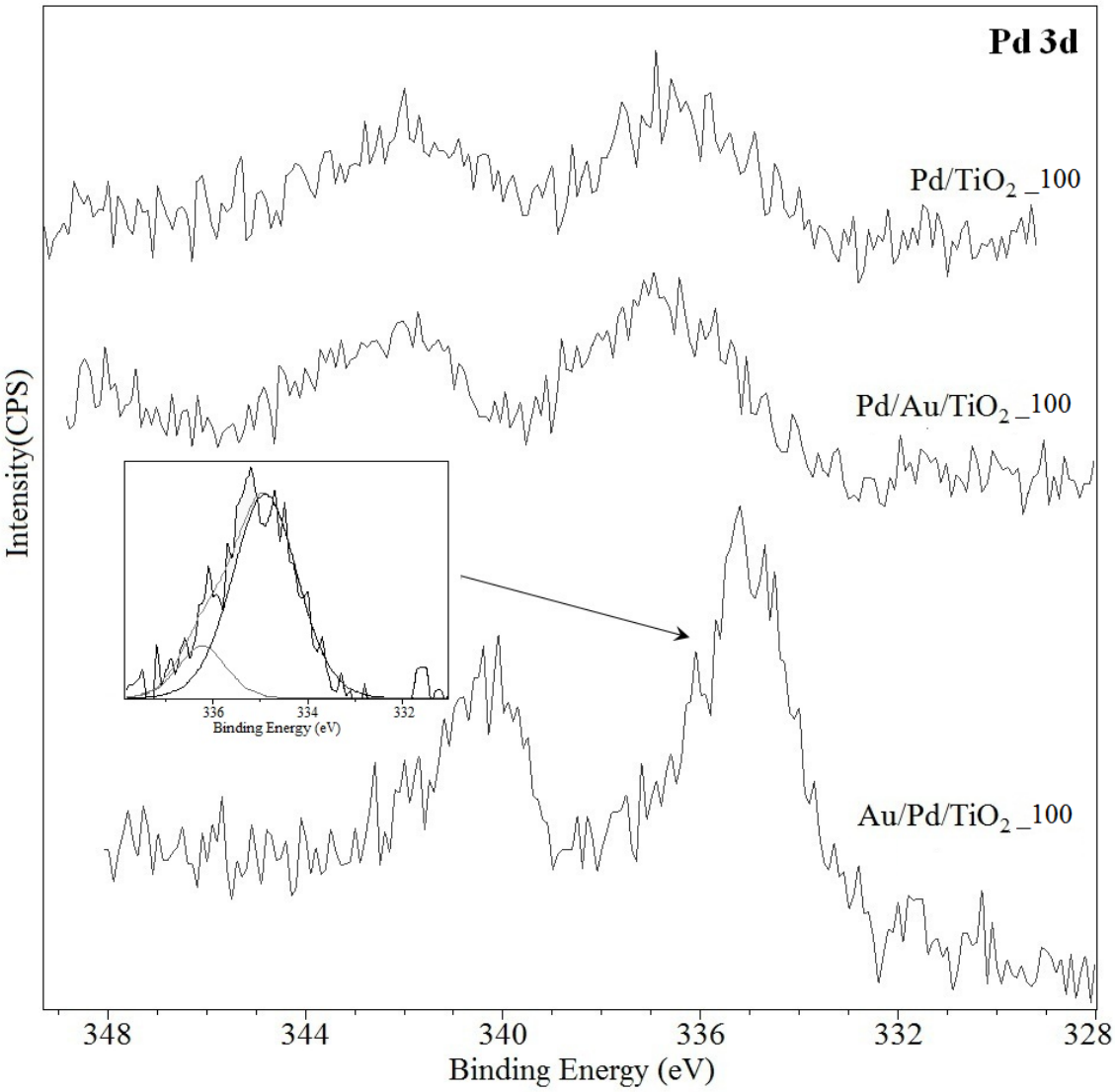

Figure 4.7 XPS Pd 3d core level spectra of Pd/TiO_2_100, $Pd/Au/TiO_2$_100, and $Au/Pd/TiO_2$_100

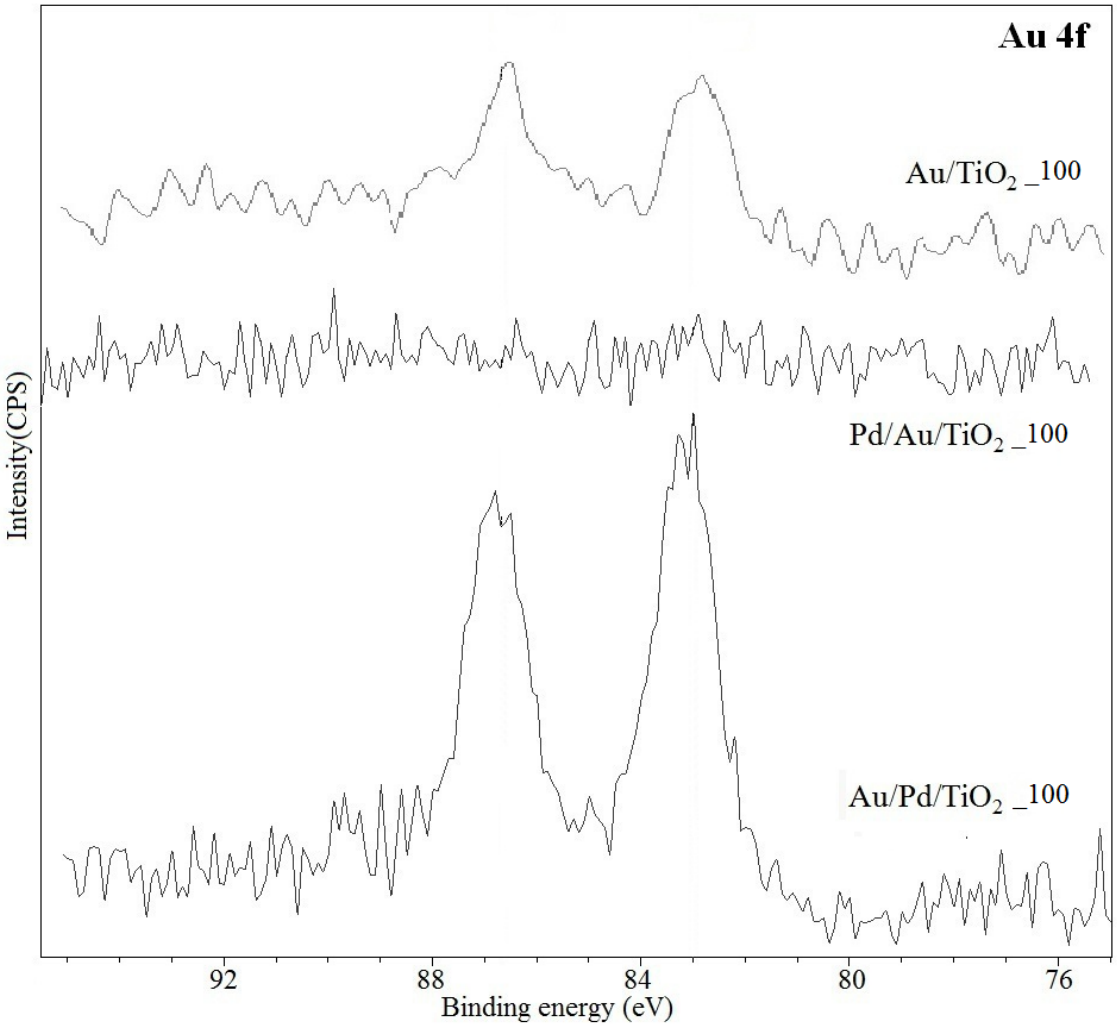

Figure 4.8 XPS Au 4f core level spectra of Au/TiO_2_100, $Pd/Au/TiO_2$_100, and $Au/Pd/TiO_2$_100

4.1.1.4 Metal active sites

The metal active sites measurement is based on chemisorptions technique. Chemisorption is relatively strong, selective adsorption of chemically reactive gases on available metal sites or metal oxide surfaces at relatively higher temperatures (i.e. 25-400^{o}C); the adsorbate-adsorbent interaction involves formation of chemical bonds and heats of chemisorptions in the order of 50-300 kJ mol^{-1}.

Since H_2 chemisorption on Pd bridge bonding may occur so there is no precise ratio of atom to Pd metal surface. H/Pd stiochiometry may be varied from 1, 1/2 or 1/3. However, for CO chemisorption, CO/Pd stiochiometry is normally equal to 1. Exposed active surface areas of Pd of the catalysts were calculated from the irreversible pulse CO chemisorptions technique base on the assumption that one CO molecule adsorbs on one palladium site.

The CO chemisorption results are given in **Table 4.2**. The dispersion of Pd increased in the order: Au/Pd/TiO_2_100 > Pd/TiO_2_100 > Pd/Au/TiO_2_100. The calculated Pd^0 particle size of the Pd/TiO_2_100 was in good agreement with that observed by TEM. For the bimetallic Pd/Au/TiO_2_100 and Au/Pd/TiO_2_100, the calculated Pd^0 particle sizes were larger and smaller than the monometallic Pd/TiO_2_100, respectively. For the Pd/Au/TiO_2_100, the presence of large Au aggregates probably lowers the dispersion of Pd on the TiO_2 due to limited surface area of the support and some PdO species may form on the Au particles. On the contrary, the higher dispersion of Pd on the Au/Pd/TiO_2_100 was ascribed to the

restructuring/redispersion of Pd particles during the deposition-precipitation of Au particles.

Table 4.2 Results from CO chemisorption of all samples

Sample	CO Chemisorption	
	%D	**d_p Pd^0 (nm)**
Au/TiO_2_100	n/a	n/a
Pd/TiO_2_100	13.4	8.4
$Pd/Au/TiO_2$_100	6.8	16.4
$Au/Pd/TiO_2$_100	27.6	4.0

4.1.1.5 UV/Vis spectra

The UV/Vis spectra of the mono and bimetallic catalysts are shown in **Figure 4.9**. The Au/TiO_2_100 exhibited the typical Au plasmon band at 570 nm [56]. The dampening and broadening of the Au plasmon band for the $Au/Pd/TiO_2$_100 corresponded to the Pd–Au alloy formation [20]. The Pd/TiO_2_100 and $Pd/Au/TiO_2$_100 did not show any well-resolved surface plasmon band, which is typical for the monometallic Pd catalysts. The surface of Au particles may be covered by Pd in the $Pd/Au/TiO_2$_100, resulting in the disappearance of Au plasmon

band. The UV–Vis spectra also suggested that most of the Au particles existed in the Pd–Au alloy and that there was no separate formation of pure Au nanoparticles in the bimetallic catalyst systems.

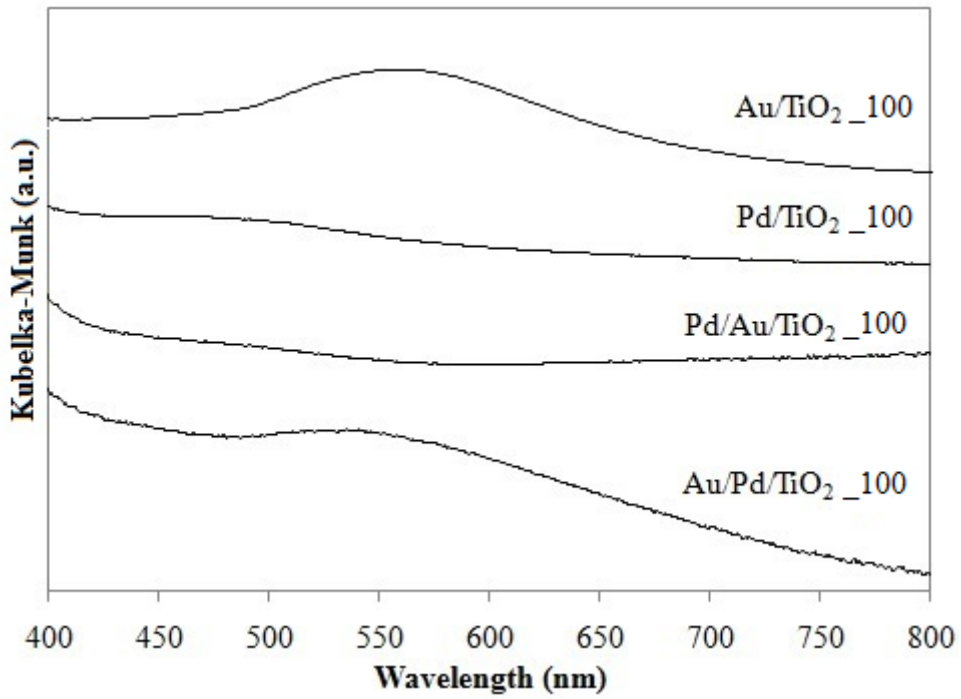

Figure 4.9 UV-vis spectra of Au/TiO_2_100, Pd/TiO_2_100, $Pd/Au/TiO_2$_100, and $Au/Pd/TiO_2$_100

4.1.1.6 Structural features

Figure 4.10 illustrates the morphology of the different catalysts based on the characterization results. The monometallic Pd/TiO_2_100 and Au/TiO_2_100 contained small metal particles with average particle sizes of ca. 6 and 10 nm, respectively. However, these Pd and Au particles were not so stable upon the addition of another metal in the second step. Impregnation of Pd on the Au/TiO_2_100 led to the formation of large Au particles (~30–50 nm). The aggregation of Au occurred during the drying and calcination steps after the incipient impregnation of HCl solution containing $PdCl_2$. The XPS results showed only Pd species in the form of PdO on the surface at similar binding energies to those of the monometallic Pd/TiO_2_100, suggesting no alloying in the Pd/Au/TiO_2_100 catalyst. However, the dispersion of Pd was lower in the presence of large Au aggregates, and some of the Pd particles may be located on the Au surface. Addition of Au by deposition-precipitaton on the Pd/TiO_2 also changed the state of dispersion of Pd species on TiO_2, but in an opposite trend to that of the Pd/Au/TiO_2_100. The dispersion of Pd increased upon the addition of Au and small Au–Pd alloy particles was formed. The XPS results also suggest the modification of the electronic properties of Pd and the formation of the Pd–Au alloy particles. In fact, the redispersion/restructuring of Pd particles occurred during deposition-precipitation even in the absence of Au precursor. In the presence of Au precursor (Au/Pd/TiO_2_100), Au particles may precipitate on these small Pd particles, forming Au–Pd alloys with Au rich on the surface.

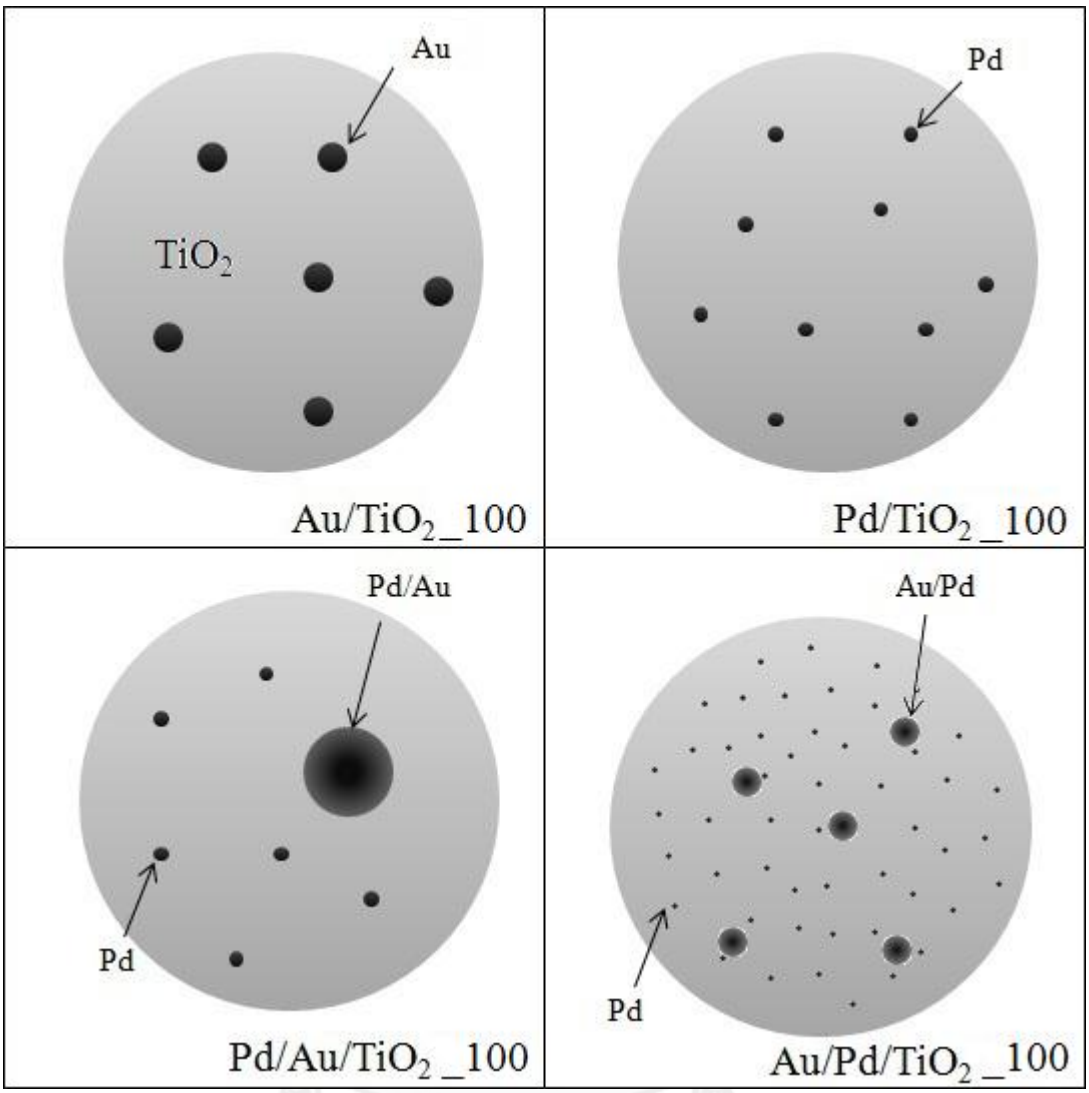

Figure 4.10 A schematic drawing illustrating the catalyst morphology

4.1.2 Catalytic behavior

4.1.2.1 Hydrogenation of 1-heptyne

The liquid-phase hydrogenation of 1-heptyne (98%, Aldrich) was carried out in a magnetically stirred 100-cm^3 Teflon-lined stainless steel autoclave reactor. Prior to the reaction testing, the catalyst sample was reduced by hydrogen gas at a flow rate of 50cm^3/min at 40 $^{\circ}C$ for 2 hour. Then, 0.01 g of the sample was dispersed in 10 cm^3 of toluene containing 2 vol.% 1-heptyne. The effect of mass transfer on the reaction rate was negligible by using a high stirring rate (1000 rpm). The reaction was carried out under flowing hydrogen at 2 bars and 30 $^{\circ}C$ for 10–120 minnute. The liquid reactants and products were analyzed by a gas chromatograph equipped with an FID detector.

The catalytic behavior of the TiO_2-supported Au, Pd, Pd/Au, and Au/Pd catalysts was evaluated in the liquid-phase semihydrogenation of 1-heptyne. The conversion of 1-heptyne and the selectivity to 1-heptene as a function of reaction time are shown in **Figure 4.11**. The hydrogenation rate was in the order: Au/Pd/TiO_2_100 > Pd/TiO_2_100 > Pd/Au/TiO_2_100 >> Au/TiO_2_100. The conversion of 1-heptyne was completed in 30 minute and 60 minute for the Au/Pd/TiO_2_100 and the Pd/Au/TiO_2_100, respectively, under the conditions used. The hydrogenation activity was in accordance with the exposed Pd surface as determined by the CO chemisorption. The very low catalytic activity of the Au/TiO_2_100 corresponded to the relatively large Au particles being formed. The size of Au particles that was

reported to be highly active in hydrogenation reactions usually falls in the range of 2–4 nm [42]. The Au particle size effect, however, varied largely depending on the nature of the substrate molecules. For examples, the reaction with Au/TiO_2 is structure sensitive in the hydrogenation of crotonaldehyde, in which the specific activity of small Au particles (ca. 2 nm) is larger by almost an order of magnitude compared to that of larger Au particles (5–9 nm) [42], whereas it exhibited a structure insensitive characteristic in the 1,3-butadiene hydrogenation [58].

Comparison of the specific activity of supported Au and Pd catalysts in the liquid-phase alkyne hydrogenation has been scarcely reported. Parvulescu et al. [78] reported the catalytic properties of SiO_2-embedded Pd, Au, and Pd–Au alloy colloids with particle sizes in the range of 3–5 nm in the liquid-phase hydrogenation. For the hydrogenation of styrene, the activity of monometallic Pd surpassed those of Pd–Au and Au (Pd > Pd–Au >> Au), whereas in the hydrogenation of cinnamaldehyde and 3-hexyn-1-ol, the catalyst activity was in the order Pd–Au > Pd >> Au. The poor hydrogenation activity of Au colloids embedded in SiO_2, however, was in line with the results of 1-heptyne hydrogenation over Au/TiO_2_100 in this study.

All the present catalysts exhibited high selectivity of 1-heptene (>95%) up to nearly full conversion of 1-heptyne. It is suggested that heptene products were adsorbed more weakly than 1-heptyne on these catalysts. Hence, once formed, heptene molecules were more easily desorbed than the alkyne molecules [79]. Generally, the selectivity of Pd is based on the triple bond being more strongly adsorbed on the active centers than the corresponding double bond, which is due to

its high electron density and restricted rotation [80, 81]. In the partial hydrogenation of alkyne, a decrease in alkene selectivity usually occurs at close to complete conversion of the alkyne because of the ability of alkene to be re-adsorbed under such conditions [82]. In the liquid-phase hydrogenation of 1-heptyne under mild conditions (reaction temperature 30 $^{\circ}$C and H_2 pressure 1.5 bar), the commercial Lindlar catalysts was reported to exhibit 50–85% selectivity to 1-heptene at 47–90% conversion of 1-heptyne [36, 38, 83]. Improvement in the catalyst performances has been recently reported over the bimetallic W-Pd/c-Al_2O_3 (95% 1-heptene selectivity at 100% heptyne conversion) [81] and the Pd/TiO_2 synthesized by one-step flame spray pyrolysis (90% 1-heptene selectivity at 100% heptyne conversion) [5]. However, the selectivity trend after complete conversion of 1-heptyne was seldom concerned while providing better comparison of the catalyst performances in the alkyne hydrogenation.

During 120 minute reaction time, the selectivity of 1-heptene decreased further after complete conversion of 1-heptyne due to the hydrogenation of 1-heptene to heptane. However, the selectivity of 1-heptene still remained >60% for the Pd/Au/TiO_2_100 and Pd/TiO_2_100 catalysts, whereas it drastically decreased to 0% for the Au/Pd/TiO_2_100. The DP_IM_Pd/TiO_2_100, which was prepared by treating the Pd/TiO_2 under deposition-precipitation conditions without Au precursor, exhibited the Pd-like behavior (similar to Pd/TiO_2_100). It is suggested that in the bimetallic Au–Pd alloy, the Au species should act as an electronic promoter for Pd and greatly promote the second step of hydrogenation of 1-heptene to heptane. The performance plot in terms of selectivity to 1-heptene versus conversion of 1-heptyne is shown in **Figure 4.12**. It shows that 1-heptene hydrogenation occurred only at nearly complete conversion of 1-heptyne over the catalysts.

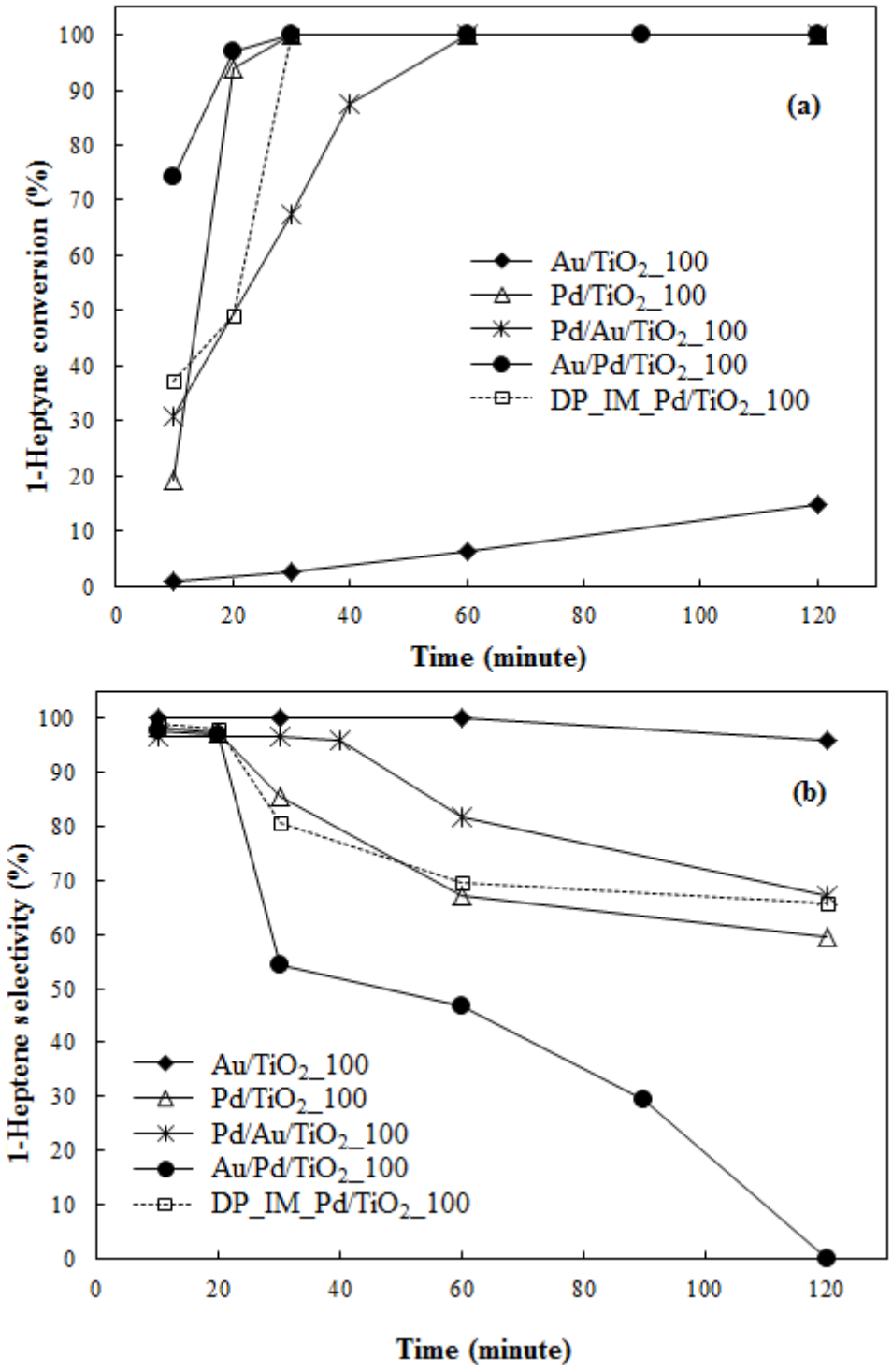

Figure 4.11 Hydrogenation of 1-heptyne on Pd/TiO_2_100, $Pd/Au/TiO_2$_100, and $Au/Pd/TiO_2$_100: %heptyne conversion (a) and %1-heptene selectivity (b)

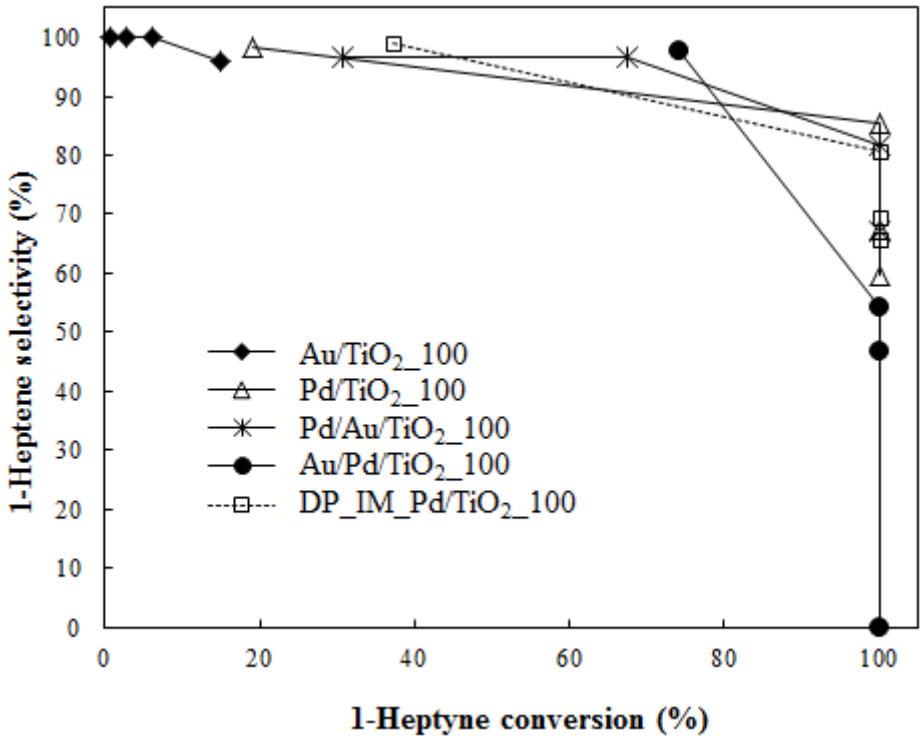

Figure 4.12 The performance plots of 1-heptyne hydrogenation over the various catalysts

4.1.2.2 Hydrogenation of 1-heptene

The hydrogenation of 1-heptene was carried out in the same manner as that of 1-heptyne hydrogenation under similar conditions. The conversion of 1-heptene as a function of reaction time of the Pd/TiO_2_100 and the Pd–Au bimetallic catalysts is shown in **Figure 4.13**. The conversion of 1-heptene at 120 min reaction time was in the order: $Au/Pd/TiO_2$_100 (100%) > Pd/TiO_2_100 (46%) > $Pd/Au/TiO_2$_100 (37%), which was found to be in good agreement with the selectivity of 1-heptene after full conversion of 1-heptyne in 1-heptyne hydrogenation. These results confirm that the hydrogenation of 1-heptene occurred only at nearly or full conversion of 1-heptyne on these catalysts. It has been suggested that the alkyne compound displaces the alkene from the catalyst surface and prevents its readsorption, thereby exerting a poisoning effect for the subsequent alkene hydrogenation, which holds as long as the alkyne species is present [83, 84]. In other words, the adsorption coefficient of 1-heptyne was greater than that of 1-heptene.

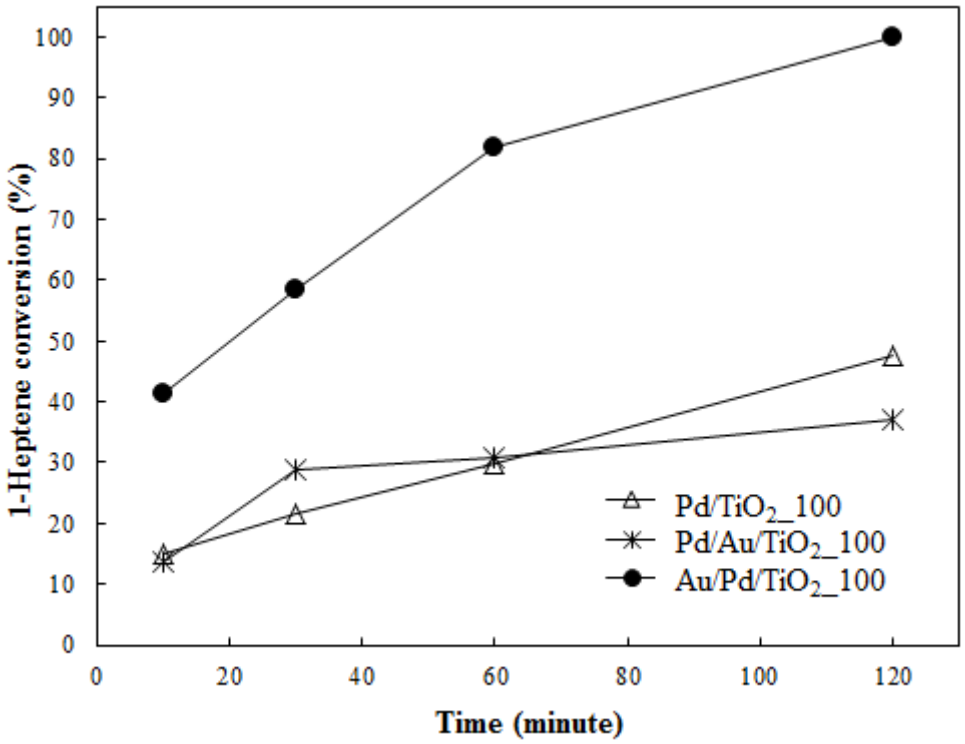

Figure 4.13 Hydrogenation of 1-heptene on Pd/TiO_2_100, $Pd/Au/TiO_2$_100, and $Au/Pd/TiO_2$_100

4.2 Effect of TiO_2 crystallite size on the catalytic behavior of Au-Pd/TiO_2 catalysts in the liquid-phase selective hydrogenation of 1-heptyne

4.2.1 Characterization of the catalysts

4.2.1.1 X-Ray Diffraction (XRD)

The XRD patterns of the TiO_2 supports and TiO_2 supported Au–Pd catalysts are shown in **Figure 4.14**. All the samples showed the characteristic peaks of pure anatase phase titania at 2θ degrees = 25° (major), 37°, 48°, 55°, 56°, 62°, 71°, and 75° without contamination of the other phases such as rutile and brookite [67]. The average crystallite sizes of TiO_2 were calculated from the full width at half maximum of the XRD peak at $2\theta = 25^\circ$ using the Sherrer equation. As shown in **Table 4.3**, the solvothermal-derived TiO_2 had the average crystallite sizes of 9 and 15 nm with specific surface area 145 and 79 m^2/g, respectively whereas the commercial TiO_2 had the average crystallite size 100 nm and surface area 10 m^2/g. The XRD characteristic peaks corresponding to palladium and gold species were not detected for all the catalysts due probably to the low amount of metals present and/or the relatively high intensity of the TiO_2 peaks compared to the metals.

Table 4.3 Properties of TiO_2 support

TiO_2 support	Source	Phase	Crystallite size (nm)	BET surface area (m^2/g)	Pore volume (cm^3/g)	Average pore diameter (nm)
TiO_2_9	SV	Anatase	9	145	0.42	8.1
TiO_2_15	SV	Anatase	15	79	0.40	14.9
TiO_2_100	Aldrich	Anatase	100	10	0.02	7.6

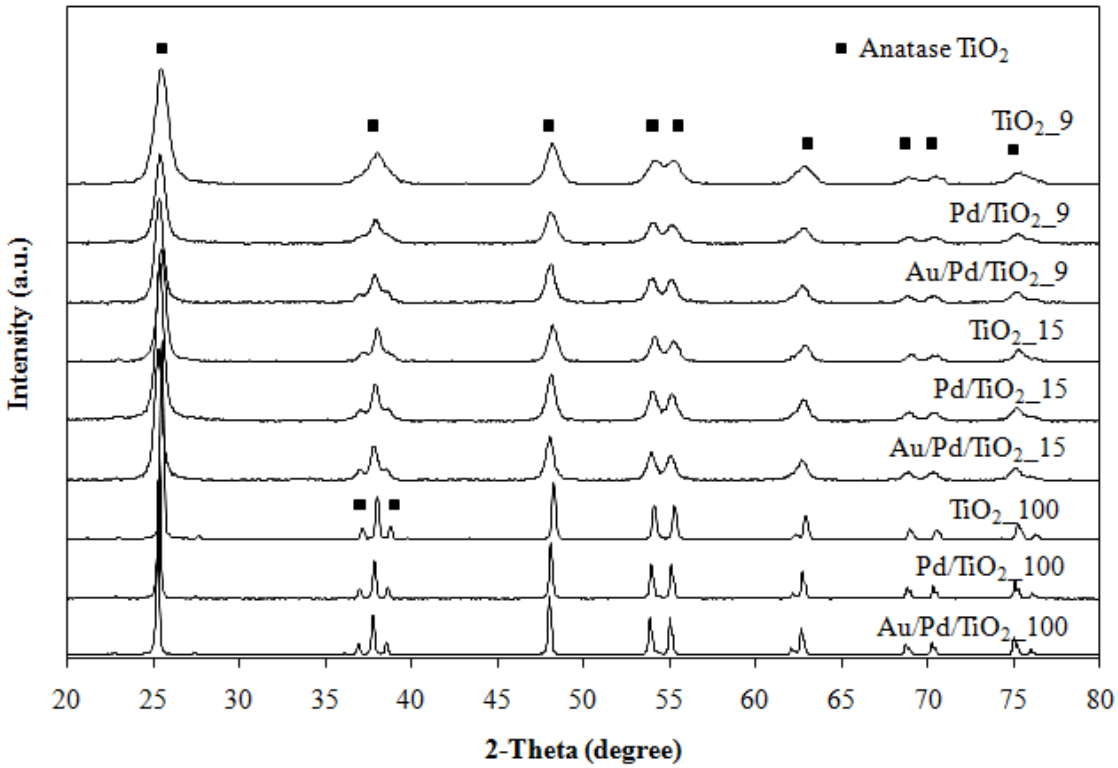

Figure 4.14 XRD patterns of TiO_2_9, Pd/TiO_2_9, Au/Pd/TiO_2_9, TiO_2_15, Pd/TiO_2_15, Au/Pd/TiO_2_15, TiO_2_100, Pd/TiO_2_100, and Au/Pd/TiO_2_100

4.2.1.2 Transmission Electron Microscopy (TEM)

Typical TEM images and particle size distributions of the monometallic Pd and the bimetallic Au–Pd catalysts are shown in **Figure 4.15-4.17**. The TiO_2_9 and TiO_2_15 supports obtained from the solvothermal method showed uniform particle size of average size 9 and 15 nm, respectively. On the other hand, the TiO_2_100 support comprised of larger particles with average size 0.1-0.2 μm. The metal dispersion on the catalysts can be observed from the TEM images. The average Pd particles size on the monometallic Pd/TiO_2_9 and Pd/TiO_2_15 catalysts were in the range of sub-nano particles (< 1 nm) whereas those on the TiO_2_100 were much larger ($đ_P$ ~ 6.9 nm). Similarly, for the bimetallic Au–Pd catalysts much smaller Au–Pd particles were seen on the Au/Pd/TiO_2_9 and the Au/Pd/TiO_2_15 than on the Au/Pd/TiO_2_100. The metal particles on the Au/Pd/TiO_2_9 and Au/Pd/TiO_2_15 had a uniform particle size distribution in the range of sub-nano particles (< 1 nm) and 2 nm, respectively. In contrast, bimodal particle size distribution with average sizes 1.7 and 7.9 nm were observed on the Au/Pd/TiO_2_100. It is suggested that the size of Au–Pd particles depended on the original size of the Pd particles, which itself a function of the TiO_2 crystallite size. Moreover, there is some research from our group studied about the effect of Ti^{3+} defective sites present on the nanocrystalline TiO_2 surface, which as itself is a function of the TiO_2 crystallite size. The solvothermal-derived TiO_2 with larger crystallite sizes (higher amounts of Ti^{3+} surface defects) resulted in stronger interaction of the TiO_2 surface and the cobalt precursor, and consequently, higher dispersion of Co on the TiO_2 supports [85].

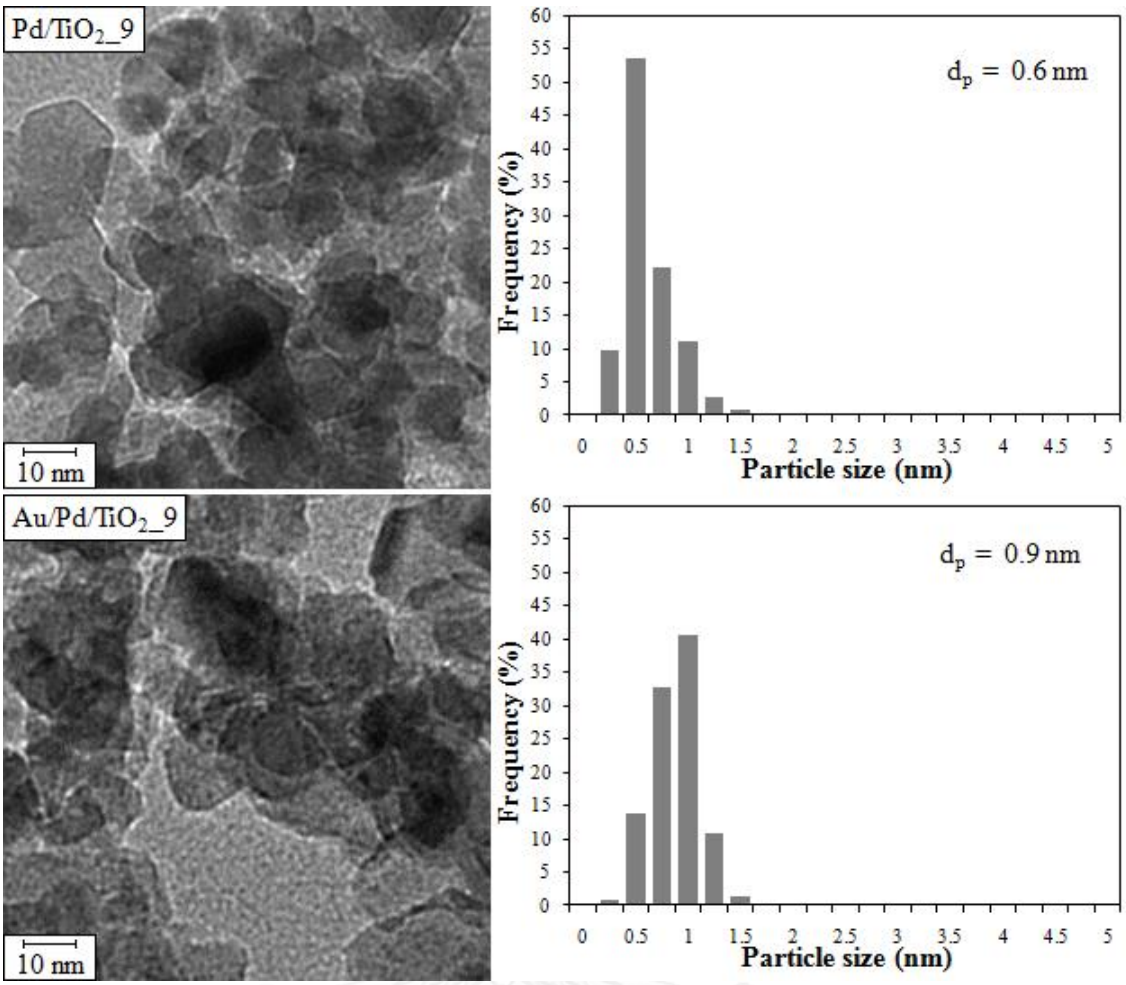

Figure 4.15 TEM images and distribution size of Pd/TiO_2_9 and $Au/Pd/TiO_2$_9

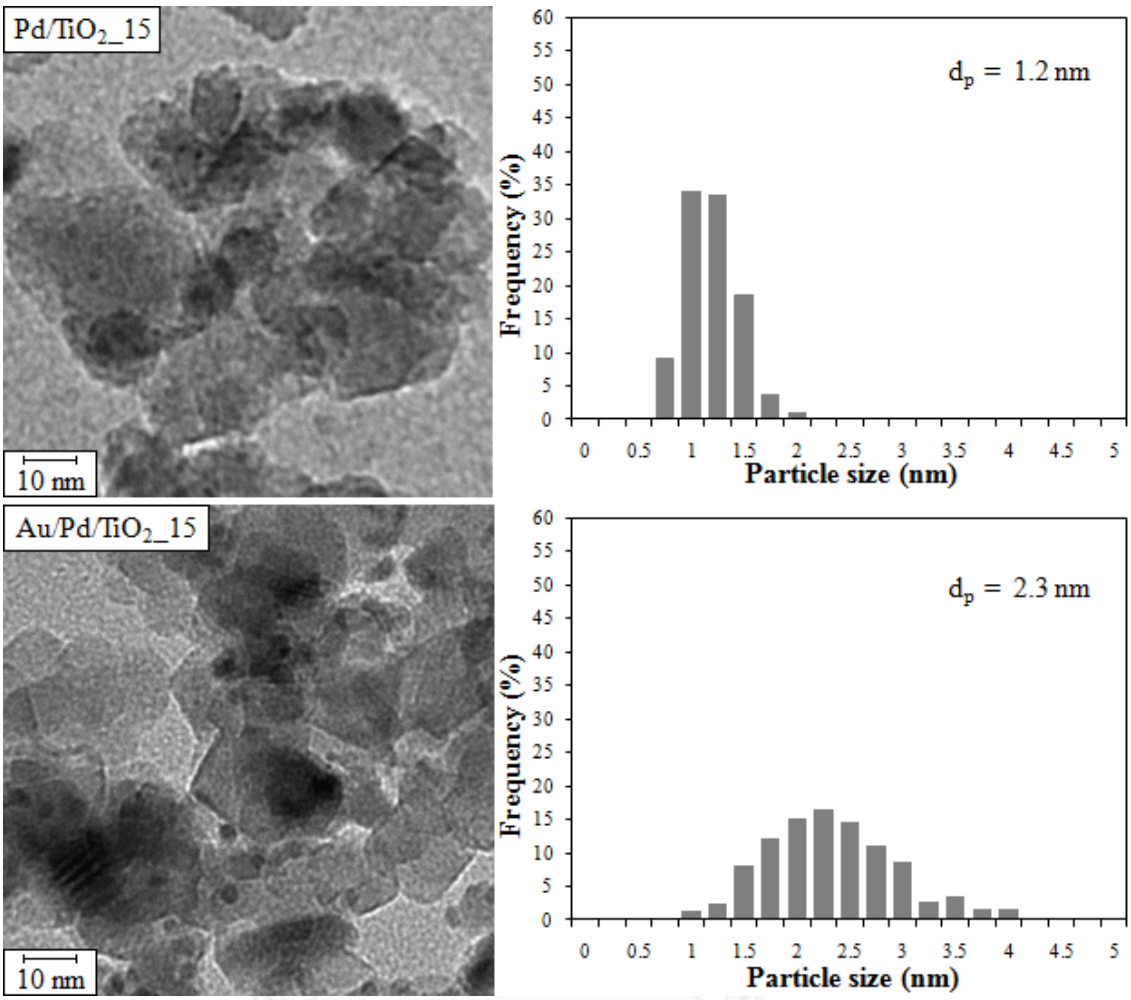

Figure 4.16 TEM images and distribution size of Pd/TiO_2_15 and $Au/Pd/TiO_2$_15

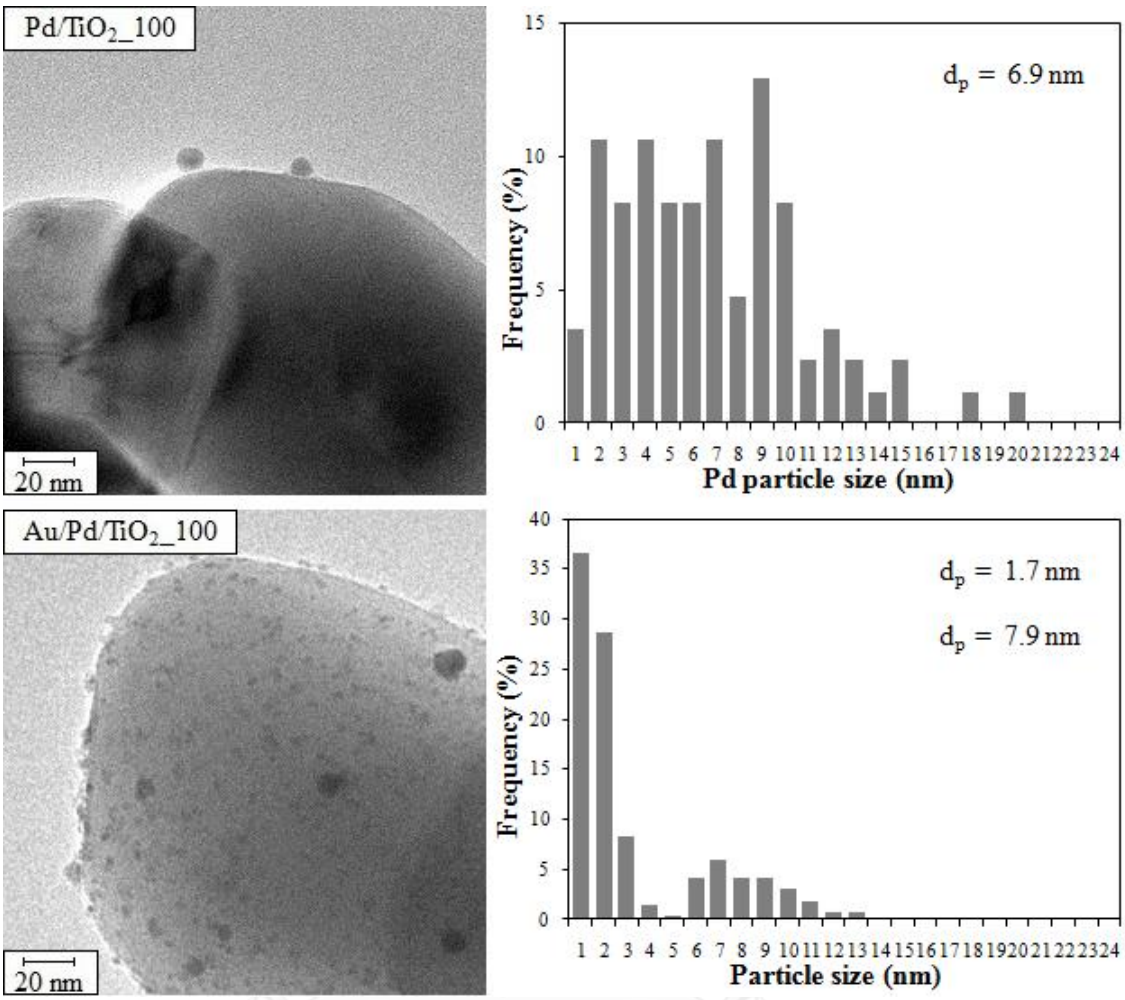

Figure 4.17 TEM images and distribution size of Pd/TiO_2_100 and $Au/Pd/TiO_2$_100

4.2.1.3 X-ray Photoelectron Spectroscopy (XPS)

Surface compositions of the catalyst were analyzed using a Kratos Amicus X-ray photoelectron spectroscopy. The XPS analysis were carried out with following conditions: Mg Ka X-ray source at current of 20 mA and 12 keV, resolution 0.1 eV/step, and pass energy 75 eV. The operating pressure is approximately $1x10^{-6}$ Pa.

A survey scan was performed in order to determine the elements on the catalyst surface. The elemental scan was carried out in the next step for C 1s, O 1s, Ti 2p, Pd 3d and Au 4f. Binding energies of each element was calibrated internally with carbon C1s at 285.0 eV. Photoemission peak areas are determined by using a linear routine. Deconvolution of complex spectra was done by fitting with Gaussian (70%)-Lorentzian (30%) shapes using VISION2 software equipped with the XPS system.

The surface properties and the chemical states of Pd and Au on the different catalysts were investigated by XPS. The Pd 3d spectra of the monometallic and bimetallic catalysts are shown in **Figure 4.18** and **4.19**, respectively. For the Pd/TiO_2_9, Pd/TiO_2_15 and Pd/TiO_2_100 catalysts, the binding energies (B.E.) of Pd $3d_{5/2}$ were detected at 336.5-337.1 eV which could be attributed to the presence of palladium in the form of PdO. On the other hand, the Pd 3d spectra of the $Au/Pd/TiO_2$_9, $Au/Pd/TiO_2$_15 and $Au/Pd/TiO_2$_100 catalysts were fitted by two peaks at higher and lower binding energies of 336.0-336.2 eV and 334.8-335.2 eV, which were attributed to Pd–Au alloy and metallic Pd^0, respectively [75, 76]. Such results

reveal that Pd particles in the bimetallic catalysts were highly resistant to oxidation, compared to those of the monometallic catalysts. Previous studies by Qian and Huang [77] and Yang et al. [56] suggested that the addition of Au was helpful to the reduction of Pd^{2+} to metallic Pd and/or the protection of Pd^{0} from being oxidized into PdO. The atomic percent of the species at 336.0-336.2 eV (Au–Pd alloy) for the Au/Pd/TiO_2_9, the Au/Pd/TiO_2_15, and the Au/Pd/TiO_2_100 were determined by peak fitting to be 19%, 18% and 15%, respectively. The percentages of Au–Pd alloy formation were not significantly different among the various bimetallic Au–Pd catalysts. The Au 4f spectra of the bimetallic catalysts are shown in **Figure 4.20**. The Au 4f peaks were detected at the binding energy of 83.0-83.2 eV, which is shift from the typical metallic gold (B.E. 84.0 ± 0.1). The small shift of binding energies could be attributed to a charge transfer from Pd to Au on the grounds of the bulk electronegativity differences and could also be indicative of alloy formation [77].

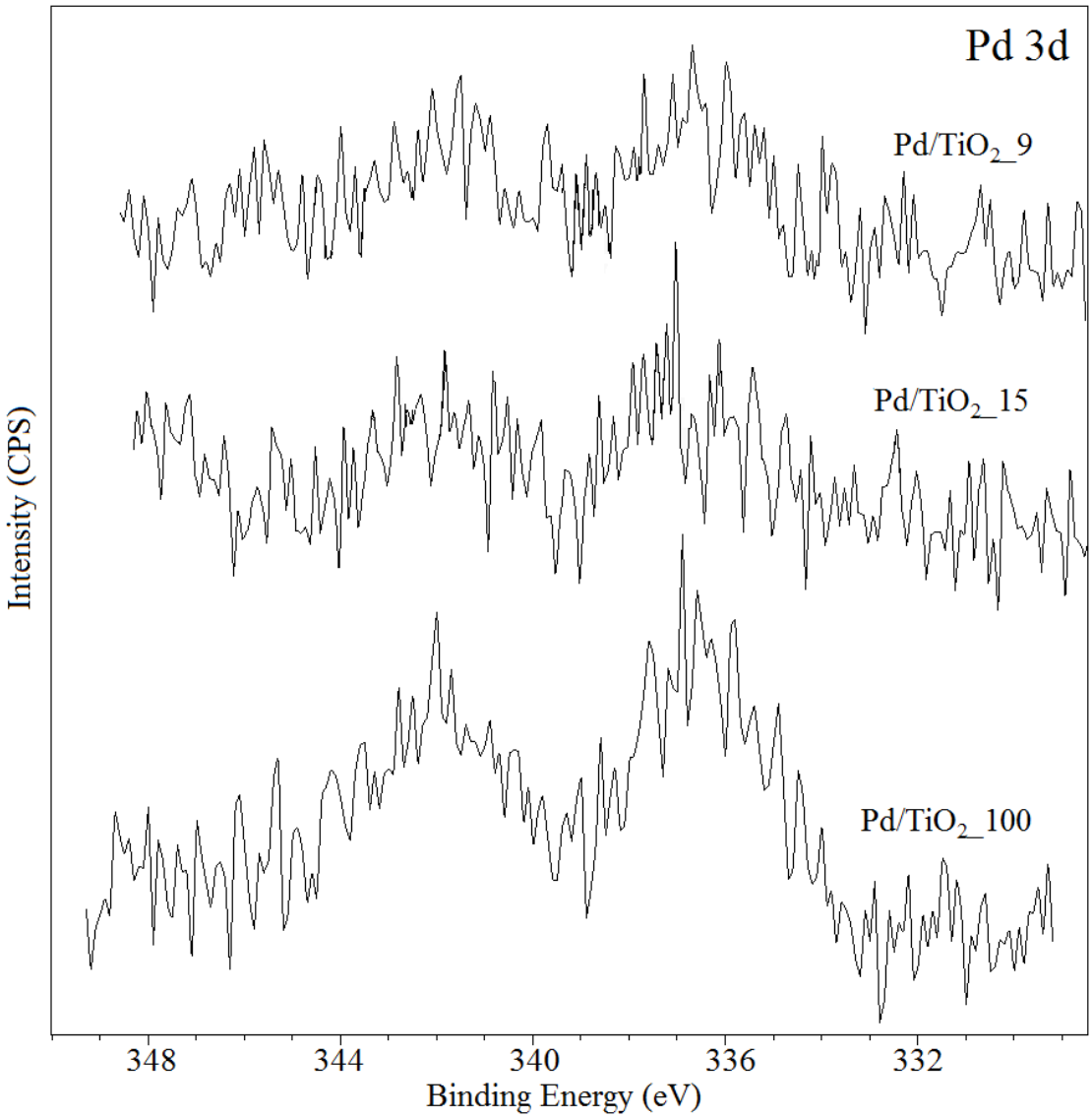

Figure 4.18 XPS Pd 3d core level spectra of Pd/TiO_2_9, Pd/TiO_2_15, and Pd/TiO_2_100

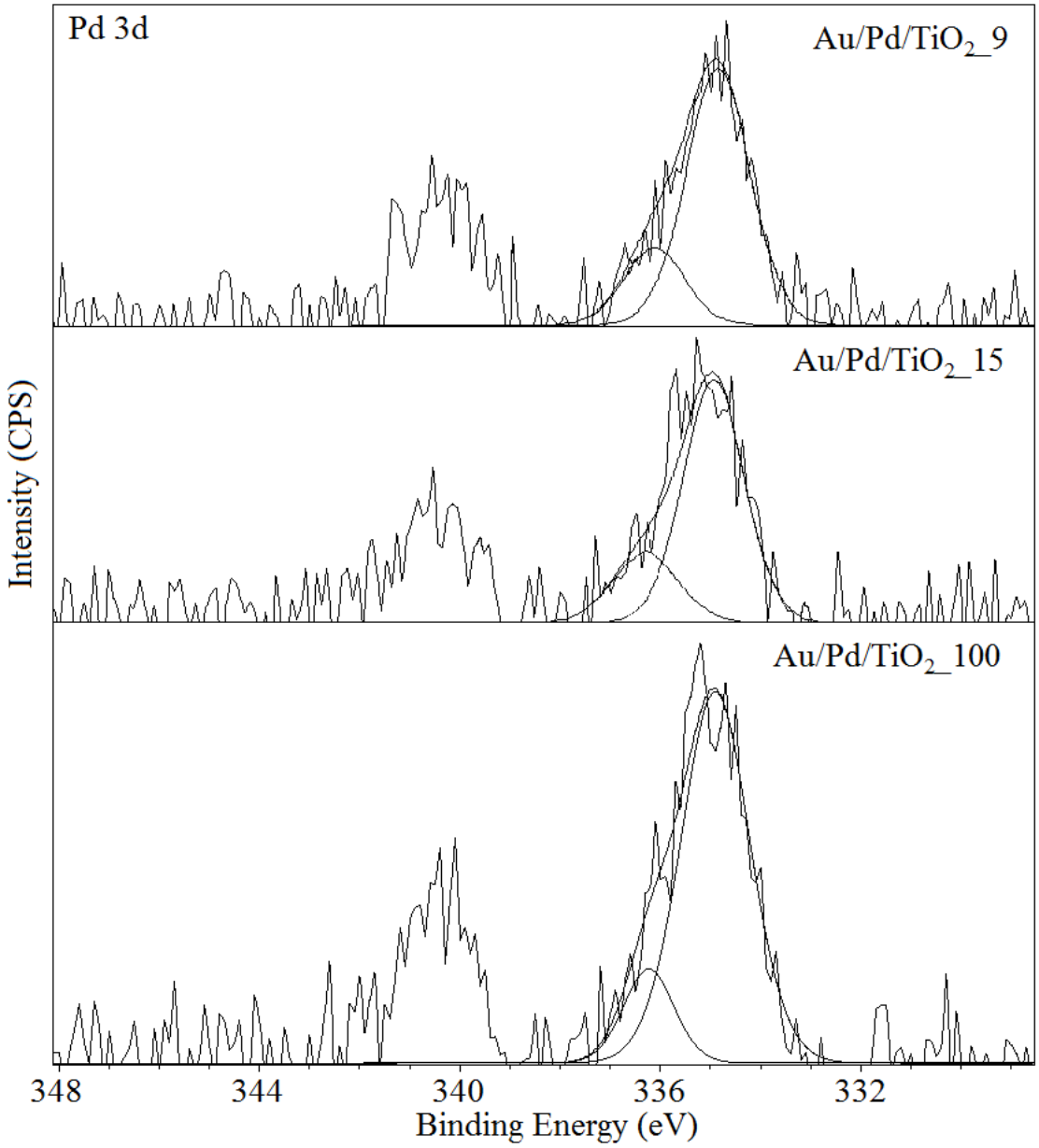

Figure 4.19 XPS Pd 3d core level spectra of Au/Pd/TiO_2_9, Au/Pd/TiO_2_15, and Au/Pd/TiO_2_100

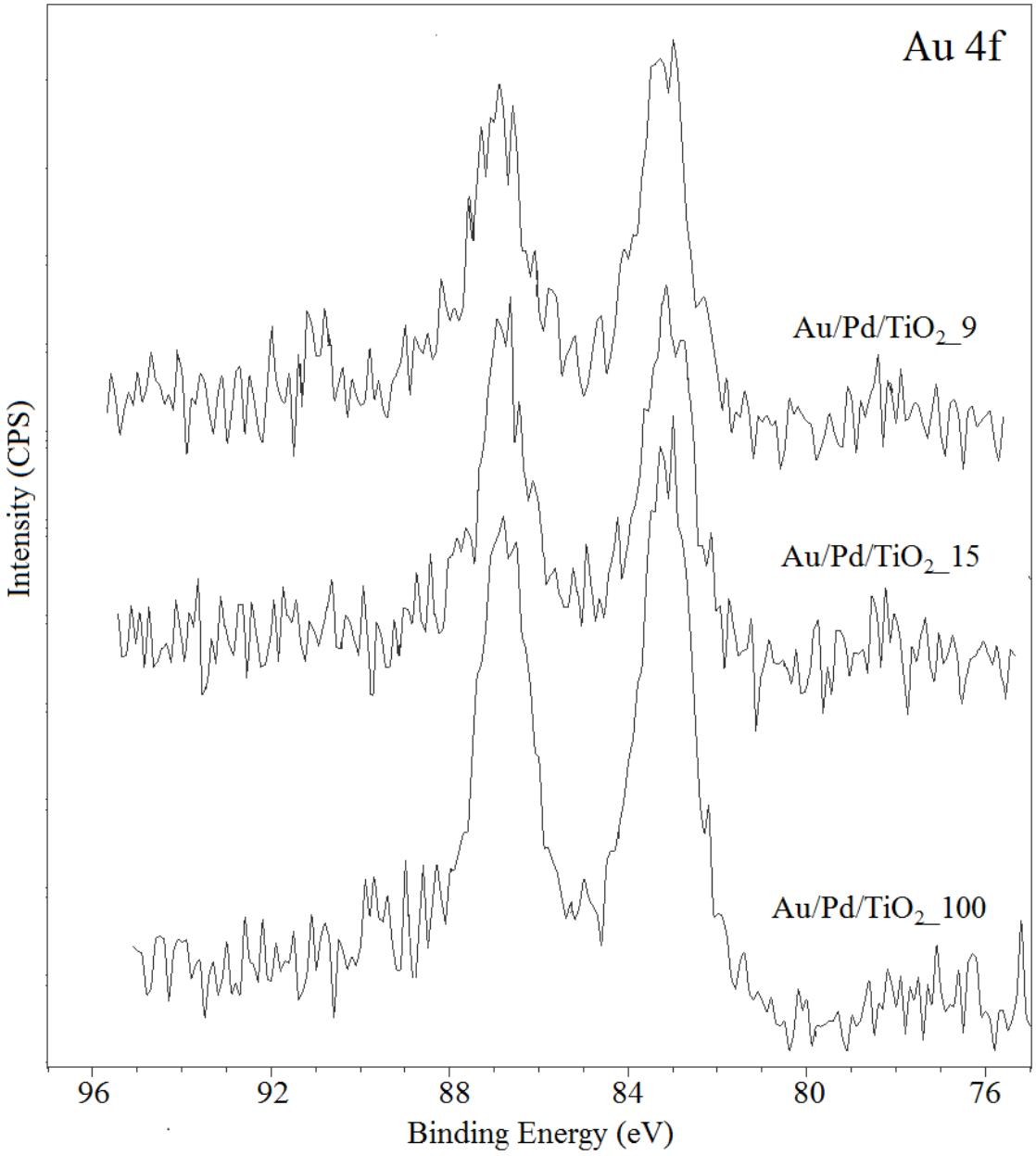

Figure 4.20 XPS Au 4f core level spectra of Au/Pd/TiO_2_9, Au/Pd/TiO_2_15, and Au/Pd/TiO_2_100

Table 4.4 XPS results of TiO_2 supported Pd and Au/Pd catalysts

Sample	Pd $3d_{5/2}$		Au $4f_{7/2}$		Atomic concentration	
	B.E. (eV)	FWHM (eV)	B.E. (eV)	FWHM (eV)	Pd (%)	Au (%)
Pd/TiO_2_9	336.7	0.924	n/a	n/a	0.12	n/a
$Au/Pd/TiO_2$_9	(1) 334.9 (2) 336.0	1.336 1.372	83.2	1.173	(1) 0.69 (2) 0.16	0.50
Pd/TiO_2_15	337.1	0.775	n/a	n/a	0.07	n/a
$Au/Pd/TiO_2$_15	(1) 334.8 (2) 336.2	1.365 1.452	83.0	1.226	(1) 0.46 (2) 0.10	0.43
Pd/TiO_2_100	336.5	1.844	n/a	n/a	0.28	n/a
$Au/Pd/TiO_2$_100	(1) 335.2 (2) 336.2	1.161 1.611	83.1	1.287	(1) 0.91 (2) 0.17	0.67

4.2.1.4 UV/Vis spectra

The UV/Vis spectra of the mono and bimetallic catalysts are shown in **Figure 4.21**. The dampening and broadening of the plasmon band for the Au/Pd/TiO_2_9, Au/Pd/TiO_2_15, and Au/Pd/TiO_2_100 corresponded to the Pd–Au alloy formation [20]. The Pd/TiO_2_9, Pd/TiO_2_15 and Pd/TiO_2_100 did not show any well-resolved surface plasmon band, which is typical for the monometallic Pd catalysts. The UV-Vis spectra also suggested that most of the Au particles existed in the Pd–Au alloy and that there was no separate formation of pure Au nanoparticles in the bimetallic catalyst systems.

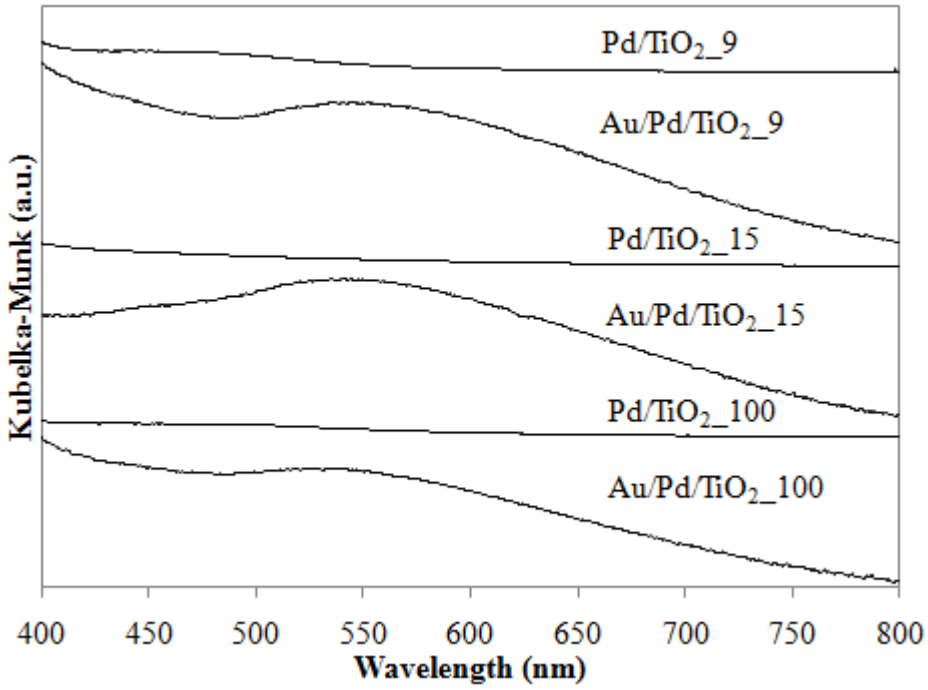

Figure 4.21 UV-Vis spectra of Pd/TiO_2_9, Au/Pd/TiO_2_9, Pd/TiO_2_15, Au/Pd/TiO_2_15, Pd/TiO_2_100, and Au/Pd/TiO_2_100

4.2.1.5 CO infrared spectra

The infrared spectra obtained after CO adsorption at 30°C on the Pd monometallic and Au–Pd bimetallic catalysts are shown in **Figure 4.22-4.24**. The spectral envelopes were deconvoluted into individual vibrational bands in order to identify the specific adsorbed species. The CO adsorption on Pd-based catalysts generally reveals two main regions: a first one between 2100 and 2030 cm^{-1} and a larger second one in 2000–1800 cm^{-1} range. The IR spectra for Pd monometallic and Au–Pd bimetallic catalysts represent four adsorption modes of CO, linear (2100-2030 cm^{-1}), compressed bridged (1995-1975 cm^{-1}), isolated bridged (1960-1925 cm^{-1}), and tricoordinated (1890-1870 cm^{-1}) bonds, as described in Ref. [86]. Compared to the monometallic Pd catalysts, the peaks corresponding to linear CO adsorbed species were shifted to lower wavenumbers after Au addition for all the Au–Pd bimetallic catalysts suggesting the Pd–Au alloy formation [86, 87].

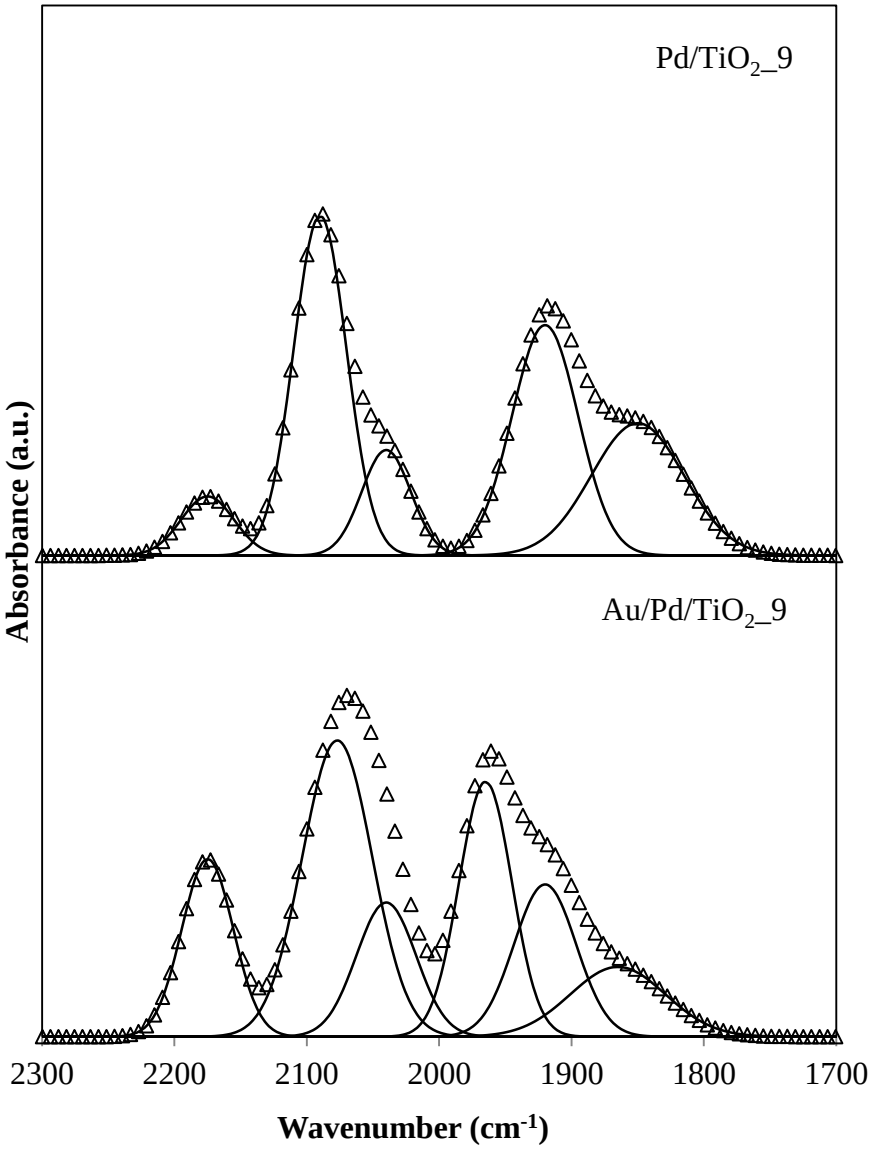

Figure 4.22 FTIR spectra of adsorbed CO at room temperature on Pd/TiO_2_9 and $Au/Pd/TiO_2$_9

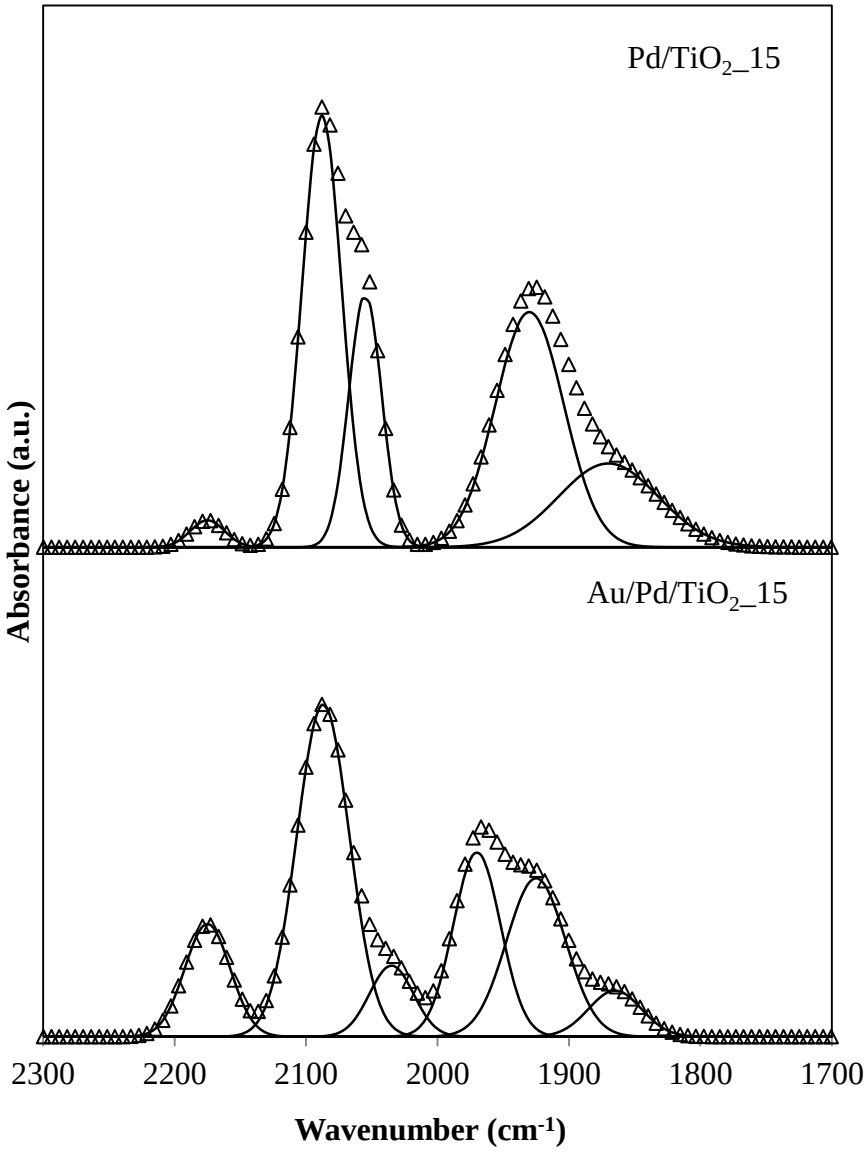

Figure 4.23 FTIR spectra of adsorbed CO at room temperature on Pd/TiO_2_15 and $Au/Pd/TiO_2$_15

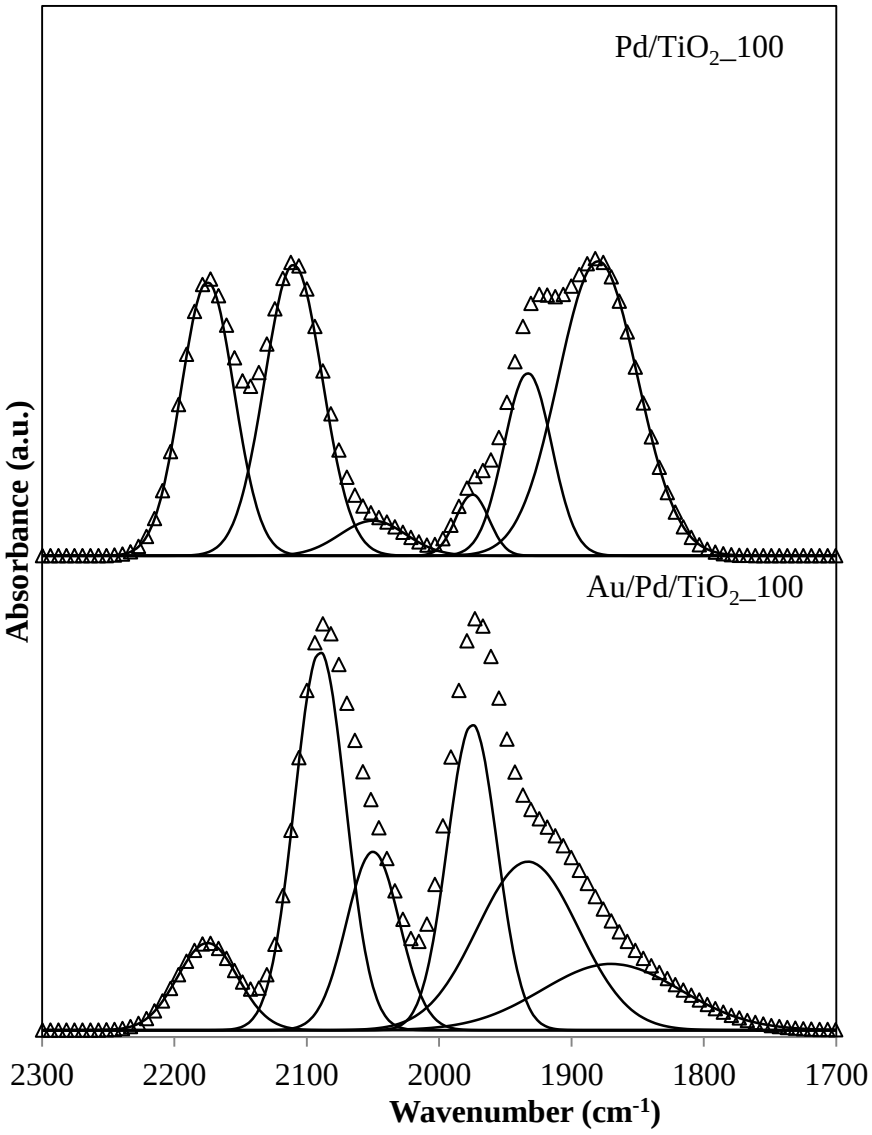

Figure 4.24 FTIR spectra of adsorbed CO at room temperature on Pd/TiO_2_100 and $Au/Pd/TiO_2$_100

4.2.2 Catalytic behavior

4.2.2.1 Hydrogenation of 1-heptyne

The catalytic behavior of the mono and bimetallic catalysts was evaluated in the liquid-phase hydrogenation of 1-heptyne under mild conditions (2 bar of H_2 and 30 $^{\circ}C$). The conversion of 1-heptyne and the selectivity to 1-heptene as a function of reaction time are shown in **Figure 4.25**. The hydrogenation rates of the bimetallic Au–Pd catalysts were higher than the monometallic Pd ones and were found to be in the order: Au/Pd/TiO_2_100 > Au/Pd/TiO_2_15 > Au/Pd/TiO_2_9 ≈ Pd/TiO_2_100 > Pd/TiO_2_15 > Pd/TiO_2_9. The conversion of 1-heptyne was completed in 30 min for all the catalysts, except Pd/TiO_2_9 in which complete conversion was achieved after 40 minute reaction time under the conditions used. The dependence of hydrogenation activity of supported Pd catalysts on Pd particle size has been investigated extensively. Typically, specific activity of Pd in the liquid-phase selective hydrogenation decreases as Pd particle size decreases especially when the average Pd size is very small (≤ 3-5 nm) [88]. Diminishing activity of small metal particles was probably due to the different band structure characteristics of nano-sized metal compared to bulk metals and that they appear to be electron deficient [80]. The results were consistent to the previous study on the comparison of Pd catalysts supported on micron- and solvothermal-derived nanocrystalline TiO_2 in the liquid-phase selective hydrogenation of phenylacetylene. The activity for hydrogenation of phenylacetylene of Pd supported TiO_2 with large crystallite size is higher than that of supported TiO_2 with small crystallite size, due to the Pd particle size decreased when

deposited on the smaller crystallite size of TiO_2. However, the selectivity of catalyst supported on the small crystallite size of TiO_2 is still higher than that of catalyst supported on the large crystallite size of TiO_2. Moreover, the used of nanocrystalline TiO_2 exhibited strong metal–support interaction (SMSI) when reduced at 500 °C [8, 34].

All the present catalysts exhibited high selectivity of 1-heptene (> 97%) up to nearly full conversion of 1-heptyne. During 120 minute reaction time, the selectivity of 1-heptene decreased further after complete conversion of 1-heptyne due to the hydrogenation of 1-heptene to heptane. Nonetheless, the selectivities of 1-heptene of the monometallic catalysts were higher than those of the bimetallic catalysts. The selectivity of 1-heptene for the bimetallic catalysts at 120 min decreased in the order: Au/Pd/TiO_2_9 (54 %) > Au/Pd/TiO_2_15 (41 %) >> Au/Pd/TiO_2_100 (0 %) whereas they were not much different among the monometallic catalysts (70%).

Unlike the alkyne hydrogenation activity, the selectivity to alkene formation was irrespective of Pd particle diameter for most reactants in the selective alkyne hydrogenation [89-91]. It is rather affected by electronic modification of Pd metal (i.e., alloy formation and presence of the strong metal-support interaction effect). In our recent papers [92], the rate of 1-heptene hydrogenation in the second step was greatly enhanced as the Pd species became electron-rich in the Au–Pd alloy particles. In other words, the Au species acted as an electronic promoter for Pd and greatly promoted the second step of hydrogenation of 1-heptene to heptane. In our previous studies, the formation of Au–Pd alloy was found to be dependent on the

loading sequence [92] and the preparation method used [93]. The results in the present work emphasized that the formation of Au–Pd alloy was responsible for the increased hydrogenation activity of 1-heptene to heptane in the selective hydrogenation of 1-heptyne and it suggests the dependence of alkene hydrogenation rate on the Au–Pd particle size.

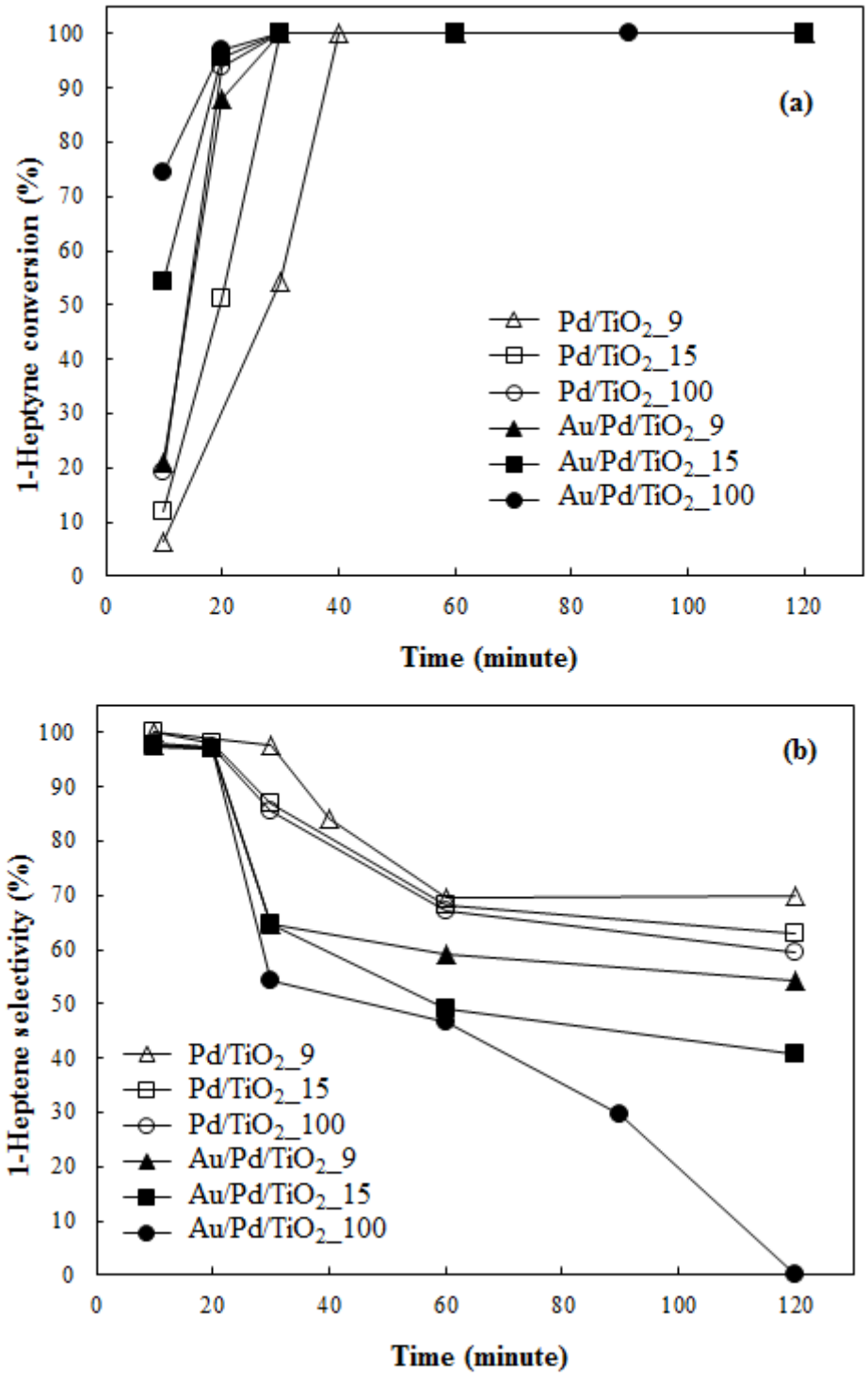

Figure 4.25 Hydrogenation of 1-heptyne on Pd/TiO_2_9, $Au/Pd/TiO_2$_9, Pd/TiO_2_15, $Au/Pd/TiO_2$_15, Pd/TiO_2_100, and $Au/Pd/TiO_2$_100: %heptyne conversion (a) and %heptenes selectivity (b)

4.2.2.2 Hydrogenation of 1-heptene

The hydrogenation of 1-heptene was carried out in the same manner as that of 1-heptyne hydrogenation under similar conditions. The conversion of 1-heptene as a function of reaction time of the Pd/TiO_2 and the Pd–Au bimetallic catalysts is shown in **Figure 4.26**. The conversion of 1-heptene at 120 minute reaction time was in the order: $Au/Pd/TiO_2\_100$ > $Au/Pd/TiO_2\_15$ > $Au/Pd/TiO_2\_9$ > Pd/TiO_2_100 > Pd/TiO_2_15 = Pd/TiO_2_9, which was found to be in good agreement with the selectivity of 1-heptene after full conversion of 1-heptyne in 1-heptyne hydrogenation. These results confirm that the hydrogenation of 1-heptene occurred only at nearly or full conversion of 1-heptyne on these catalysts. It has been suggested that the alkyne compound displaces the alkene from the catalyst surface and prevents its readsorption, thereby exerting a poisoning effect for the subsequent alkene hydrogenation, which holds as long as the alkyne species is present [83, 84]. In other words, the adsorption coefficient of 1-heptyne was greater than that of 1-heptene.

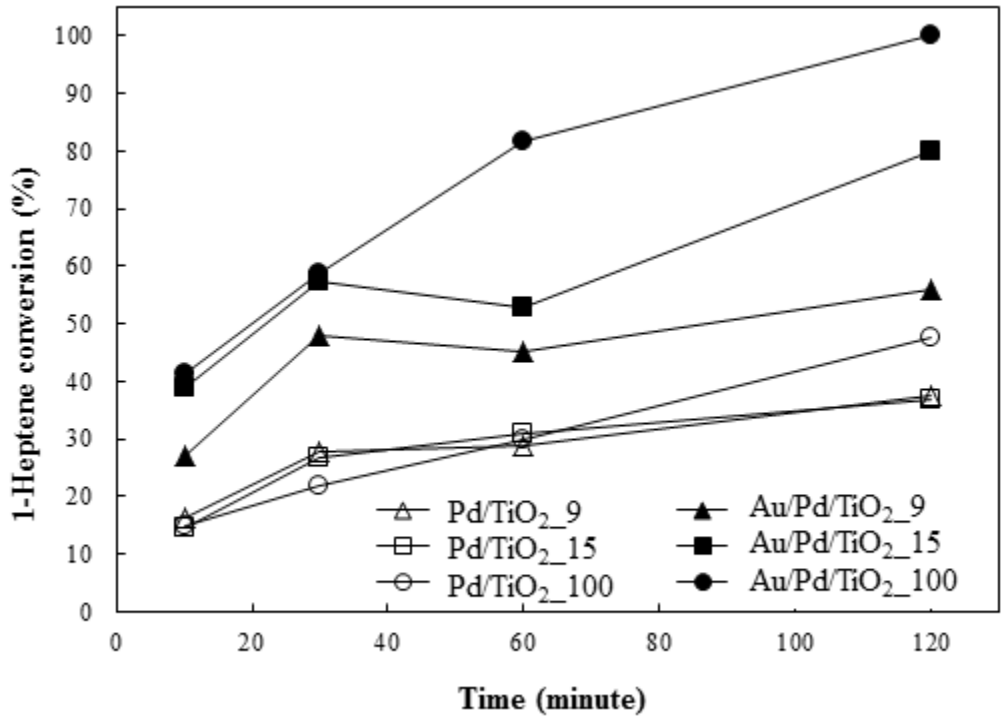

Figure 4.26 Hydrogenation of 1-heptene on Pd/TiO_2_9, $Au/Pd/TiO_2$_9, Pd/TiO_2_15, $Au/Pd/TiO_2$_15, Pd/TiO_2_100, and $Au/Pd/TiO_2$_100

4.3 Effect of Pd loading on the catalytic behavior of Pd/TiO_2 and $Au\text{-}Pd/TiO_2$ catalysts in the liquid-phase selective hydrogenation of 1-heptyne

The liquid-phase hydrogenation of 1-heptyne (98%, Aldrich) was carried out in a magnetically stirred 100 ml Teflon-lined stainless steel autoclave reactor. The reaction was carried out under flowing hydrogen at 2 bars and 30 $^{\circ}C$ for 10–120 minnute. The catalytic behavior of the Pd/TiO_2_9, $2\%Pd/TiO_2\_9$, $Au/Pd/TiO_2\_9$, and $Au/2\%Pd/TiO_2\_9$ catalysts was evaluated in the liquid-phase hydrogenation of 1-heptyne. The conversion of 1-heptyne and the selectivity to 1-heptene as a function of reaction time are shown in **Figure 4.27**. The conversion of 1-heptyne increased with increasing Pd loading from 0.5 to 2 wt% for Pd/TiO_2_9 catalyst. After complete conversion of 1-heptyne, the hydrogenation of 1-heptene occurred. The conversion of 1-heptene also increased with increasing Pd loading. However the hydrogenation rate of 1-heptene was lower than 1-heptyne because the adsorption of 1-heptene was lower than 1-heptyne. The similar result was observed for $Au/Pd/TiO_2\_9$ catalyst with increased Pd loading. Moreover, this result was in good agreement with previous work by S. Somboonthanakij et al. [6] which found that the conversion of 1-heptyne increased from 42 to 75% as Pd loading increased from 0.5 to 5 wt.% and remained relatively constant when Pd loading was increased to 10 wt.%. The selectivities for 1-heptene were in the range of 92–95% for all the Pd/SiO_2 catalysts.

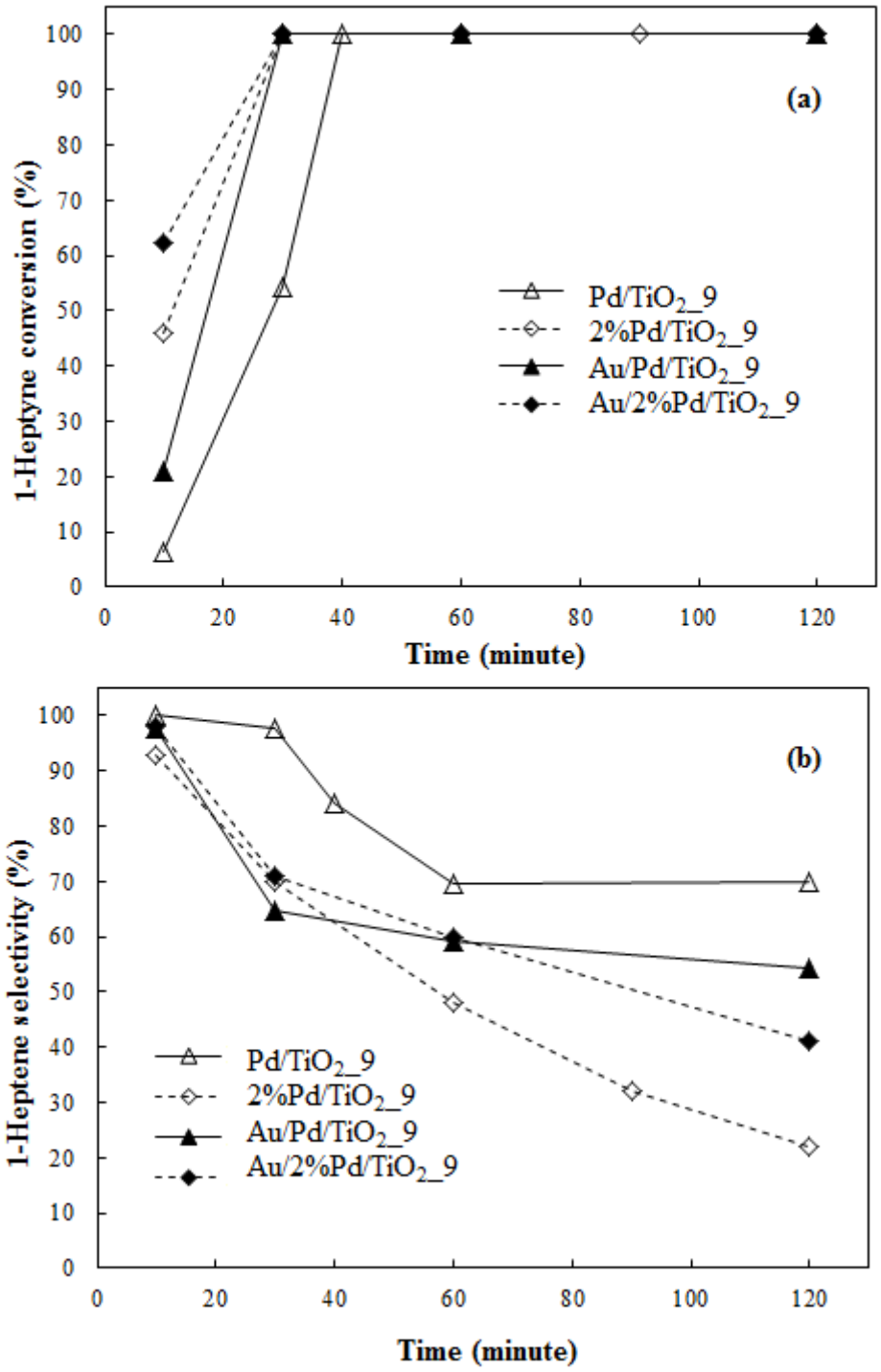

Figure 4.27 Hydrogenation of 1-heptyne on Pd/TiO_2_9, 2%Pd/TiO_2_9, $Au/Pd/TiO_2$_9, and $Au/2\%Pd/TiO_2$_9: % heptyne conversion (a) and % heptenes selectivity (b)

4.4 Effect of H_2 pressure on the catalytic behavior of Pd/TiO_2 catalysts in the liquid-phase hydrogenation of 1-heptene

The liquid-phase hydrogenation of 1-heptene on Pd/TiO_2_9 catalyst was carried out in a magnetically stirred 100 ml Teflon-lined stainless steel autoclave reactor. The solution was contained 1.53 mmol of 1-heptene in 9.8 ml of toluene. The reaction was carried out under flowing hydrogen (2 and 10 bars) at 30 $^{\circ}C$ for 10–120 min. The conversion of 1-heptene as a function of reaction time is shown in **Figure 4.28**. The conversion of 1-heptene increased from 37% to 85% as H_2 pressure increased from 2 to 10 bars at 120 minute. The amount of H_2 required for liquid-phase hydrogenation of 1-heptene was 1.53 mmol (equal to the amount of 1-heptene). In case of total hydrogenation of 1-heptyne to n-heptane, the amount of H_2 requirement was 3.06 mmol (2 time of hydrogenation of 1-heptene to n-heptane). Since the H_2 using in each experiment was 2 bars or 7.14 mmol, it is indicted that the amount of H_2 was excess in each experiment. However the conversion of 1-heptene at 10 bars of H_2 was higher than at 2 bars, probably because of the higher solubility of H_2 in the solution at high pressure.

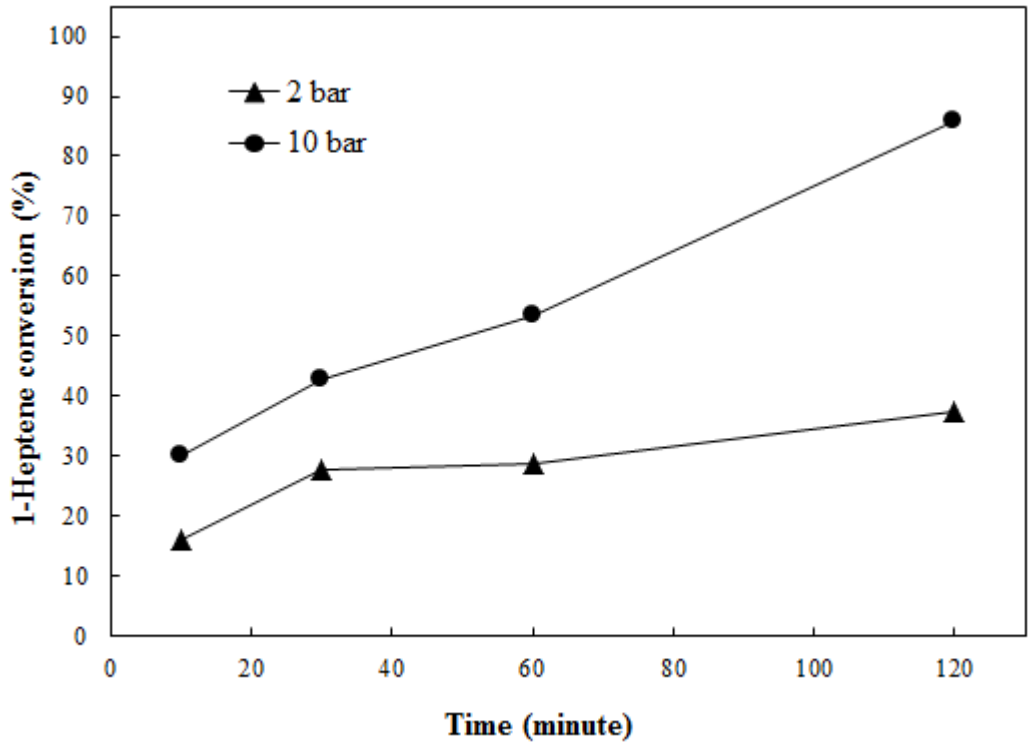

Figure 4.28 Hydrogenation of 1-heptene on Pd/TiO_2_9 catalyst under H_2 pressure of 2 and 10 bars

4.5 The deactivation of catalyst

4.5.1 The deactivation of catalyst in the liquid-phase hydrogenation of 1-heptyne

The liquid-phase hydrogenation of 1-heptyne on Pd/TiO_2_9 catalyst was carried out in a magnetically stirred 100 ml Teflon-lined stainless steel autoclave reactor. The reaction was carried out under flowing hydrogen 2 bars at $30^{o}C$. The amount of catalyst used was 0.01 g. For the 1^{st} run, the solution contained 1.528 mmol (0.215 ml) of 1-heptene in 9.8 ml of toluene. After the reaction was preformed for 1 hour, a small sampling of product was analyzed by GC. The moles of 1-heptene and heptane were calculated to be 1.088 and 0.440 mmol, respectively (**Figure 4.29**). After that the 2^{nd} experiment was performed by addition of 1-heptyne (1.528 mmol or 0.2 ml) into the reactor without taking the 1^{st} run solution out. The reaction was then carried out for another 1 hour and then the product was analyzed by GC. There was no 1-heptyne left in the product solution (100% conversion of 1-heptyne). Within 1 hour for the 2^{nd} run, all of 1-heptyne was hydrogenated to 1-heptene and then 1-heptene hydrogenation occurred and converted to heptane. The moles of 1-heptene and heptane for 2^{nd} run were 0.972 and 0.556 mmol, respectively. From the result, it is implied that no catalyst deactivation occurred in the liquid-phase hydrogenation of 1-heptyne.

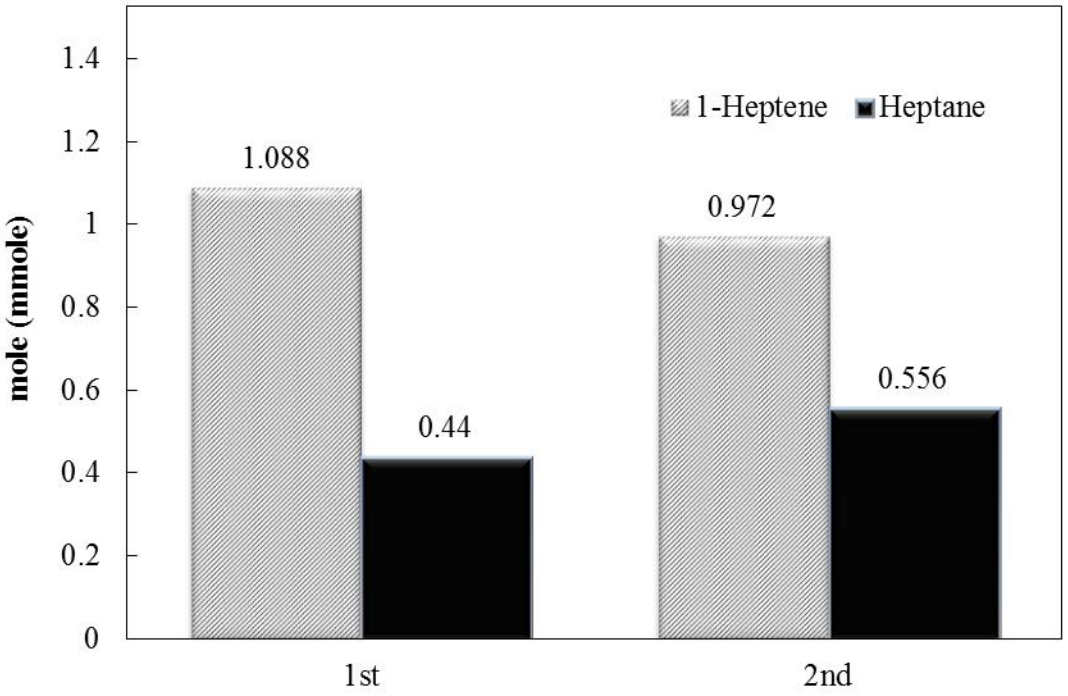

Figure 4.29 The catalyst deactivation test for hydrogenation of 1-heptyne on Pd/TiO_2_9 catalyst

4.5.2 The deactivation of catalyst in the liquid-phase hydrogenation of 1-heptene

The liquid-phase hydrogenation of 1-heptene on Pd/TiO_2_9 catalyst was carried out in a magnetically stirred 100 ml Teflon-lined stainless steel autoclave reactor. The solution was contained 7.64 mmol (1.075 ml) of 1-heptene in 49 ml of toluene. The amount of catalyst used was 0.05 g. The reaction was carried out under flowing hydrogen 5 bars at 30°C for 0–180 minute. The Pd/TiO_2_9 catalyst using for the 1st run was fresh catalyst after reduced under H_2 flow. After the reaction for the 1st run was completed at 180 minute, the products was analyzed by GC and the catalyst was wash with 50 ml of toluene for 2 times. Then the 2nd run was performed. After the 2nd run was finished, the catalyst was wash with toluene for 2 times and then the 3rd run was performed. After the reaction for the 3rd run was completed at 180 minute, the solution was take off from the reactor and then the solution for the 4th run was introduced to the reactor without washing with toluene. The reaction for the 4th run was carried out in the same manner as that of 1st run. The conversion of 1-heptene as a function of reaction time is shown in **Figure 4.30**. The conversion of 1-heptene was about 40% in all cycle. The results indicated that no catalyst deactivation occurred in liquid-phase hydrogenation of 1-heptene.

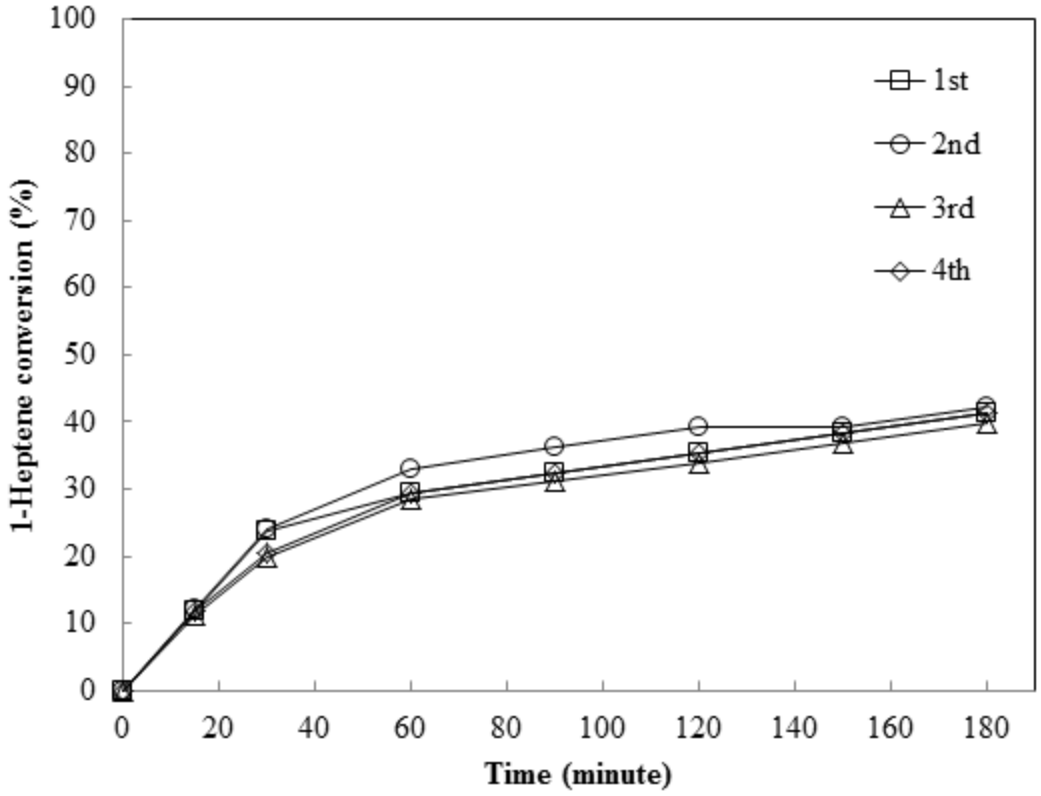

Figure 4.30 The catalyst deactivation test for hydrogenation of 1-heptene on Pd/TiO_2_9 catalyst

CHAPTER V
CONCLUSIONS AND RECOMMENDATIONS

5.1 Conclusions

1. The TiO_2-supported Pd/Au catalysts were prepared with the combination of IM and DP methods. DP of Au first followed by IM of Pd (Pd/Au/TiO_2_100) led to large Au aggregates (30–50 nm) and lower Pd dispersion, whereas smaller Pd–Au alloy particles (4–10 nm) and higher Pd dispersion were obtained when Au was added on the Pd/TiO_2 (Au/Pd/TiO_2_100).
2. The Pd metal and/or Pd-Au alloy formed on the TiO_2_9 (< 1 nm) were smaller than on TiO_2_15 (2-3 nm) and on TiO_2_100 (4-10 nm).
3. The catalytic behavior of Au/Pd/TiO_2 strongly depended on the crystallite size of TiO_2 and Au-Pd alloy particle size. The smaller particles size of Pd and/or Pd-Au alloy provided a higher selectivity to 1-heptene in the selective hydrogenation of 1-heptyne under mild reaction conditions.
4. In the presence of alloying effect in the Au/Pd/TiO_2, the Au species acted as an electronic promoter for Pd, which greatly promoted the second-step hydrogenation of 1-heptene to heptane.
5. No deactivation of catalyst occurred during the liquid-phase hydrogenation of 1-heptyne and 1-heptene

5.2 Recommendation

1. The catalysts should be reduced at higher temperature (500°C) to investigate the SMSI effect.

2. The other metal (such as Ni) should be used as the promoter of Pd supported catalyst.

3. The other alkynes should be used as the reactant for hydrogenation reaction over Au-Pd supported catalyst.

4. TiO_2 (P-25), mostly used for supported Au catalyst, should be more preferable used for supported Pd and Au-Pd catalysts to study the effect of other TiO_2-phase on the catalytic behavior of liquid-phase hydrogenation reaction.

REFERENCES

[1] Al-Herz, M., Simmons, M.J.H., and Wood, J. Selective Hydrogenation of 1-Heptyne in a Mini Trickle Bed Reactor. Industrial and Engineering Chemistry Research 51 (2012): 8815-8825.

[2] Crespo-Quesada, M., Dykeman, R.R., Laurenczy, G., Dyson, P.J., and Kiwi-Minsker, L. Supported nitrogen-modified Pd nanoparticles for the selective hydrogenation of 1-hexyne. Journal of Catalysis 279 (2011): 66-74.

[3] Liprandi, D.A., Cagnola, E.A., Quiroga, M.E., and L'Argentiere, P.C. Influence of the reaction temperature on the 3-hexyne semi-hydrogenation catalyzed by a palladium(II) complex. Catalysis Letters 128 (2009): 423-433.

[4] Lederhos, C.R., L'Argentiere, P.C., and Figoli, N.S. 1-Heptyne selective hydrogenation over Pd supported catalysts. Industrial and Engineering Chemistry Research 44 (2005): 1752-1756.

[5] Mekasuwandumrong, O., Somboonthanakij, S., Praserthdam, P., and Panpranot, J. Preparation of nano-Pd/SiO_2 by one-step flame spray pyrolysis and its hydrogenation activities: comparison to the conventional impregnation method. Industrial and Engineering Chemistry Research 48 (2009): 2819-2825.

[6] Somboonthanakij, S., et al. Characteristics and Catalytic Properties of Pd/SiO_2 Synthesized by One-step Flame Spray Pyrolysis in Liquid-phase Hydrogenation of 1-Heptyne. Catalysis Letters 119 (2007): 346-352.

[7] Papp, A., Molnar, A., and Mastalir, A. Catalytic investigation of Pd particles supported on MCM-41 for the selective hydrogenations of terminal and internal alkynes. Applied Catalysis A: General 289 (2005): 256-266.

[8] Weerachawanasak, P., Mekasuwandumrong, O., Arai, M., Fujita, S.-I., Praserthdam, P., and Panpranot, J. Effect of strong metal–support interaction on the catalytic performance of Pd/TiO_2 in the liquid-phase semihydrogenation of phenylacetylene. Journal of Catalysis 262(2) (2009): 199-205.

[9] Panpranot, J., Phandinthong, K., Sirikajorn, T., Arai, M., and Praserthdam, P. Impact of palladium silicide formation on the catalytic properties of Pd/SiO_2 catalysts in liquid-phase semihydrogenation of phenylacetylene. Journal of Molecular Catalysis A: Chemical 261(1) (2007): 29-35.

[10] Marin-Astorga, N., Pecchi, G., Fierro, J.L.G., and Reyes, P. A comparative study of Pd supported on MCM-41 and SiO2 in the liquid phase hydrogenation of

phenyl alkyl acetylenes mixtures. Journal of Molecular Catalysis A: Chemical 231 (2005): 67-74.

[11] Neurock, M. and Mei, D. Effects of alloying Pd and Au on the hydrogenation of ethylene: an ab initio-based dynamic Monte Carlo study. Topics in Catalysis 20 (2002): 5-23.

[12] Liu, R. and Zhao, F. Selective hydrogenation of citral over Au-based bimetallic catalysts in supercritical carbon dioxide. Science China Chemistry 53 (2010): 1571-1577.

[13] Pawelec, B., Cano-Serrano, E., Campos-Martin, J.M., Navarro, R.M., Thomas, S., and Fierro, J.L.G. Deep aromatics hydrogenation in the presence of DBT over Au–Pd/γ-alumina catalysts. Applied Catalysis A: General 275(1–2) (2004): 127-139.

[14] Venezia, A.M., Parola, V.L., Pawelec, B., and Fierro, J.L.G. Hydrogenation of aromatics over Au-Pd/SiO_2-Al_2O_3 catalysts; support acidity effect. Applied Catalysis A: General 264(1) (2004): 43-51.

[15] Sárkány, A., Horváth, A., and Beck, A. Hydrogenation of acetylene over low loaded Pd and Pd-Au/SiO_2 catalysts. Applied Catalysis A: General 229 (2002): 117-125.

[16] Sarkany, A., Geszti, O., and Safran, G. Preparation of Pdshell–Aucore/SiO_2 catalyst and catalytic activity for acetylene hydrogenation. Applied Catalysis A: General 350 (2008): 157-163.

[17] Krauth, A.C., Bernstein, G.H., and Wolf, E.E. Novel microfabricated Pd-Au/SiO_2 bimetallic model catalysts for the hydrogenation of 1,3-butadiene. Catalysis Letters 45 (1997): 177-186.

[18] Harada, M., Asakura, K., and Toshima, N. Catalytic Activity and Structural Analysis of Polymer-Protected Au/Pd Bimetallic Clusters Prepared by the Successive Reduction of $HAuCl_4$ and $PdCl_2$. Journal of Physical Chemistry 97 (1993): 5103-5114.

[19] Yang, X., et al. High-performance Pd–Au bimetallic catalyst with mesoporous silica nanoparticles as support and its catalysis of cinnamaldehyde hydrogenation. Journal of Catalysis 291 (2012): 36-43.

[20] Liu, R., et al. Physically and chemically mixed TiO_2-supported Pd and Au catalysts: unexpected synergistic effects on selective hydrogenation of citral in supercritical CO_2. Journal of Catalysis 269(1) (2010): 191-200.

[21] Menegazzo, F., Canton, P., Pinna, F., and Pernicone, N. Bimetallic Pd–Au catalysts for benzaldehyde hydrogenation: Effects of preparation and of sulfur poisoning. Catalysis Communications 9 (2008): 2353-2356.

[22] Enache, D.I., et al. Solvent-free oxidation of benzyl alcohol using titania-supported gold–palladium catalysts: Effect of Au–Pd ratio on catalytic performance. Catalysis Today 122(3–4) (2007): 407-411.

[23] Miedziak, P.J., et al. Oxidation of benzyl alcohol using supported gold–palladium nanoparticles. Catalysis Today 163(1) (2011): 47-54.

[24] Miedziak, P., et al. Oxidation of benzyl alcohol using supported gold–palladium nanoparticles. Catalysis Today 164(1) (2011): 315-319.

[25] Dimitratos, N., Lopez-Sanchez, J.A., Lennon, D., Porta, F., Prati, L., and Villa, A. Effect of particle size on monometallic and bimetallic (Au,Pd)/C on the liquid phase oxidation of glycerol. Catalysis Letters 108 (2006): 147-153.

[26] Choudhary, T.V., Sivadinarayana, C., Datye, A.K., Kumar, D., and Goodman, D.W. Acetylene hydrogenation on Au-based catalysts. Catalysis Letters 86 (2003): 1-8.

[27] Garron, A., Lázár, K., and Epron, F. Characterization by Mössbauer spectroscopy of trimetallic Pd–Sn–Au/Al_2O_3 and Pd–Sn–Au/SiO_2 catalysts for denitration of drinking water. Applied Catalysis B: Environmental 65(3–4) (2006): 240-248.

[28] Kolli, N.E., Delannoy, L., and Louis, C. Bimetallic Au–Pd catalysts for selective hydrogenation of butadiene: Influence of the preparation method on catalytic properties. Journal of Catalysis 297(0) (2013): 79-92.

[29] Li, G., Edwards, J., Carley, A.F., and Hutchings, G.J. Direct synthesis of hydrogen peroxide from H_2 and O_2 using zeolite-supported Au-Pd catalysts. Catalysis Today 122(3–4) (2007): 361-364.

[30] Smolentseva, E., et al. Selective oxidation of arabinose to arabinonic acid over Pd–Au catalysts supported on alumina and ceria. Applied Catalysis A: General 392(1–2) (2011): 69-79.

[31] Edwards, J.K., Thomas, A., Solsona, B.E., Landon, P., Carley, A.F., and Hutchings, G.J. Comparison of supports for the direct synthesis of hydrogen peroxide from H_2 and O_2 using Au–Pd catalysts. Catalysis Today 122(3–4) (2007): 397-402.

[32] Celorrio, V., Montes de Oca, M.G., Plana, D., Moliner, R., Fermín, D.J., and Lázaro, M.J. Electrochemical performance of Pd and Au–Pd core–shell

nanoparticles on surface tailored carbon black as catalyst support. International Journal of Hydrogen Energy 37(8) (2012): 7152-7160.

[33] Edwards, J.K., et al. The effect of heat treatment on the performance and structure of carbon-supported Au–Pd catalysts for the direct synthesis of hydrogen peroxide. Journal of Catalysis 292(0) (2012): 227-238.

[34] Weerachawanasak, P., Praserthdam, P., Arai, M., and Panpranot, J. A comparative study of strong metal–support interaction and catalytic behavior of Pd catalysts supported on micron- and nano-sized TiO_2 in liquid-phase selective hydrogenation of phenylacetylene. Journal of Molecular Catalysis A: Chemical 279(1) (2008): 133-139.

[35] Panpranot, J., Kontapakdee, K., and Praserthdam, P. Selective hydrogenation of acetylene in excess ethylene on micron-sized and nanocrystalline TiO_2 supported Pd catalysts. Applied Catalysis A: General 314(1) (2006): 128-133.

[36] Lederhos, C.R., et al. Hept-1-yne partial hydrogenation reaction over supported Pd andWcatalysts. Applied Catalysis A: General 396 (2011): 170-176.

[37] Mekasuwandumrong, O., Phothakwanpracha, S., Jongsomjit, B., Shotipruk, A., and Panpranot, J. Liquid-phase selective hydrogenation of 1-heptyne over Pd/TiO_2 catalyst synthesized by one-step flame spray pyrolysis. Catalysis Letters 136 (2010): 164-170.

[38] Lederhos, C.R., Badano, J.M., Quiroga, M.E., and L'Argentière, P.C. Influence of Ni addition to a low-loaded palladium catalyst on the selective hydrogenation of 1-heptyne. Química Nova 33 (2010): 816-820.

[39] Bond, G.C. and Thompson, D.T. Catalysis by gold. Catalysis Reviews: Science and Engineering 41 (1999): 319-388.

[40] Lopez-Sanchez, J.A. and Lennon, D. The use of titania- and iron oxide-supported gold catalysts for the hydrogenation of propyne. Applied Catalysis A: General 291 (2005): 230-237.

[41] Nikolaev, S.A. and Smirnov, V.V. Synergistic and size effects in selective hydrogenation of alkynes on gold nanocomposites. Catalysis Today 147S (2009): S336–S341.

[42] Zanella, R., Louis, C., Giorgio, S., and Touroude, R. Crotonaldehyde hydrogenation by gold supported on TiO_2: structure sensitivity and mechanism. Journal of Catalysis 223(2) (2004): 328-339.

[43] Jia, J., Haraki, K., Kondo, J.N., Domen, K., and Tamaru, K. Selective Hydrogenation of Acetylene over Au/Al_2O_3 Catalyst. Journal of Physical Chemistry B 104 (2000): 11153-11156.

[44] Liu, Y., Xing, T., Wei, Z., Li, X., and Yan, W. Liquid phase selective hydrogenation of phthalic anhydride to phthalide over titania supported gold catalysts. Catalysis Communications 10 (2009): 2023-2026.

[45] Milone, C., Trapani, M.C., and Galvagno, S. Synthesis of cinnamyl ethyl ether in the hydrogenation of cinnamaldehyde on Au/TiO_2 catalysts. Applied Catalysis A: General 337 (2008): 163-167.

[46] Prati, L., Villa, A., Porta, F., Wang, D., and Su, D. Single-phase gold/palladium catalyst: The nature of synergistic effect. Catalysis Today 122 (2007): 386-390.

[47] Ketchie, W.C., Murayama, M., and Davis, R.J. Selective oxidation of glycerol over carbon-supported AuPd catalysts. Journal of Catalysis 250 (2007): 264-273.

[48] Dimitratos, N., Porta, F., and Prati, L. Au, Pd (mono and bimetallic) catalysts supported on graphite using the immobilisation method Synthesis and catalytic testing for liquid phase oxidation of glycerol. Applied Catalysis A: General 291 (2005): 210-214.

[49] Moreau, F., Bond, G.C., and Taylor, A.O. Gold on titania catalysts for the oxidation of carbon monoxide: control of pH during preparation with various gold contenets. Journal of Catalysis 231 (2005): 105-114.

[50] Moreau, F. and Bond, G.C. Gold on titania catalysts, influence of some physicochemical parameters on the activity and stability for the oxidation of carbon monoxide. Applied Catalysis A: General 302 (2006): 110-117.

[51] Denkwitz, Y., et al. Influence of the crystalline phase and surface area of the TiO_2 support on the CO oxidation activity of mesoporous Au/TiO_2 catalysts. Applied Catalysis B: Environmental 91 (2009): 470–480.

[52] Denkwitz, Y., Schumacher, B., Kucerova, G., and Behm, R.J. Activity, stability, and deactivation behavior of supported Au/TiO_2 catalysts in the CO oxidation and preferential CO oxidation reaction at elevated temperatures. Journal of Catalysis 267 (2009): 78-88.

[53] Yu, W., Lee, W., Yang, C., and Wan, B. Low-temperature preferential oxidation of CO in a hydrogen rich stream (PROX) over Au/TiO_2: Thermodynamic study and effect of gold-colloid pH adjustment time on catalytic activity. Journal of the Chinese Institute of Chemical Engineers 38 (2007): 151-160.

[54] Zanella, R., Giorgio, S., Shin, C., Henry, C.R., and Louis, C. Characterization and reactivity in CO oxidation of gold nanoparticles supported on TiO_2 prepared by deposition-precipitation with NaOH and urea. Journal of Catalysis 222 (2004): 357–367.

[55] Ou, T., Chang, F., and Roselin, L.S. Production of hydrogen via partial oxidation of methanol over bimetallic Au–Cu/TiO2 catalysts. Journal of Molecular Catalysis A: Chemical 293 (2008): 8-16.

[56] Huang, J., Dai, W.-L., Li, H., and Fan, K. Au/TiO_2 as high efficient catalyst for the selective oxidative cyclization of 1,4-butanediol to γ-butyrolactone. Journal of Catalysis 252(1) (2007): 69-76.

[57] Moreau, F., Bond, G.C., and Taylor, A.O. The influence of metal loading and pH during preparation on the CO oxidation activity of Au/TiO_2 catalysts. Chemical Communications (2004): 1642-1643.

[58] Okumura, M., Akita, T., and Haruta, M. Hydrogenation of 1,3-butadiene and of crotonaldehyde over highly dispersed Au catalysts. Catalysis Today 74 (2002): 265-269.

[59] Sárkány, A. Acetylene hydrogenation on SiO_2 supported gold nanoparticles. Reaction Kinetics and Catalysis Letters 96 (2009): 43-54.

[60] Konova, P., Naydenov, A., Venkov, C., Mehandjiev, D., Andreev, D., and Tabakov, T. Activity and deactivation of Au/TiO_2 catalyst in CO oxidation. Journal of Molecular Catalysis A: Chemical 213 (2004): 235-240.

[61] Tsubota, S., Nakamura, T., Tanaka, K., and Haruta, M. Effect of calcination temperature on the catalytic activity of Au colloids mechanically mixed with TiO2 powder for CO oxidation. Catalysis Letters 56 (1998): 131-135.

[62] Grunwaldt, J.-D., Kiener, C., Wogerbauer, C., and Baiker, A. Preparation of Supported Gold Catalysts for Low-Temperature CO Oxidation via “Size-Controlled” Gold Colloids. Journal of Catalysis 181 (1999): 223–232.

[63] Grunwaldt, J.-D., Maciejewski, M., Becker, O.S., Fabrizioli, P., and Baiker, A. Comparative Study of Au/TiO2 and Au/ZrO2 Catalysts for Low-Temperature CO Oxidation. Journal of Catalysis 186 (1999): 458–469.

[64] Dimitratos, N., Villaa, A., Bianchi, C.L., Prati, L., and Makkee, M. Gold on titania: Effect of preparation method in the liquid phase oxidation. Applied Catalysis A: General 311 (2006): 185-192.

[65] Kang, M., et al. Characterization of a TiO_2 photocatalyst synthesized by the solvothermal method and its catalytic performance for $CHCl_3$ decomposition.

Journal of Photochemistry and Photobiology A: Chemistry 144 (2001): 185-191.

[66] Payakgul, W. Crystallization and precipitation mechanism of titanium (IV) oxide under the solvothermal condition and the effect of second element on titanium (IV) oxide products. Master's thesis Department of chemical Engineering Chulalongkorn University, (2002).

[67] Watson, S.S., Beydoun, D., Scott, J.A., and Amal, R. The effect of preparation method on the photoactivity of crystalline titanium dioxide particles. Chemical Engineering Journal 95 (2003): 213-220.

[68] Daté, M., Ichihashi, Y., Yamashita, T., Chiorino, A., Boccuzzi, F., and Haruta, M. Performance of Au/TiO_2 catalyst under ambient conditions. Catalysis Today 72 (2002): 89-94.

[69] Haruta, M., Tsubota, S., Kobayashi, T., Kageyama, H., Genet, M.J., and Delmon, B. Low-Temperature Oxidation of CO over Gold Supported on TiO_2, α-Fe_2O_3, and Co_3O_4. Journal of Catalysis 144(1) (1993): 175-192.

[70] Herzing, A.A., Carley, A.F., Edwards, J.K., Hutchings, G.J., and Kiely, C.J. Microstructural Development and Catalytic Performance of Au-Pd Nanoparticles on Al_2O_3 Supports: The Effect of Heat Treatment Temperature and Atmosphere. Chemistry of Materials 20 (2008): 1492-1501.

[71] Enache, D.I., et al. Solvent-Free Oxidation of Primary Alcohols to Aldehydes Using Au-Pd/ TiO_2 Catalysts. Science 311 (2006): 362-365.

[72] Zanella, R., Delannoy, L., and Louis, C. Mechanism of deposition of gold precursors onto TiO_2 during the preparation by cation adsorption and deposition–precipitation with NaOH and urea. Applied Catalysis A: General 291 (2005): 62-72.

[73] Ivanova, S., Pitchon, V., Petit, C., Herschbach, H., Dorsselaer, A.V., and Leize, E. Preparation of alumina supported gold catalysts: Gold complexes genesis, identification and speciation by mass spectrometry. Applied Catalysis A: General 298 (2006): 203-210.

[74] Pollmanna, J., Frankea, R., Hormesa, J., Bo¨nnemannb, H., Brijouxb, W., and Tillingb, A.S. An X-ray photoelectron spectroscopy investigation of a novel Pd–Pt colloid catalyst. Journal of Electron Spectroscopy and Related Phenomena 94 (1998): 219-227.

[75] Venezia, A.M., La Parola, V., Nicolì, V., and Deganello, G. Effect of Gold on the HDS Activity of Supported Palladium Catalysts. Journal of Catalysis 212(1) (2002): 56-62.

[76] Venezia, A.M., La Parola, V., Deganello, G., Pawelec, B., and Fierro, J.L.G. Synergetic effect of gold in Au/Pd catalysts during hydrodesulfurization reactions of model compounds. Journal of Catalysis 215(2) (2003): 317-325.

[77] Qian, K. and Huang, W. Au–Pd alloying-promoted thermal decomposition of PdO supported on SiO_2 and its effect on the catalytic performance in CO oxidation. Catalysis Today 164(1) (2011): 320-324.

[78] Parvulescu, V.I., et al. Characterization and Catalytic-Hydrogenation Behavior of SiO2-Embedded Nanoscopic Pd, Au, and Pd–Au Alloy Colloids. Chemistry - A European Journal 12 (2006): 2343-2357.

[79] Nijhuis, T.A., Koten, G.v., and Moulijn, J.A. Optimized palladium catalyst systems for the selective liquid-phase hydrogenation of functionalyzed alkynes. Applied Catalysis A: General 238 (2003): 259-271.

[80] Molnár, Á., Sárkány, A., and Varga, M. Hydrogenation of carbon–carbon multiple bonds: chemo-, regio- and stereo-selectivity. Journal of Molecular Catalysis A: Chemical 173(1–2) (2001): 185-221.

[81] Molero, H., Bartlett, B.F., and Tysoe, W.T. The hydrogenation of acetylene catalyzed by palladium: hydrogen pressure dependence. Journal of Catalysis 181 (1999): 49-56.

[82] Bond, G.C. Metal-Catalysed Reactions of Hydrocarbons Springer, New York. (2005).

[83] L'Argentière, P.C., Cagnola, E.A., Quiroga, M.E., and Liprandi, D.A. A palladium tetra-coordinated complex as catalyst in the selective hydrogenation of 1-heptyne. Applied Catalysis A: General 226 (2002): 253-263.

[84] Varga, M., Molnár, Á., Mohai, M., Bertóti, I., Janik-Czachor, M., and Szummer, A. Selective hydrogenation of pentynes over PdZr and PdCuZr prepared from amorphous precursors. Applied Catalysis A: General 234 (2002): 167-178.

[85] Kongsuebchart, W., Panpranot, J., Satayaprasert, C., and Praserthdam, P. Effect of TiO_2 crystallite size on the dispersion of Co on nanocrystalline TiO_2. Reaction Kinetics and Catalysis Letters 91 (2007): 119-126.

[86] Vicente, A., Lafaye, G., Especel, C., Marécot, P., and Williams, C.T. The relationship between the structural properties of bimetallic Pd–Sn/SiO_2 catalysts and their performance for selective citral hydrogenation. Journal of Catalysis 283(2) (2011): 133-142.

[87] Pattamakomsan, K., et al. Selective hydrogenation of 1,3-butadiene over Pd and Pd–Sn catalysts supported on different phases of alumina. Catalysis Today 164(1) (2011): 28-33.

[88] Domínguez-Domínguez, S., Berenguer-Murcia, Á., Linares-Solano, Á., and Cazorla-Amorós, D. Inorganic materials as supports for palladium nanoparticles: Application in the semi-hydrogenation of phenylacetylene. Journal of Catalysis 257(1) (2008): 87-95.

[89] Sárkány, A., Beck, A., Horváth, A., Révay, Z., and Guczi, L. Acetylene hydrogenation on sol-derived Pd/SiO_2. Applied Catalysis A: General 253(1) (2003): 283-292.

[90] Ulan, J.G., Maier, W.F., and Smith, D.A. Rational design of a heterogeneous palladium catalyst for the selective hydrogenation of alkynes. The Journal of Organic Chemistry 52(14) (1987): 3132-3142.

[91] Albers, P., Seibold, K., Prescher, G., and Müller, H. XPS and SIMS studies of carbon deposits on Pt/Al_2O_3 and Pd/SiO_2 catalysts applied in the synthesis of hydrogen cyanide and selective hydrogenation of acetylene. Applied Catalysis A: General 176(1) (1999): 135-146.

[92] Kittisakmontree, P., Pongthawornsakun, B., Yoshida, H., Fujita, S.-i., Arai, M., and Panpranot, J. The liquid-phase hydrogenation of 1-heptyne over Pd–Au/TiO_2 catalysts prepared by the combination of incipient wetness impregnation and deposition–precipitation. Journal of Catalysis 297(0) (2013): 155-164.

[93] Pongthawornsakun, B., Fujita, S.-i., Arai, M., Mekasuwandumrong, O., and Panpranot, J. Mono- and bi-metallic Au–Pd/TiO_2 catalysts synthesized by one-step flame spray pyrolysis for liquid-phase hydrogenation of 1-heptyne. Applied Catalysis A: General 467 (2013): 132-141.

APPENDICES

APPENDIX A
CALCULATION FOR CATALYST PREPARATION

- The calculation for the preparation of 0.5%Pd/TiO_2

  Base on 100 g of catalyst used, the composition of catalyst was as followed:

  Pd = 0.5 g

  TiO_2 = 100-0.5 = 99.5 g

  For 2 g of TiO_2

  Pd required = 2 × (0.5/99.5) = 0.0101 g

  Pd (Mw = 106.42) 0.0101g was prepared from $PdCl_2$ (Mw = 177.32)

  $$PdCl_2 \text{ required} = \frac{\text{Mw of } PdCl_2 \times \text{Pd required}}{\text{Mw of Pd}}$$

  $$= \frac{177.32 \times 0.0101}{106.42} = 0.0168 \text{ g}$$

- The calculation for the preparation of 1.0%Au/TiO_2

Base on 100 g of catalyst used, the composition of catalyst was as followed:

Au = 1.0 g

TiO_2 = 100-1.0 = 99 g

For 2 g of TiO_2

Au required = 2×(1.0/99) = 0.0202 g

Au (Mw = 196.97) 0.0202g was prepared from $HAuCl_4.3H_2O$ (Mw = 393.83)

$$HAuCl_4.3H_2O \text{ required} = \frac{\text{Mw of } HAuCl_4.3H_2O \times \text{Au required}}{\text{Mw of Au}}$$

$$= \frac{393.83 \times 0.0202}{196.97} = 0.0404 \text{ g}$$

- The calculation for the preparation of 0.5%Pd-1.0%Au/TiO_2

Base on 100 g of catalyst used, the composition of catalyst was as followed:

Pd = 0.5 g

Au = 1.0 g

TiO_2 = 100-0.5-1.0 = 98.5 g

For 2 g of TiO_2

Pd required = 2×(0.5/98.5) = 0.0102 g

Au required = 2×(1.0/98.5) = 0.0203 g

$$PdCl_2 \text{ required} = \frac{\text{Mw of } PdCl_2 \times \text{Pd required}}{\text{Mw of Pd}}$$

$$= \frac{177.32 \times 0.0102}{106.42} = 0.0170 \text{ g}$$

$$HAuCl_4.3H_2O \text{ required} = \frac{\text{Mw of } HAuCl_4.3H_2O \times \text{Au required}}{\text{Mw of Au}}$$

$$= \frac{393.83 \times 0.0203}{196.97} = 0.0406 \text{ g}$$

APPENDIX B
CALCULATION OF THE CRYSTALLITE SIZE

Calculation of the crystallite size by Debye-Scherrer equation

The crystallite size was calculated from the half-heigh width of the diffraction peak of XRD pattern using the Debye-Scherrer equation.

From Scherrer equation: $$D = \frac{K\lambda}{\beta\cos\theta}$$

where D = Crystallite size, Å

K = Crystallite-shape factor = 0.9

λ = X-ray wavelength, 1.5418 Å for CuKα

θ = Observed peak angle, degree

β = X-ray diffraction broadening, radian

The X-ray diffraction broadening (β) is the pure width of a powder diffraction free from all broadening due to the experimental equipment. α-Alumina is used as a standard sample to observe the instrument broadening since its crystallite size is lager thean 2000 Å. The X-ray diffraction broadening can be obtained from Warren's formula.

From Warren's formula: $$\beta = \sqrt{B_M^2 - B_S^2}$$

where B_M = The measured peak width in radians at half peak heigh

B_S = The corresponding width of the standard material

(0.00383 radian for α-Alumina)

APPENDIX C

CALCULATION FOR METAL ACTIVE SITES AND DISPERSION

Calculation for metal active sites and metal dispersion of the catalyst, a stoichiometry of CO/Pd = 1, measured by CO adsorption is as follows:

Let the weight of catalyst used = W g

Integral area of CO peak after adsorption = A unit

Integral area of 100 μl of standard CO peak = B unit

Amount of CO adsorbed on catalyst = B – A unit

Volume of CO adsorbed on catalyst = $100 \times \frac{(B-A)}{B}$ μl

Volume of 1 mole of CO at $30^{\circ}C$ = 24.86×10^{6} μl

Mole of CO adsorbed on catalyst = $\frac{100}{24.86 \times 10^{6}} \times \frac{(B-A)}{B}$ μmole

Molecule of CO adsorbed on catalyst

$$= [4.02 \times 10^{-6}] \times [6.02 \times 10^{23}] \times \frac{(B-A)}{B} \text{ molecules}$$

Metal active sites catalyst

$$= [2.42 \times 10^{18}] \times \frac{(B-A)}{B} \times \frac{1}{W} \text{ molecules of CO/g of catalyst}$$

Molecules of Pd loaded

$$= [6.02 \times 10^{23}] \times \frac{[\%\text{wt of Pd}]}{[\text{MW of Pd}]} \text{ molecules/g of catalyst}$$

$$\text{Metal dispersion (\%)} = 100 \times \frac{\text{moleces of Pd from CO adsorption}}{\text{molecules of Pd loaded}}$$

In this study, the formula from Chemisorp 2750 Operator's Manual can used for determined the % metal dispersion as follow:

$$\%D = S_f \times \left[\frac{V_{ads}}{V_g}\right] \times \left[\frac{Mw}{\%M}\right] \times 100\% \times 100\%$$

$$V_{ads} = \left[\frac{V_{inj}}{m}\right] \times \sum_{i=1}^{n} \left(1 - \frac{Ai}{Af}\right)$$

where D% = %metal dispersion

S_f = stoichiometry factor, (CO on Pd* =1)

V_{ads} = volume adsorbed (cm^3/g)

V_g = molar volume of gas at STP = 22414 cm^3/mol

Mw = molecular weight of metal (g/mol)

%M = %metal loading

V_{inj} = volume injected = 0.1 cm^3

m = weight of sample (g)

Ai = Area of peak i

Af = Area of last peak

The average crystallite size of Pd metal was calculated base on active metal surface area per gram of metal

$$d_p^{\circ} = \frac{Fg}{\rho \times MSAm} \times \left[\frac{m^3}{10^6 cm^3}\right] \times \left[\frac{10^9 nm}{m}\right]$$

$$MSAm = S_f \times \left[\frac{V_{ads}}{V_g}\right] \times \left[\frac{100\%}{\%M}\right] \times N_A \times \sigma_m \times \left[\frac{m^2}{10^{18} nm^2}\right]$$

where d_p^o = average crystallite size of Pd metal

Fg = crystallite geometry factor (hemisphere = 6)

ρ = specific gravity of the active metal (Pd = 12.0 g/cm^3)

MSAm = active metal suface area/g of metal (m^2/g)

N_A = Avogado's number (6.02×10^{23} molecules/mol)

σ_m = cross-sectional area of active metal atom

(Pd=0.0787nm^2)

APPENDIX D
CALIBRAION CURVES

This appendix showed the calibration curve for calculation of composition of reactant and products in 1-heptyne hydrogenation. The reactant is 1-heptyne and products are 1-heptene and n-heptane.

The GS-alumina column was used with a gas chromatography equipped with a flame ionization detector (FID), Shimadzu modal 14B, for analyzing the concentration of 1-heptyne, 1-heptene and n-heptane. Condition uses in GC are illustrated in **Table D.1**.

Mole of the reagent in y-axis and area, which was reported by gas chromatography, in x-axis is exhibited in the curves. The calibration curves of 1-heptyne, 1-heptene, and heptane are shown in **Figure D.1**, **Figure D.2**, and **Figure D.3**, respectively.

Table D.1 Conditions used in Shimadzu model GC-14B

Parameters	Conditions of Shimadzu GC-14B
Width	5
Slope	29
Drift	0
Min.area	50
T.DBL	2.7
Stop time	10
Atten.	0
Speed	2
Method	1
Format	1
SPL.WT	100
IS.WT	0

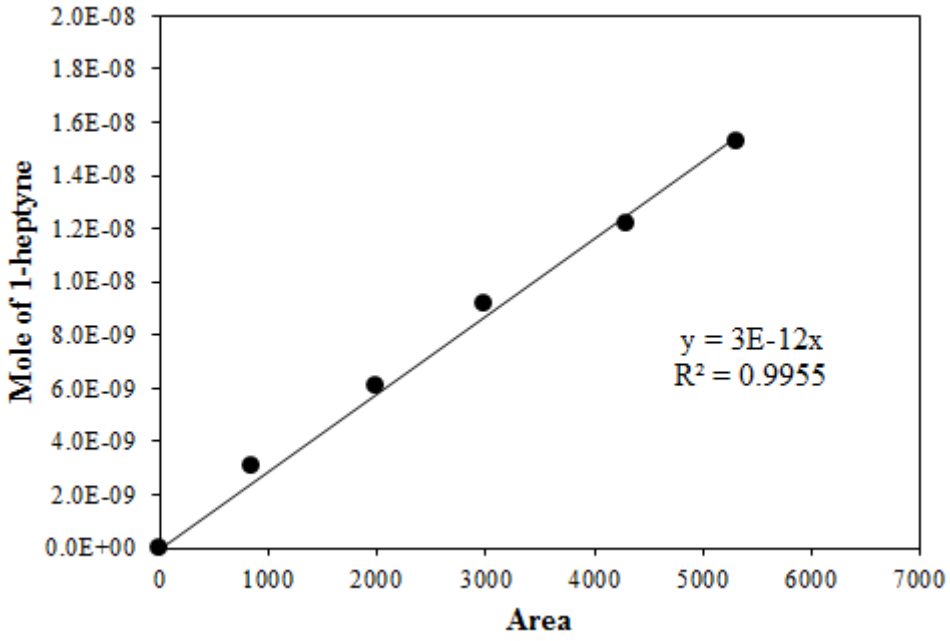

Figure D.1 The calibration curve of 1-heptyne

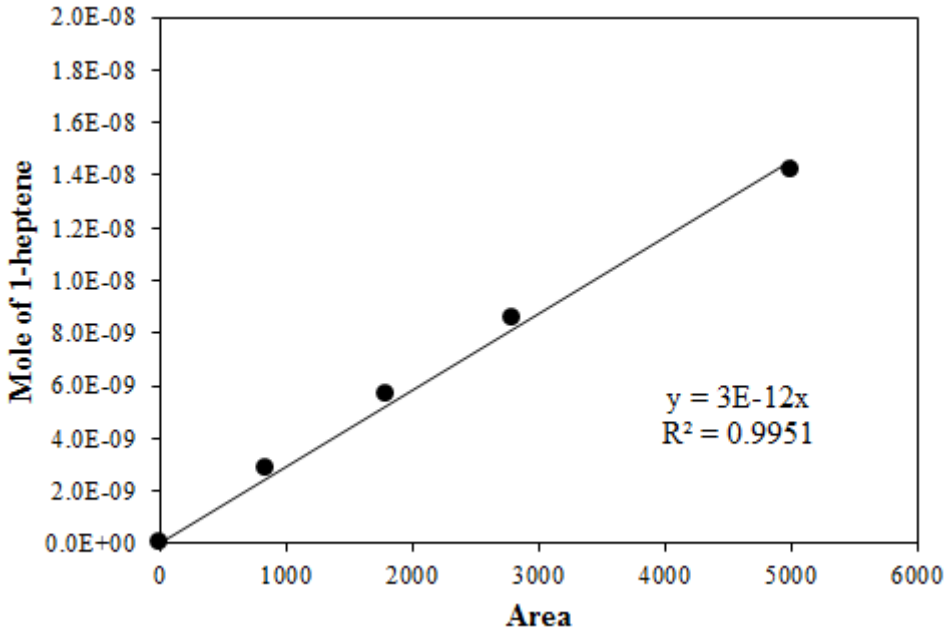

Figure D.2 The calibration curve of 1-heptene

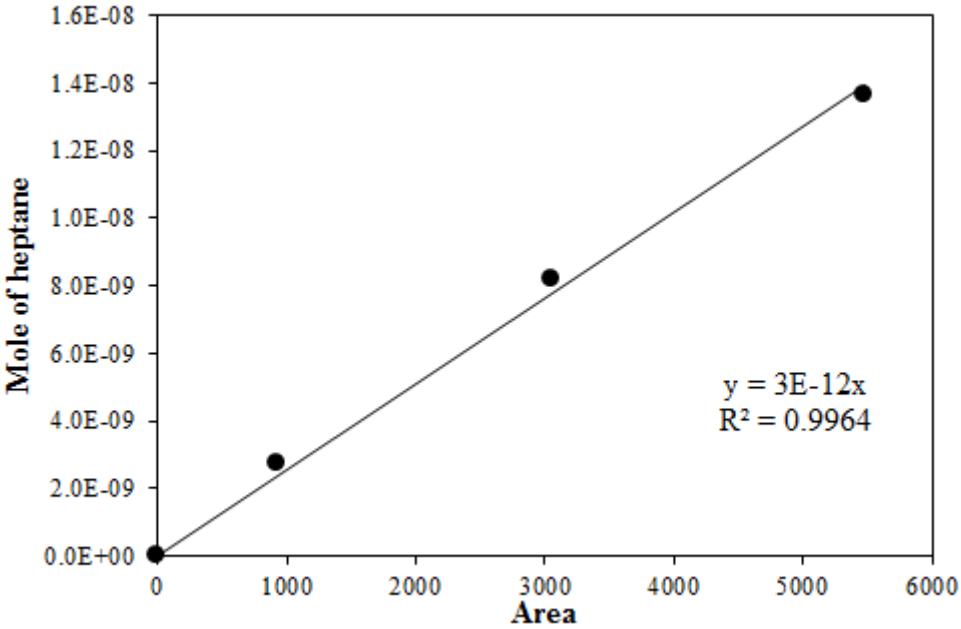

Figure D.3 The calibration curve of heptane

APPENDIX E
CALCULATION OF 1-HEPTYNE AND 1-HEPTENE CONVERSION AND 1-HEPTENE SELECTIVITY

The catalytic performance for the 1-heptyne hydrogenation was evaluated in terms of activity for 1-heptyne conversion and 1-heptene selectivity.

Activity of the catalyst performed in term of 1-heptyne conversion. 1-Heptyne conversion is defined as moles of 1-heptyne converted with respect to 1-heptyne in feed:

$$\text{1-heptyne conversion (\%)} = \frac{\text{Mole of 1-heptyne in (feed – product)}}{\text{Mole of 1-heptyne in feed}} \times 100$$

; Where the mole of 1-heptyne can be measure employing the calibration curve of 1-heptyne in **Figure D.1**.

$$\text{Mole of 1-heptyne} = \left[\begin{array}{c} \text{Area of 1-heptyne peak} \\ \text{from integrator plot on GC-14B} \end{array} \right] \times (3 \times 10^{-12})$$

Selectivity of the product is defined as mole of 1-heptene formed with respect to mole of 1-heptyne converted:

$$\text{1-heptene selectivity (\%)} = \frac{\text{Mole of 1-heptene}}{\text{Mole of total product}} \times 100$$

; Where mole of 1-heptene and heptane can be measured employing the calibration curve of 1-heptene in **Figure D.2** and **Figure D.3**

$$\text{Mole of 1-heptene} = \left[\begin{array}{c} \text{Area of 1-heptene peak} \\ \text{from integrator plot on GC-14B} \end{array} \right] \times (3 \times 10^{-12})$$

$$\text{Mole of 1-heptane} = \left[\begin{array}{c} \text{Area of 1-heptane peak} \\ \text{from integrator plot on GC-14B} \end{array} \right] \times (3 \times 10^{-12})$$

The catalytic performance for the 1-heptene hydrogenation was evaluated in terms of activity for 1-heptene conversion. 1-Heptene conversion is defined as moles of 1-heptene converted with respect to heptane in feed:

$$\text{1-heptene conversion (\%)} = \frac{\text{Mole of 1-heptene in (feed – product)}}{\text{Mole of 1-heptene in feed}} \times 100$$

APPENDIX F
LIST OF PUBLICATIONS

1. Prathan Kittisakmontree, Boontida Pongthawornsakun, Hiroshi Yoshida, Shin-ichiro Fujita, Masahiko Arai, and Joongjai Panpranot, The liquid-phase hydrogenation of 1-heptyne over Pd–Au/TiO_2 catalysts prepared by the combination of incipient wetness impregnation and deposition–precipitation, *Journal of Catalysis* 297 (2013) 155-164.

2. Prathan Kittisakmontree, Boontida Pongthawornsakun, and Joongjai Panpranot, Effect of TiO_2 crystallite size on the catalytic behavior of Au-Pd/TiO_2 catalysts in the liquid-phase hydrogenation of 1-heptyne, *The 2nd International Conference on Engineering and Applied Science 2013*, Tokyo, Japan, Mar 15-17, 2013.

3. Chayanin Na-Chiangmai, Napaporn Tiengchad, Prathan Kittisakmontree, Okorn Mekasuwandumrong, Jonathan Powell, and Joongjai Panpranot, Characteristics and catalytic properties of mesocellular foam silica supported Pd nanoparticles in the liquid-phase selective hydrogenation of phenylacetylene, *Catalysis Letters* 141 (2011) 1149-1155.

VITA

Mister Prathan Kittisakmontree was born in November 1st, 1984 in Lopburi, Thailand. He finished high school from Pibulwittayalai School, Lopburi in 2003, and received bachelor's degree in Chemical Engineering from the department of Chemical Engineering, Faculty of Engineering, Burapha University, Chonburi, Thailand in 2007.